

**A STUDY OF DIESEL HEAT TRANSFER DISTRIBUTION
USING A RAPID COMPRESSION MACHINE**

Robert S. Wolf

M.S., Stanford University (1979)
S.B., Massachusetts Institute of Technology (1978)

Submitted to the Department of Aeronautics and Astronautics
in partial fulfillment of the requirements for the degree of

DOCTOR OF SCIENCE

at the

MASSACHUSETTS INSTITUTE OF TECHNOLOGY

September 1988

© Massachusetts Institute of Technology 1988

Signature of Author

Department of Aeronautics and Astronautics
September 1988

Certified by

Prof. Wai K. Cheng, Thesis Supervisor
Associate Professor of Mechanical Engineering

Certified by

Prof. John B. Heywood
Professor of Mechanical Engineering

Certified by

Prof. Anthony T. Patera
Associate Professor of Mechanical Engineering

Certified by

Prof. Manuel M. Martinez-Sanchez
Associate Professor of Aeronautics and Astronautics

Accepted by

Prof. Harold Y. Wachman
Chairman, Departmental Graduate Committee

Acknowledgements

It is difficult to condense into a couple of pages the impact that MIT has had on me. I was an undergraduate here, spent five years elsewhere, and returned for another five years. Some of my old friends were (and are) still around, and I met plenty of new ones. In many ways, MIT often seems like home. It's not the pristine architecture or the splendor of Cambridge by the river; it's the people that make it so special. I would like to acknowledge some of those people, but if a name is omitted here rest assured that it is not omitted in my memory.

First, I would like to thank my advisor, Wai Cheng. He was always available for help whenever I wanted it, and left me alone when I wanted to flounder on my own. I couldn't have asked for a better "doctor-father". I also want to thank the other members of my thesis committee; John Heywood, the very epitome of the British Gentleman, from whom I learned as much by example as from his wisdom and engineering insight; Manuel Martinez, my mentor in the field of rocket propulsion, for which I will always be grateful; and Tony Patera, who introduced me to the greater world of computational fluid mechanics. Believe it or not, they even made thesis committee meetings enjoyable.

All of my colleagues in the Sloan Automotive Lab deserve special mention, but space limits me to thank only two. Rick Frank and Stefan Pischinger taught me almost everything I know about working in a research lab; they tolerated two years of continual harassment from me without complaining (at least not much, anyways) and loaned me their equipment whenever I needed it. Without these two I would still be struggling along in the test cell, trying to figure out what was going on.

The Space Systems Lab deserves my highest accolades. I cannot begin to describe the positive impact that the SSL has had on my life. The people in the lab have been, almost without exception, terrific to work with and play with. My highest thanks go to my good friend Dave Akin, whose confidence in me five years ago made it possible for me to come back to MIT and ultimately finish the doctoral program.

I would also like to thank my family. Without their support I would still be "the family underachiever".

Finally, I am eternally indebted to my son Stevie. Being a graduate student is work, a single parent even more so, and both together should by all rights be too much altogether. However, Stevie made it all seem fun. Stevie, you're the best thing that ever happened to me. Daddy loves you.

This work was funded in part by the MIT Consortium for Engine Research, and in part by the MIT Consortium for the Use of Ceramics in Internal Combustion Engines. Member companies have included Cummins Engine Company, Ford Motor Company, General Motors Corporation, Kolbenschmidt AG, Martin Marietta, Peugeot Societe Anonyme, Regie Nationale des Usines Renault, the United States Department of Energy, and the U.S. Army Tank Automotive Command.

A STUDY OF DIESEL HEAT TRANSFER DISTRIBUTION USING A RAPID COMPRESSION MACHINE

TITLE PAGE

ABSTRACT

ACKNOWLEDGEMENTS

I	INTRODUCTION	1
	1.1 Motivation	1
	1.2 Previous Experiments	2
	1.3 Present Work	3
	1.3.1 The Fuel Spray as a Submerged Jet	3
	1.3.2 Effect of Swirl on Heat Transfer	4
	1.3.3 Effect of Charge Air Temperature on Heat Transfer	4
	1.4 Scope of Present Effort	5
II	APPARATUS AND INSTRUMENTATION	6
	2.1 Rapid Compression Machine	6
	2.2 Experiment Geometry and Nomenclature	7
	2.3 Fuel Injection System	8
	2.4 Instrumentation	12
	2.5 Data Acquisition System	13
	2.6 High-Speed Movies	14
III	ANALYSIS TECHNIQUES	15
	3.1 Heat Transfer Determination	15
IV	EXPERIMENTAL RESULTS	21
	4.1 Test Conditions	21
	4.2 Impingement Point Heat Transfer	22
	4.3 Effect of Injection Distance on Impingement Point Heat Transfer	23
	4.4 Repeatability	25
	4.5 Heat Transfer Surveys	26

4.5.1	Horizontal Surveys	27
4.5.2	Vertical Surveys	28
4.5.3	Miscellaneous Surveys	29
V	COMPARISON TO STEADY SUBMERGED JET	30
5.1	Motivation	30
5.2	Quasi-Steady-State Heat Transfer	31
5.3	Determination of Quasisteady Heat Flux	33
5.4	Modeling Fuel Spray as Submerged Jet	33
5.4.1	Equivalent Nozzle Diameter	34
5.4.2	Determination of Nozzle Exit Velocity	34
5.4.3	Entrained Mass	35
5.4.4	Estimation of Jet Temperature	35
5.5	Impingement Point Heat Transfer	37
5.6	Circumferential Variation of Heat Transfer	41
VI	EFFECT OF SWIRL	44
6.1	Motivation	44
6.2	Test Conditions	44
6.3	Results	45
VII	EFFECT OF CHARGE TEMPERATURE	47
7.1	Motivation	47
7.2	Test Conditions	47
7.3	Results	48
7.3.1	Net Heat Release Rate	48
7.3.2	Correlation of Heat Transfer Rates with Other Events	49
7.3.3	Quasisteady Heat Transfer Rates	50
VIII	SUMMARY AND CONCLUSIONS	52
	REFERENCES	54
	APPENDICES	

Chapter 1

Introduction

1.1 MOTIVATION

Heat transfer is an area of great concern to designers of all propulsion systems. Among other things, heat transfer affects engine performance, efficiency, and emissions. These particular concerns can generally be addressed by the overall, or spatially-averaged, heat transfer rates. A rich literature exists on overall heat transfer from the combustion gases to the chamber.^[1] These heat transfer rates have been successfully correlated by applying the Nusselt number - Reynolds number relationships developed for pipe flow; an example of such is the empirical correlation of Woschni.^[2] Other researchers^[3,4] have proposed the use of flat-plate forced convection correlations.

Although the spatially-averaged correlation methods work fairly well at predicting the overall heat transfer, surprisingly little is known about the detailed structure of heat transfer and the underlying physical mechanisms which govern the process. Recent developments in low heat rejection engines have brought this lack of understanding to the forefront. Considerable effort has been expended towards reducing heat losses from internal combustion engines by means of coating critical engine components with thermally insulating materials. And yet, the efficacy of thermal insulation in reducing heat transfer rates, once universally accepted, has itself been challenged.^[5]

Local heat transfer rates are required for calculating thermal stresses. This is of particular interest to designers of low-heat-rejection engines, as the thermal stresses in these engines are greater than in conventional engines due to the higher wall temperatures. In fact, a major problem with insulating coatings is thermal stress due to differential heating within the combustion chamber. Engine life-cycle predictions are also affected by the local heat transfer rates.

Recent advances in computational problem solving have allowed the diesel combustion process to be simulated numerically. The advantage to this is that the underlying physical processes can be modeled more directly, rather than correlated empirically. Boundary conditions still need to be modeled, however, since the coarseness of practical computational grids precludes resolution of the viscous sublayers. The more sophisticated

numerical simulations^[6] evaluate the gas velocity and temperature adjacent to the wall, then use turbulent boundary layer correlations to evaluate the wall shear stress, and finally employ the Reynolds-Colburn analogy to estimate local heat transfer coefficients. This presupposes the existence of a fully developed boundary layer at all points in the combustion chamber, an assumption born primarily of necessity. The accuracy of the heat transfer predictions by this technique are as yet unknown.

Unfortunately, experimental information of the distribution of heat transfer around the combustion chamber is extremely sparse. This limits our understanding of the heat transfer process itself and makes validation of numerical simulations difficult. Fortunately, experimental techniques for measuring the unsteady, local heat flux have been developed^[3], and these may be used to gather supporting data for analysis of predictive models. Limited efforts in this area have been made; these results will be summarized below.

1.2 PREVIOUS EXPERIMENTS

The first applicable experiments on local heat transfer were performed by Gardon and Cobonpue.^[7] They were interested in the cooling of glass plates by impinging jets of air. They subjected an electrically heated aluminum plate to impinging turbulent jets of air, and measured the heat flux both at the impingement point and elsewhere. A single round jet was used, as was an array of jets. They were able to correlate the impingement point Nusselt number with a simple formula involving the jet Reynolds number and the distance from the nozzle to the plate. Further, for nozzle-to-plate distances large enough to ensure fully developed jet behavior (about 10 nozzle diameters or greater) they correlated the local heat transfer coefficients to those at the impingement point. The local heat transfer coefficients were found to decrease monotonically with increasing distance from the impingement point.

More directly applicable experiments were conducted by Kamimoto, et.al.^[8] They performed experiments in a rapid compression machine using a single fuel spray impinging on a flat cylinder head. Local heat transfer rates were extracted for two injection distances and two jet impingement angles. Their results showed that the heat flux from an impinging diesel flame is distributed approximately evenly on the contact surface, and the heated area → spreads out with time. Their interpretation was that the heat transfer coefficient, decreasing with distance from the impingement point, is being counteracted by increasing local gas

temperatures. They also found that, for the rather small range of injection distances used (28 and 40 mm), that the heat transfer rate was insensitive to injection distance. Finally, a single run was performed using nitrogen gas instead of air, so that spray-induced heat transfer could be separated from flame-induced heat transfer. Surprisingly, the impingement point heat transfer with nitrogen equaled that with air, although this result was of peripheral interest and did not receive intense scrutiny.

Similar experiments have been done in a combustion bomb,^[9,10] they offer heat transfer rates for a single injection distance with and without swirl, but cannot offer companion data without combustion due to the limitations of the experimental apparatus. Their results are intended to be a database for validation of numerical models.

1.3 PRESENT WORK

The present work follows along similar lines to the work of Kamimoto. A rapid compression machine was used to determine local heat transfer rates from impinging diesel flames. The injection distance was varied in five increments from 29mm to 105 mm. Runs were repeated for all distances with nitrogen in an attempt to determine local heat transfer coefficients, and to determine whether the counterbalancing of decreasing coefficients by increasing temperatures is plausible. The effect of initial charge temperature was also evaluated, as was the effect of swirl.

1.3.1 THE FUEL SPRAY AS A SUBMERGED JET

One of the goals of this research was to determine whether the burning fuel spray could be modeled as a submerged jet for heat transfer purposes. This was broken into two steps. The first step was to determine whether a non-burning fuel spray could be so modeled, hence the runs with nitrogen were performed. Next, the extension of the submerged jet analogy to the burning case was performed. The data of Gardon and Cobonpue^[7] was used to evaluate the efficacy of the submerged jet model. This necessitated varying the injection distance to see if the scaling law applicable to air jets was applicable to fuel sprays as well. It was not possible to vary the jet Reynolds number in this study.

There is ample precedent for considering the fuel spray as a steady submerged jet. Abramovich^[11] reasoned that the fuel droplets in a spray could be treated as a very dense admixture in air. Although the fuel spray is initially pure liquid, it both entrains air and

vaporizes as it moves downstream of the nozzle. The liquid fuel droplets soon become a small fraction of the jet volume. Because of the rapid entrainment, the mixture attains the same density as the surrounding fluid in approximately 10 nozzle diameters.^[12] The velocity of the small droplets relative to the gas diminishes to near zero in approximately 30 nozzle diameters.^[13] At greater distances, the characteristics of the spray (width, velocity distribution) are almost the same as a gas jet with the same initial momentum.^[14]

1.3.2 EFFECT OF SWIRL ON HEAT TRANSFER

Swirl is used in diesel engines to promote more rapid mixing between the inducted air charge and the injected fuel. It is therefore necessary to consider the effect of swirl on the fuel spray, as significant changes in the flow patterns can result from this initial air motion. A logical assumption is that the heat transfer will be profoundly affected as well, both in magnitude and in distribution. A single run with swirling air was performed in order to verify this assumption.

1.3.3 EFFECT OF CHARGE AIR TEMPERATURE ON HEAT TRANSFER

Diesel engines operate over a wide range of temperature conditions. The inlet air will be relatively cold when the engine is first started, and will gradually warm up to the vicinity of 100 C when the engine is in steady-state operation. Collella, et.al.^[15] studied the influence of charge temperature on the combustion event itself. They discovered striking variations in the instantaneous net heat release rates. Their conclusions were that decreasing the charge temperature lengthened the ignition time delay, which in turn allowed more fuel to be vaporized prior to the start of combustion. Since more fuel was burned in the characteristic premixed combustion phase, the rate of heat release was increased. Further, since less fuel remained to be burned during the mixing-controlled combustion phase, the total length of the combustion period was reduced. The effect was so strong that decreasing the inlet air temperature from 102 C to 27 C caused the peak net heat release rate to increase from 1500 kW to 5000 kW. It would be surprising if heat transfer rates were unaffected, therefore a study of diesel heat transfer would not be complete without considering the effect of charge temperature on heat transfer. This was investigated in the current research by varying the initial charge temperature from 30 C to 100 C in three increments.

1.4 SCOPE OF PRESENT EFFORT

This research effort deals with the spatial distribution of heat transfer in direct injection diesel engines. Heat transfer rates were measured at various locations along the cylinder walls of a rapid compression machine. The objectives of the research were to:

- * measure the local, instantaneous heat transfer rates in the vicinity of impinging diesel sprays, both with and without combustion.

- * assess how the magnitude of heat transfer, both at the impingement point and elsewhere, is affected by injector standoff distance, charge temperature, and swirl.

- * determine whether or not existing models for heat transfer from submerged jets can be expanded to cover two-phase burning spray flames.

- * develop an experimental database for numerical studies of diesel combustion.

Chapter 2

Apparatus and Instrumentation

2.1 RAPID COMPRESSION MACHINE

The experiments were carried out in the MIT Rapid Compression Machine (RCM); a pneumatically driven, single shot device which produces a compressed charge simulating the diesel combustion environment (fig. 2.1). The construction and operation of the RCM has previously been documented in detail by Balles.^[16] The dimensions and operating range of the RCM are summarized in table 2.1. In the following experiments, the inlet air temperature was generally maintained at 100 C with a very slow axial flow rate. For one set of experiments the air temperature was varied (30, 65, 100 C). For another experiment the inlet air was injected tangentially at high velocity to provide swirl of approximately 2500 rpm.

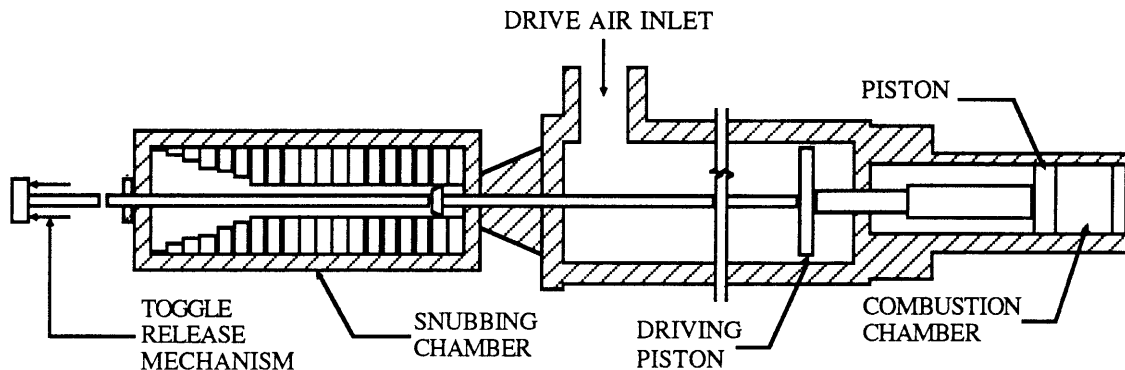


Fig. 2.1. Rapid Compression Machine

Major Characteristics

Bore:	10.16 cm	(4.00 in)
Stroke:	44.7 cm	(17.69 in)
Clearance Height:	3.07 cm	(1.21 in)
Compression Ratio:	15.5	

Range of Operating Conditions

Initial Air Temperature:	-20 to 150 C
Initial Air Velocity:	10 to 50 m/s
Initial Swirl Level:	0 to 6000 rpm
Initial Cylinder Pressure:	1 to 2 bar

Table 2.1. RCM Specifications

2.2 EXPERIMENT GEOMETRY AND NOMENCLATURE

The RCM was configured with a side-mounted fuel injector. A single fuel spray was directed at the curved cylinder wall midway between the piston face and the cylinder head. The cylinder head was equipped with a fused silica (quartz) window which covered the entire cylinder bore. This arrangement is pictured in Figure 2.2, which also identifies the nomenclature for various geometric parameters.

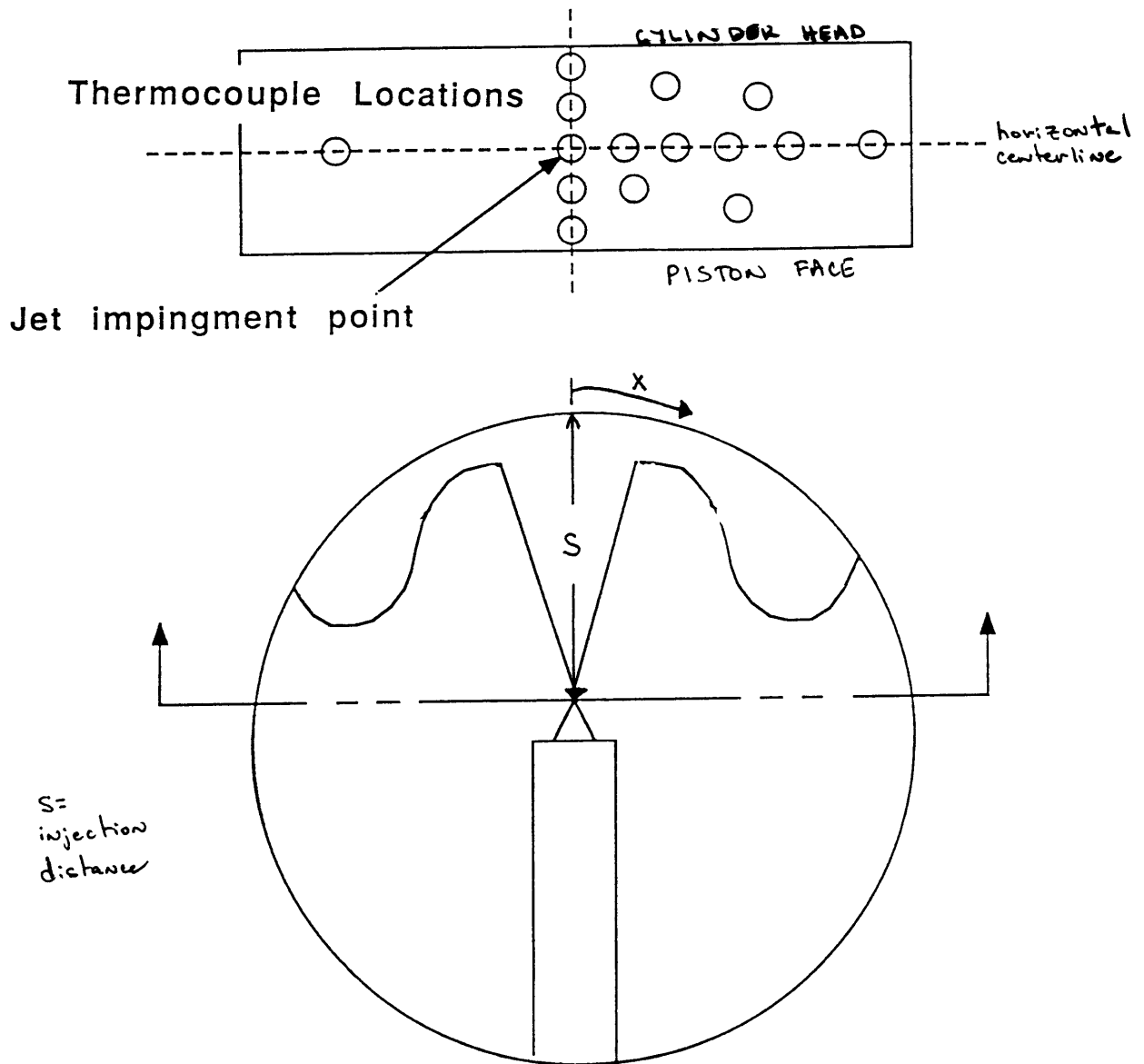


Figure 2.2. Experiment Geometry and Nomenclature

2.3 FUEL INJECTION SYSTEM

A single-shot fuel injection system was developed for use with the Rapid Compression Machine. The heart of the system was a pneumatically actuated fuel pump which presented a single pulse of high-pressure fuel to a Stanadyne Model 9.5 pencil nozzle. The nozzle exit diameter was .254 mm (.010 in). The system also contained a fuel reservoir and a pressurizing gas accumulator. The fuel injection system is illustrated in Figure 2.3.

The fuel pump (Figure 2.4) employed a piston which alternately retracted and extended to pump fuel into the nozzle. The piston was retracted before the RCM was fired to draw fuel into a small plenum. During the RCM firing sequence, a solenoid valve was opened which allowed pressurizing gas to force the piston into the extended position. The amount of fuel injected was controlled by limiting the stroke of the piston. The duration of fuel injection was controlled by adjusting the pressure in the accumulator. The delivered pressure was affected by the accumulator pressure, the nozzle orifice size, and the nozzle cracking pressure. The fuel pump delivered a dynamic, yet repeatable, pressure pulse to the pencil nozzle. Figure 2.5 shows the pressure traces for five separate injection events. For the injections depicted in figure 2.5, the accumulator pressure was 17.2 bar (250 psi) and the injected fuel mass approximately 0.025 grams. The nozzle opening pressure was set to 103 bar (1500 psi).

It is not possible to directly measure the quantity of fuel injected into the RCM. However, one can measure the fuel injected into another vessel and assume the injection event is repeatable, or one can extract the injected fuel quantity from a fuel pressure time history. Historically, the latter method is accurate only to about 10%, but substantially better results were obtained in this investigation. The actual mass injected was determined by injecting fuel into a glass bottle which was weighed before and after the injection. The fuel mass was measured to a precision of +/- 0.0001 gram using a Macalester balance scale. The quantity of fuel injected was fitted to the formula

$$\text{Fuel Mass} = \int_{T_{\text{open}}}^{T_{\text{close}}} C_D \rho A \sqrt{2 \frac{\Delta P}{\rho}} dt \quad (2-1)$$

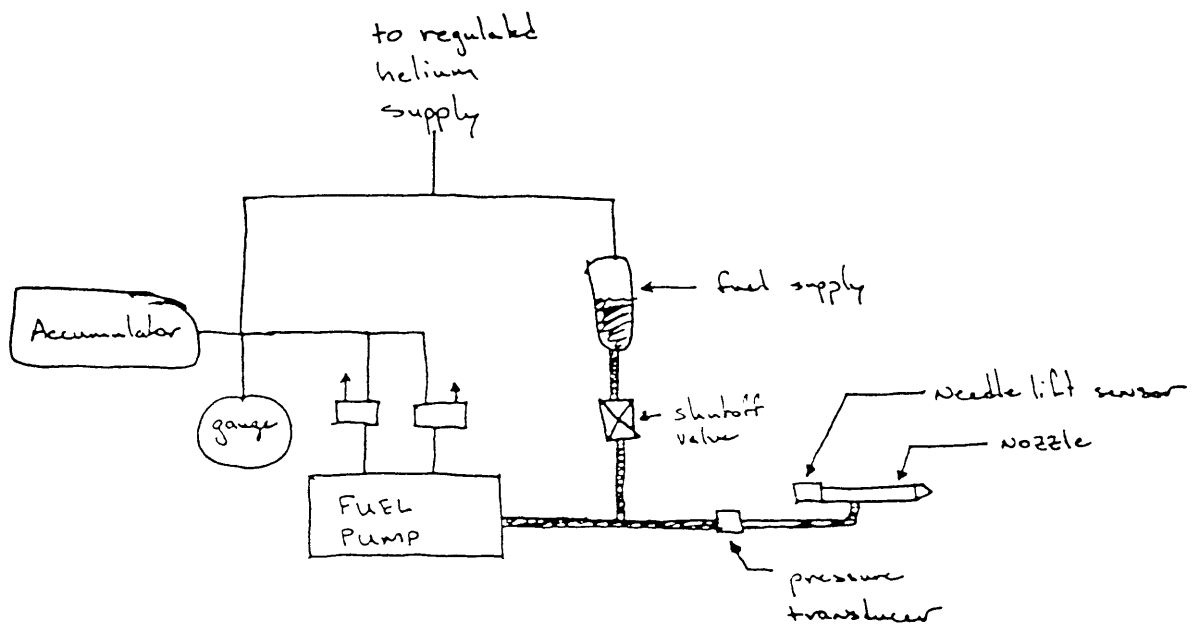


Figure 2.3. Fuel Injection System

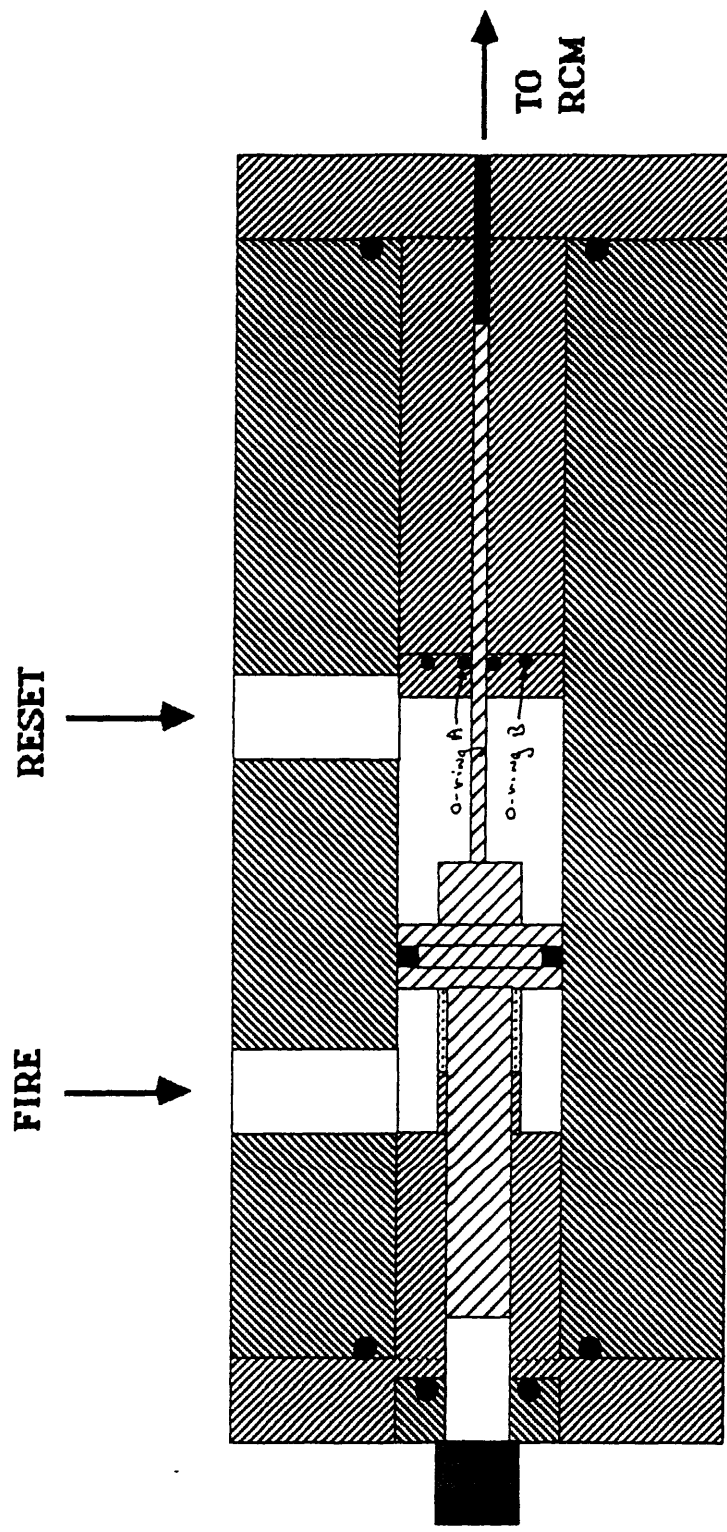


Figure 2.4. Fuel Pump

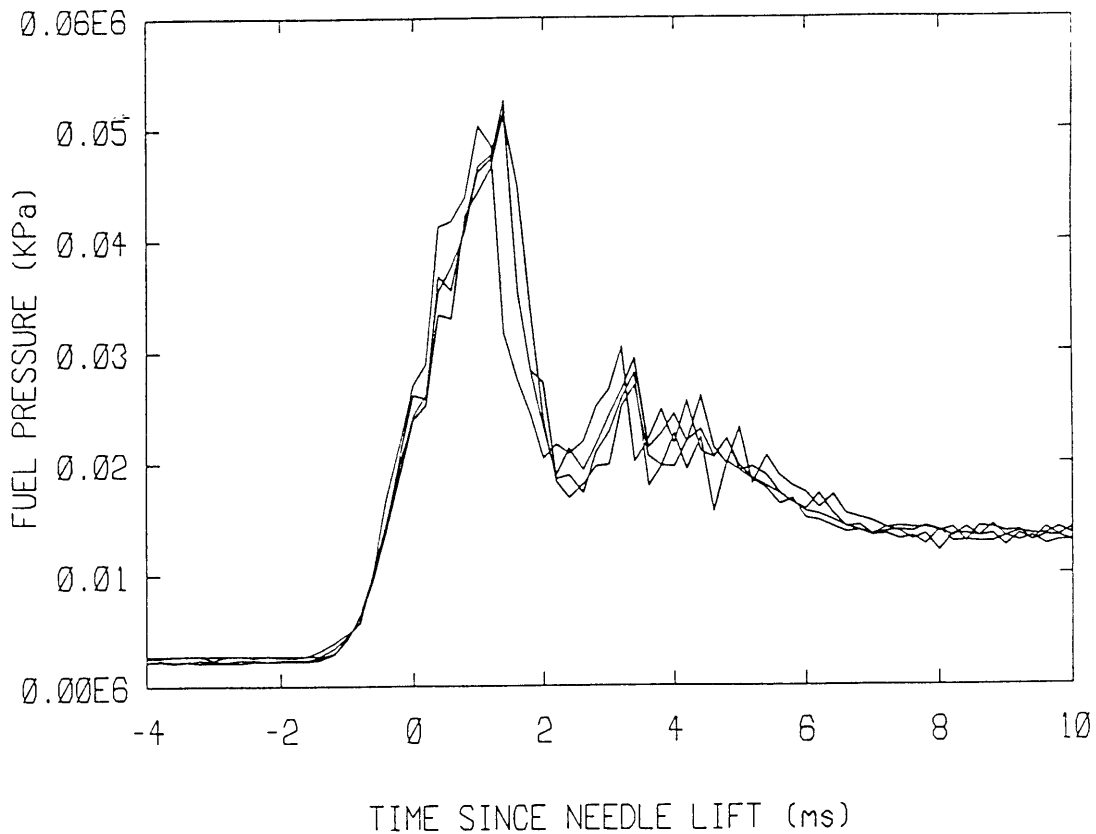


Fig. 2.5. Fuel Pressure Time-Histories for Five Injections.

where C_D = discharge coefficient, ρ = fuel density, A = nozzle area, ΔP = pressure differential across the nozzle. The quantity $C_D A$ was adjusted until the mean error between measured and calculated fuel mass was zero, using a sample size of seven injections. The standard deviation of the error was 3%. *Small*

It should be noted that the quantity determined by this analysis is not C_D alone, but the quantity $C_D A$. There is some uncertainty in nozzle area due to the method of determining nozzle exit diameter, thus there is some uncertainty in the discharge coefficient. The nozzle exit diameter was determined by inserting gauge pins of different diameters through the nozzle orifice. The gauge pin diameters come in increments of 0.025 mm (0.001 inch), thus the nozzle orifice diameter was not determined exactly, but rather was bracketed by two different size pins. The nozzle exit diameter was therefore 0.254 to 0.279 mm (0.010 to 0.011 inch), which corresponded to discharge coefficients of 0.92 to 0.76.

With use, the performance of the fuel pump degraded unacceptably. This was caused by damage to the o-ring which sealed against the sliding piston. Manifestations of o-ring damage were a) reductions in the quantity of fuel injected and b) insufficient pressure to keep the needle open continuously (needle bounce). The final solution to this required replacing the internal o-rings after approximately every second experimental run. Even so, nearly 40% of the experimental runs had to be repeated due to needle bounce. The lesson here is that a robust, high-pressure single-shot fuel pump is a critical part of RCM experimental apparatus.

2.4 INSTRUMENTATION

The cylinder pressure was measured using a quartz piezoelectric transducer (Kistler model 6123A2). The initial cylinder gas temperature was determined using type K thermocouples upstream of the inlet valve and downstream of the exhaust port under steady flow conditions. The arithmetic mean of these measurements was taken to be the cylinder gas temperature. The details of the instrumentation and calibration procedures are described in reference 16.

Cylinder wall surface temperature was measured with 14 type K surface thermocouples (Medtherm TCS-K-10368 microsecond-response) flush-mounted in the cylinder wall. An additional thermocouple (Medtherm TCS-K-375-10702) was identical except a second junction was embedded 9.5 mm (0.375 inch) below the surface so that temperature gradients normal to the surface could be measured. The thermocouples were situated essentially along horizontal and vertical lines running through the fuel jet impingement point, with a few extra located off-axis (Figure 2.6). These thermocouples were connected to a jack panel mounted next to the RCM; this jack panel formed the second junction for each thermocouple. To determine the temperature of the jack panel, a standard (slow-response) type K thermocouple was attached to the panel and referenced to an ice bath.

The thermocouple signals were amplified by a factor of 512 by two Transiac 1008 8-channel amplifier cards before being digitized and stored by the data acquisition system. Temperature could be resolved to 0.12 degrees C.

The injector needle lift was measured using an inductive, non-contacting, proximity meter. The transducer probe and signal conditioning unit were manufactured by Kaman Sciences

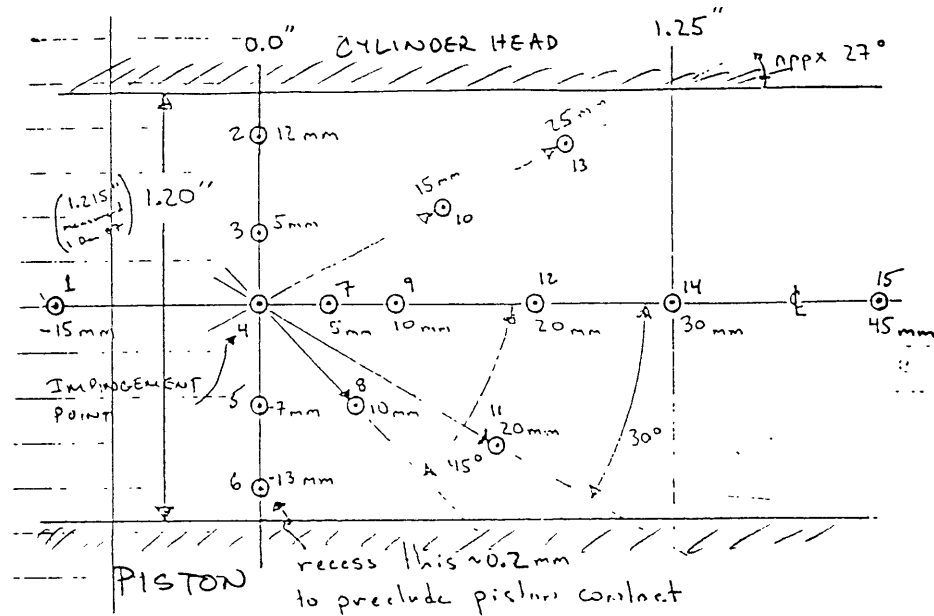


Figure 2.7. Thermocouple Locations

Corporation (KD-2400). The meter provided a signal of approximately 5 volts when the needle was closed, and approximately 4 volts when the needle was fully open. The system exhibited a 10 KHz frequency response. [17]

The fuel pressure was measured with a quartz piezoelectric transducer (Kistler model 607F122) coupled to a charge amplifier (Kistler model 504E). The pressure transducer was mounted in the fuel line between the fuel pump and the injector body. The transducer was calibrated using dead weights and showed excellent linearity.

2.5 DATA ACQUISITION SYSTEM

The analog voltages provided by the above instrumentation were digitized and recorded using the standard MIT Sloan Automotive Laboratory data acquisition system. The fifteen fast-response thermocouple signals plus a data correlation signal were digitized and recorded using a Lecroy Instruments 8212/16 digitizer. The other signals, plus the same

data correlation signal, were recorded using a Lecroy Instruments 8121/8 digitizer. Both of these units are 12 bit, bipolar (-5 to +5 volts), medium speed, multi-channel analog-to-digital transient recorders. The data was sampled at 5 KHz, providing one data point every 0.2 milliseconds. This was the maximum data rate for the 16-channel digitizer. The duration of the combustion event was on the order of 10 milliseconds, thus the resolution was adequate. Both digitizers were triggered by the same stop trigger pulse, thus data synchronization between digitizers was +/- 0.2 milliseconds. Data was transferred from local memory units to the laboratory's Digital Equipment Corporation VAX 11/750 immediately after each run for long term storage and detailed analysis.

2.6 HIGH-SPEED MOVIES

High-speed color movies (direct photography) were used in this study. An NAC E10 camera with a 28 mm f/2.0 macro lens was mounted so as to look directly through the quartz window in the cylinder head. A framing rate of 6000 frames per second was used throughout the study. A rotating shutter with a shutter constant of 1/5 was used yielding an effective exposure time of 33 microseconds. Illumination was provided by two Sylvania ELH bulbs. Eastman Ektachrome High-Speed 7250 (tungsten balanced) film was used for all runs.

Chapter 3

Data Analysis Techniques

3.1 HEAT TRANSFER DETERMINATION

Heat transfer rates were extracted from time histories of the wall surface temperature. One-dimensional conductive heat transfer within the wall was assumed, since the normal temperature gradient is large compared to the lateral one for the duration of interest (≤ 50 ms). The heat transfer rate was related to the temperature via a numerical solution to the one-dimensional heat conduction equation

$$\frac{\partial^2 T}{\partial x^2} = \frac{1}{\alpha} \frac{\partial T}{\partial t} \quad (3-1)$$

The purpose of the solution was to calculate the surface heat flux ($k_w \partial T / \partial x$ at $x=0$) using the measured surface temperature and the known initial temperature profile. Discretizing equation (3-1) using an Euler forward differencing technique, we obtained

$$\frac{T_j^{n+1} - T_j^n}{\alpha \Delta t} = \frac{1}{\Delta x^2} \left(T_{j-1}^n - 2T_j^n + T_{j+1}^n \right) \quad (3-2)$$

which is first-order accurate in Δt and second-order accurate in Δx . In the data analysis, Δt was set to match the data acquisition rate (0.2 ms) and Δx was chosen to meet criteria for stability of the numerical solution. Since equation (3-1) was discretized with a forward-differencing technique, stability could be assured if $\Delta x^2 / \alpha \Delta t \geq 2$. This was effected by setting $\Delta x = .044$ mm. Care was taken to ensure that the last point was outside the thermal skin depth during the data analysis period, so that the temperature at this point may be specified as equal to the initial temperature. 677 nodes were used, thus the last grid point was 3 cm from the surface. Setting $\Delta x^2 / \alpha \Delta t = 2$ we obtained the simple result

$$T_j^{n+1} = \frac{1}{2} \left(T_{j-1}^n + T_{j+1}^n \right) \quad (3-3)$$

We set up a virtual grid in the cylinder wall as shown in figure 3.1, where T_j represents the temperature at node j .

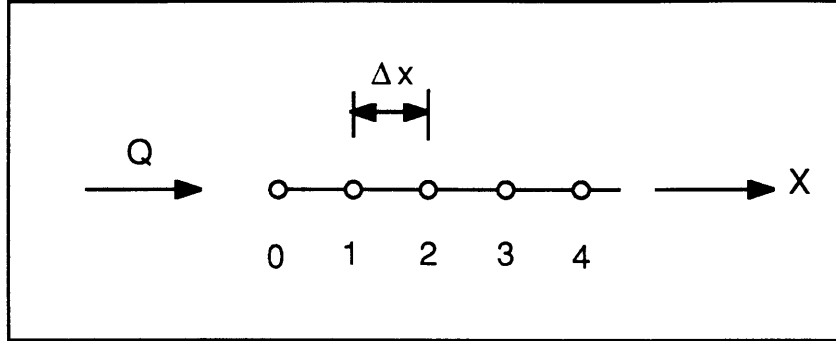


Fig. 3.1 One-dimensional Heat Conduction in Cylinder Wall

Referring to figure 3.1, an energy balance may be written for the first volume element

$$q = k_w \frac{\partial T}{\partial x} + \frac{Q}{A} \quad (3-4)$$

where q is the net heating rate, k_w is the thermal conductivity of the wall, and the temperature gradient is evaluated at $x=1/2$. Note that Q/A is the heat flux which we are trying to determine. At the wall surface (node zero) however,

$$q = \rho_w C_{p_w} \frac{\Delta x}{2} \left(\frac{T_0^{n+1} - T_0^n}{\Delta t} \right) \quad (3-5)$$

Combining (3-4) and (3-5) and using $\Delta x^2/\alpha \Delta t = 2$,

$$\frac{Q}{A} = \frac{k_w}{\Delta x} \left(T_0^{n+1} - T_1^n \right) \quad (3-6)$$

In order to obtain the heat flux time history from a recorded time history of wall surface temperature we proceed as follows.

A) Initialize the virtual grid with an appropriate initial temperature profile. The wall temperature was known both at the surface and, using the embedded thermocouple, at a depth of 9.5 mm (0.375 in). A linear gradient was assumed between these nodes and extrapolated for deeper nodes.

B) For each time step, the new wall surface temperature was provided from experimental data.

C) Eqn. (3-6) was used to infer Q/A .

D) Eqn. (3-3) was used to update the temperatures for all nodes other than the surface node (which was updated in step B above). As a boundary condition, the temperature of the deepest node remained constant.

Since this process involves differencing the wall surface temperature, any noise in the data is magnified. To reduce the apparent noise in the resulting heat transfer rate, the recorded temperature signal was digitally filtered using a first-order filter. The time constant for the filter was 1 millisecond; a compromise which gave adequate smoothing without degrading the time-response too much. Figures 3.2a and 3.2b show a representative unfiltered temperature trace and the resulting heat transfer rate. Figures 3.3a and 3.3b show the same for filtered temperatures.

The heat conduction model was verified by comparing the calculated interior wall temperature to data obtained from a thermocouple embedded in the wall. One of the wall thermocouples (# 9) had a second junction inset 9.5 mm (.375 inch) into the wall. This was provided by a Medtherm TCS-K-375-10702 dual-junction thermocouple. It was therefore possible to measure the interior wall temperature at this point and compare it to the temperature calculated with the one dimensional conduction model described above. Excellent agreement was obtained using the thermal diffusivity and conductivity of chromel (the primary thermocouple material) in the conduction model (fig. 3.4).

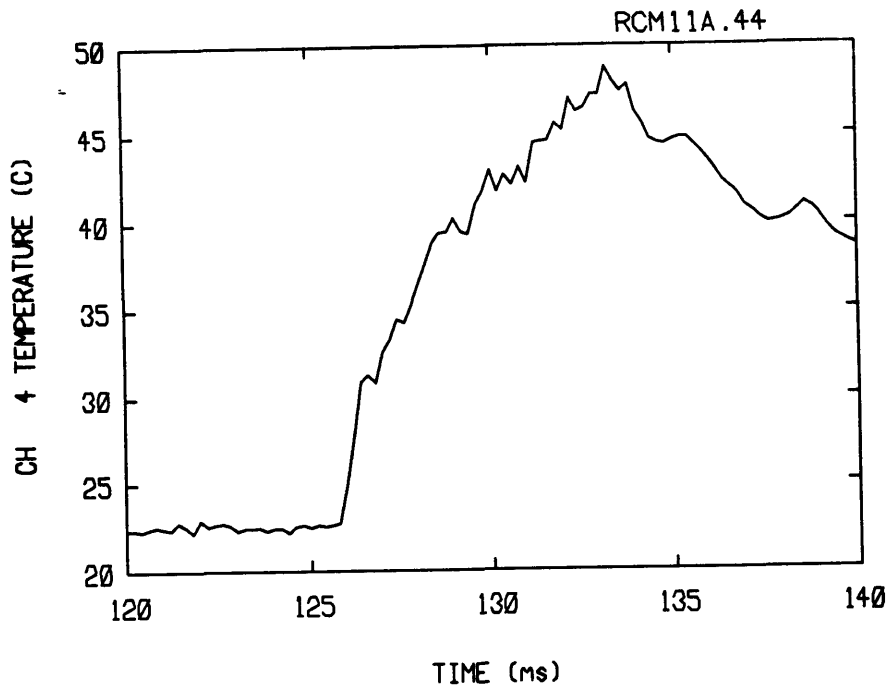


Fig. 3.2a Representative Unfiltered Temperature Trace
(Numbers refer to degrees above ambient temperature)

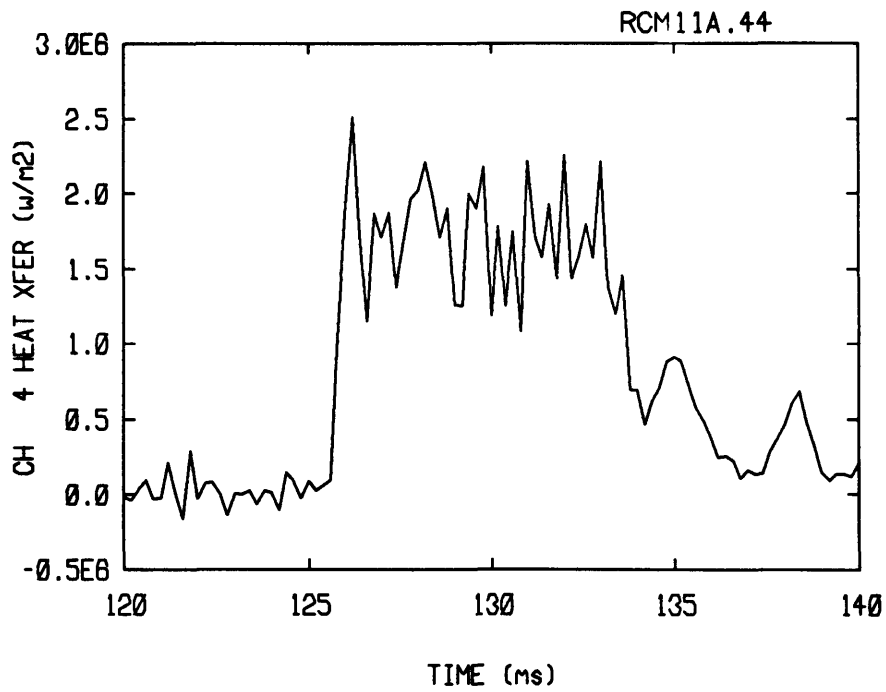


Fig. 3.2b Heat Transfer Rate using Unfiltered Temperature as Input

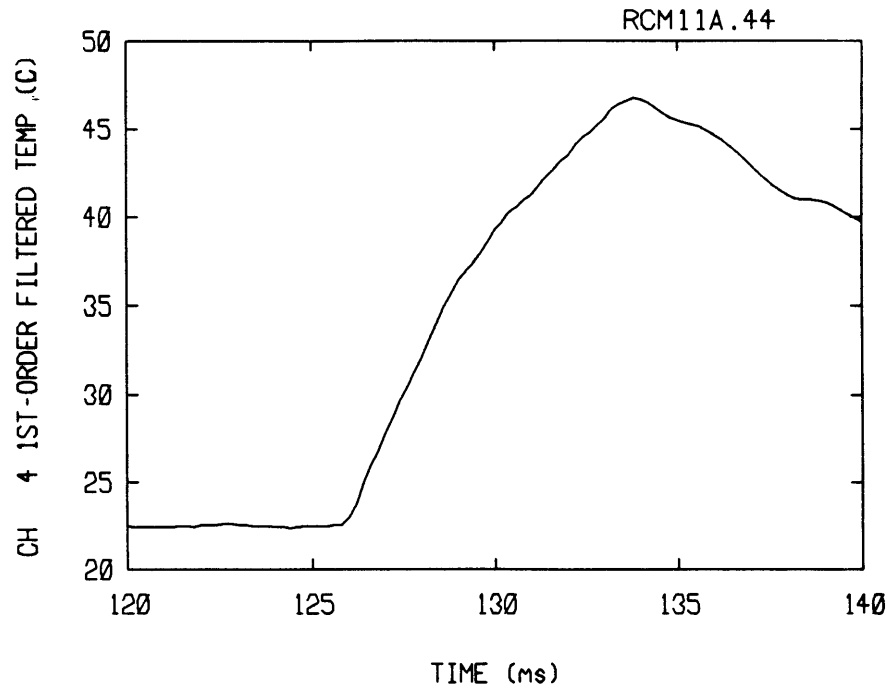


Fig. 3.3a Representative Filtered Temperature Trace using First Order Filter with Time Constant of 1 Millisecond (Numbers refer to degrees above ambient temperature)

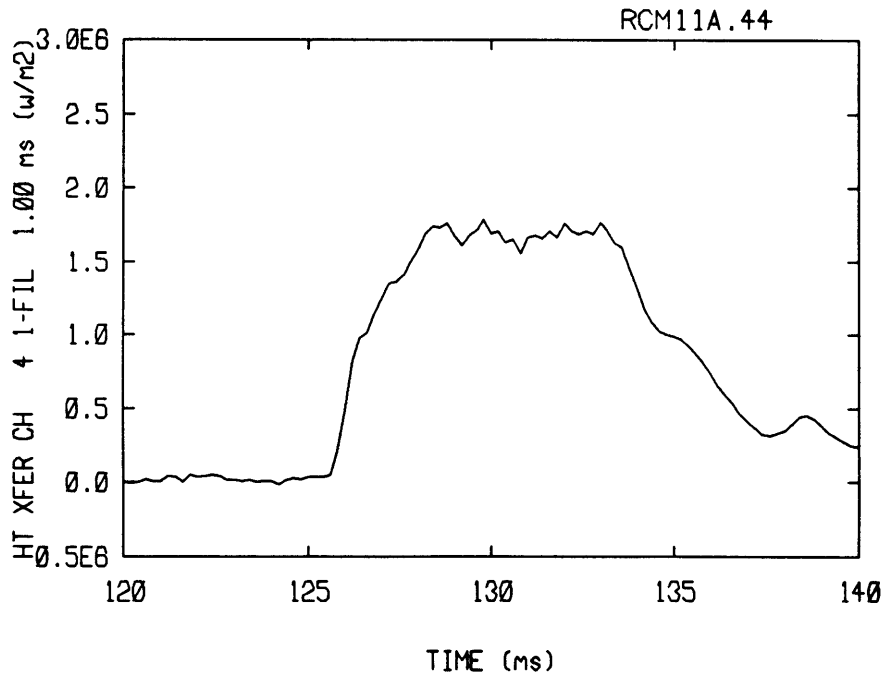


Fig. 3.3b Heat Transfer Rate using Filtered Temperature as Input

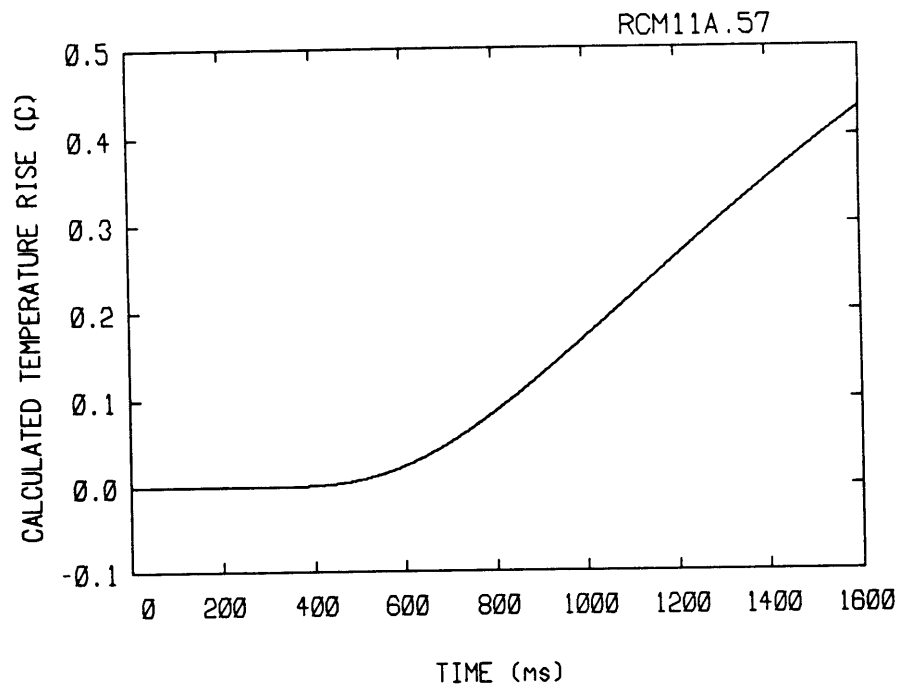


Fig. 3.4a Calculated Change of Inset Temperature using 1-Dimensional Conduction Model

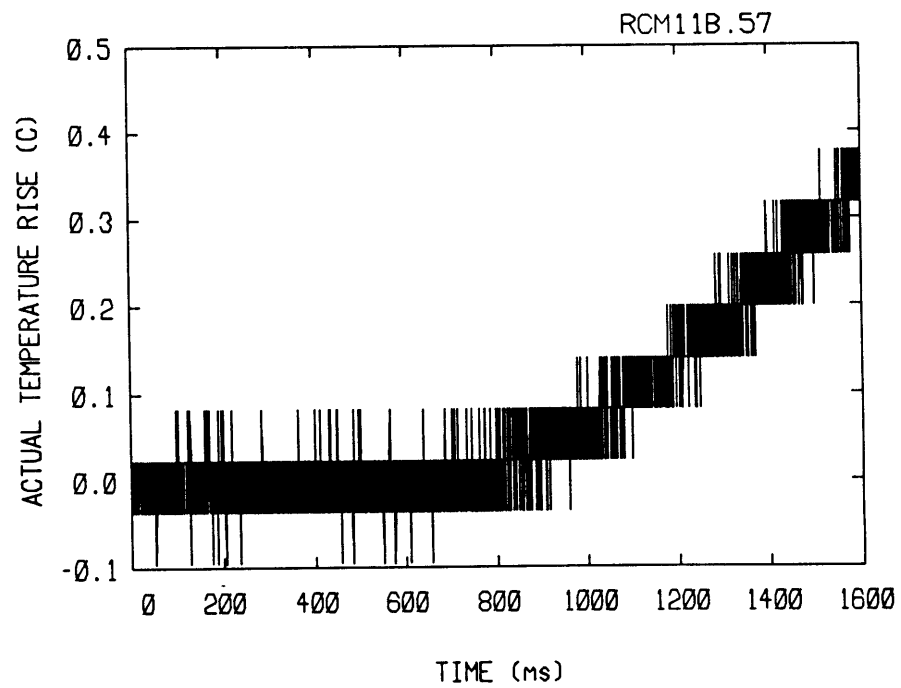


Fig. 3.4b Measured Change of Inset Temperature

Chapter 4 Experimental Results

4.1 TEST CONDITIONS

A baseline test condition was chosen, from which parameters were varied to complete a test matrix. The baseline condition was selected to match as closely as possible the conditions that would exist in an operating diesel engine. Further, a wealth of experimental data^[15,18] and numerical simulations^[19,20] have involved using the RCM with a five-jet injector, and it was desired to have the results of the current investigation bear as much similarity to these previous results as possible. The baseline case was to represent a single jet of the five-jet injector used in references 1-4.

The previous works used a five-jet injection of 0.1248 grams of fuel to simulate a medium size direct injection diesel engine operating at about 50% load. Since only one jet was used in this study, the desired fuel mass injected was one-fifth of this value, or 0.025 g. It turned out that the mean fuel mass injected during the current research was 0.0293 gm. Average injection duration was 4.88 ms. The mean injection pressure was 118.5 bar (1719 psi). This injection pressure is somewhat low compared to actual engines, but was the highest attainable due to limitations of the fuel injection system.

Most of the experiments used an initial charge temperature of 100 C with little or no air motion. The charge conditions at the time of injection for these cases were 950 K and 38.1 bar (550 psi).

The test matrix involved parametric variations of injection distance, charge gas, initial charge temperature, and swirl. The test matrix consisted of a total of 13 runs. The injection distance survey involved five different injection distances from 29 to 105 mm. These runs were performed both with air and with nitrogen as the charge gas. The effects of initial charge temperature and swirl were performed at a fixed injection distance (54 mm) and only with air. It was not possible to generate swirl with nitrogen due to the low flow rates of nitrogen available. Initial air temperatures of 30, 65, and 100 C were used, resulting in cylinder temperatures at injection of 819, 855, and 943 K respectively.

The results of 13 RCM runs are included in this thesis. The specific parameters for each run are listed in Table 4.1.

<u>Run No.</u>	<u>Injection Distance (mm)</u>	<u>Gas</u>	<u>Initial Temp (C)</u>	<u>Fuel Injected (g)</u>	<u>Injection Duration (ms)</u>	<u>Swirl (rpm)</u>
11.62	29	Air	99.5	0.0323	5.6	0
11.44	54	Air	99.5	0.0280	4.4	0
11.60	68	Air	99.8	0.0337	5.6	0
11.63	79	Air	100.0	0.0262	4.6	0
11.47	105	Air	100.0	0.0278	4.4	0
11.50	29	N ₂	100.5	0.0304	5.0	0
11.52	54	N ₂	100.0	0.0301	5.0	0
11.55	68	N ₂	100.5	0.0283	4.8	0
11.53	79	N ₂	100.5	0.0290	4.8	0
11.54	105	N ₂	100.0	0.0274	4.6	0
11.57	54	Air	30.0	0.0337	5.2	0
11.59	54	Air	65.0	0.0320	5.2	0
11.61	54	Air	100.5	0.0318	5.6	2540

Table 4.1. Test Conditions

4.2 IMPINGEMENT POINT HEAT TRANSFER

Figure 4.1 shows the impingement point heat transfer time history for a 54 mm injector standoff distance. The solid line shows the heat transfer in air; the dashed line shows the heat transfer in nitrogen. Both traces show a rapid rise in heat transfer rate at approximately the time of jet arrival. The heat transfer rate in air is about three times greater with combustion than without, however, as will be seen in Chapter 5 the relative percentages vary greatly with injection distance.

The heat transfer rate with combustion holds steady at approximately 3200 kilowatts per square meter for quite some time after injection is over. This is presumably due to continued burning of the injected fuel until it is totally consumed. The nitrogen trace is different, however, in that there is a sharp increase in heat transfer rate at the end of injection. It is believed that hot cylinder gases are convected towards the wall by the fuel jet. These gases are cooled somewhat by the evaporation of the fuel. However, when the fuel spray suddenly ceases, the cooling effect disappears immediately while the flowfield takes a finite time to decay. The sudden increase in gas temperature with no corresponding

change in gas velocity causes the spike in heat transfer rate. As the gas velocities decay, the heat transfer rate decays as well.

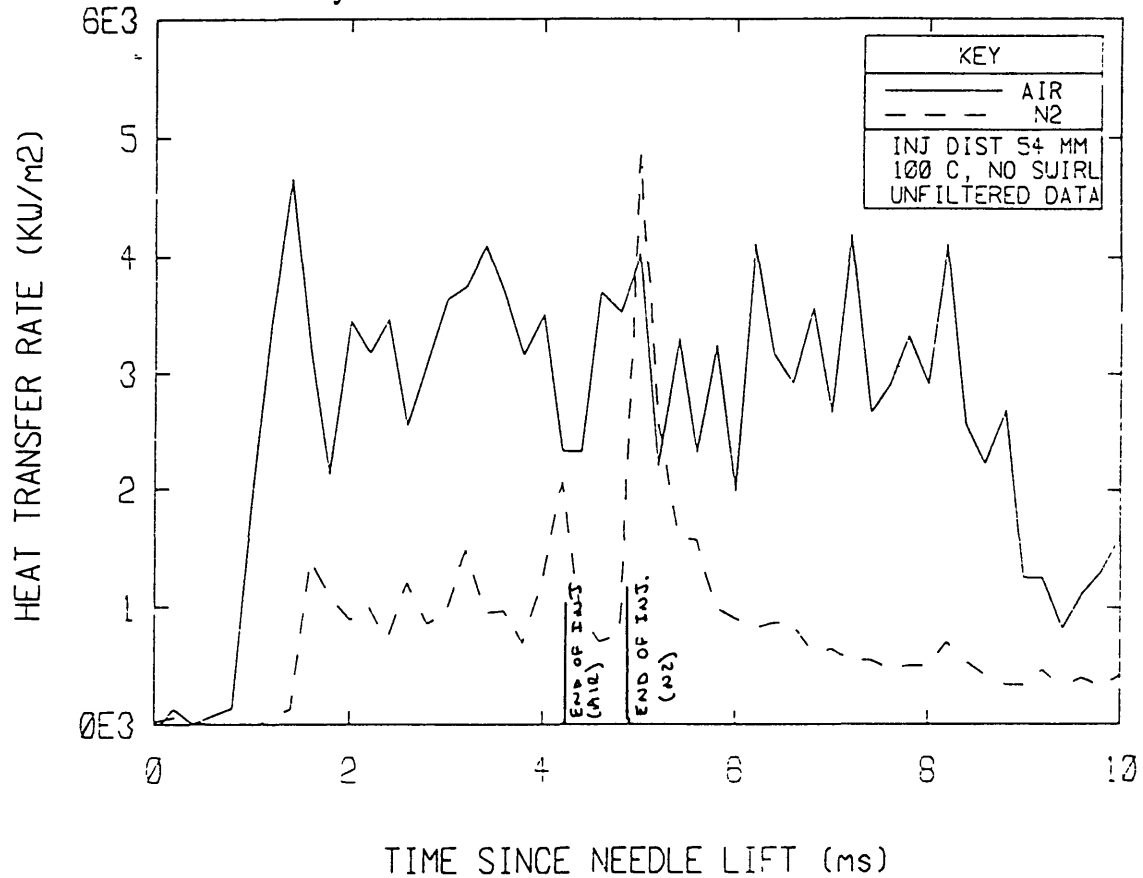


Figure 4.1. Impingement Point Heat Transfer in Air and Nitrogen (54 mm injection distance)

4.3 EFFECT OF INJECTION DISTANCE ON IMPINGEMENT POINT HEAT TRANSFER

The impingement point heat transfer rates during the steady portion were determined as explained in Chapter 5 and plotted as a function of injection distance (fig. 4.2). Note that the heat transfer rate for the 29 mm injection distance is identical for both air and nitrogen. This suggests that the spray is not burning at the impingement point, probably because the local equivalence ratio is too rich to support combustion. This can be verified by examining the heat transfer traces for the two runs; the end phase heat transfer is considerably higher in air than in nitrogen, indicating the presence of combustion in the post-injection period (fig. 4.3)

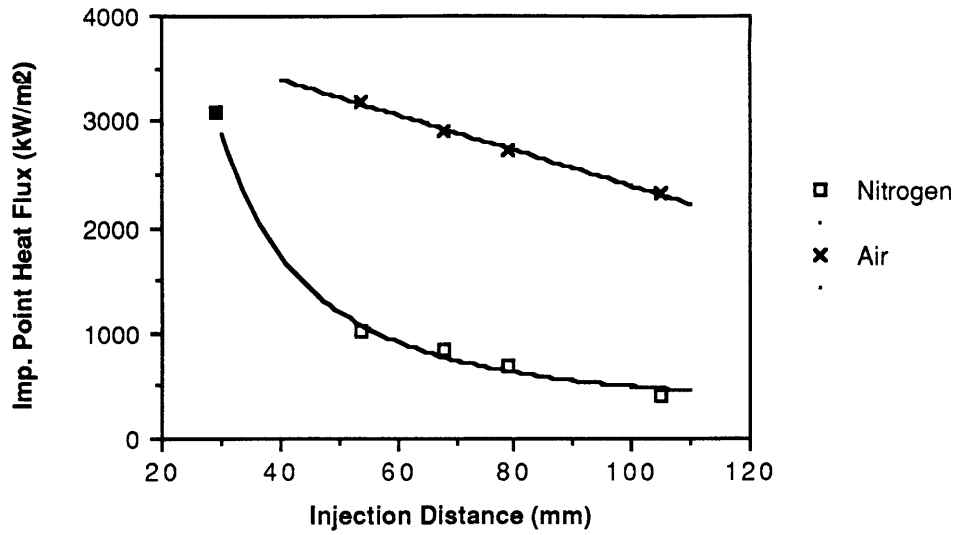


Fig. 4.2. Impingement Point Heat Transfer vs. Injection Distance (Air, Nitrogen)
 (Formula for line through nitrogen data is $y = 2.368E6 x^{-2} + 259$,
 Formula for line through air data is $y = -16.67 x + 4059$)

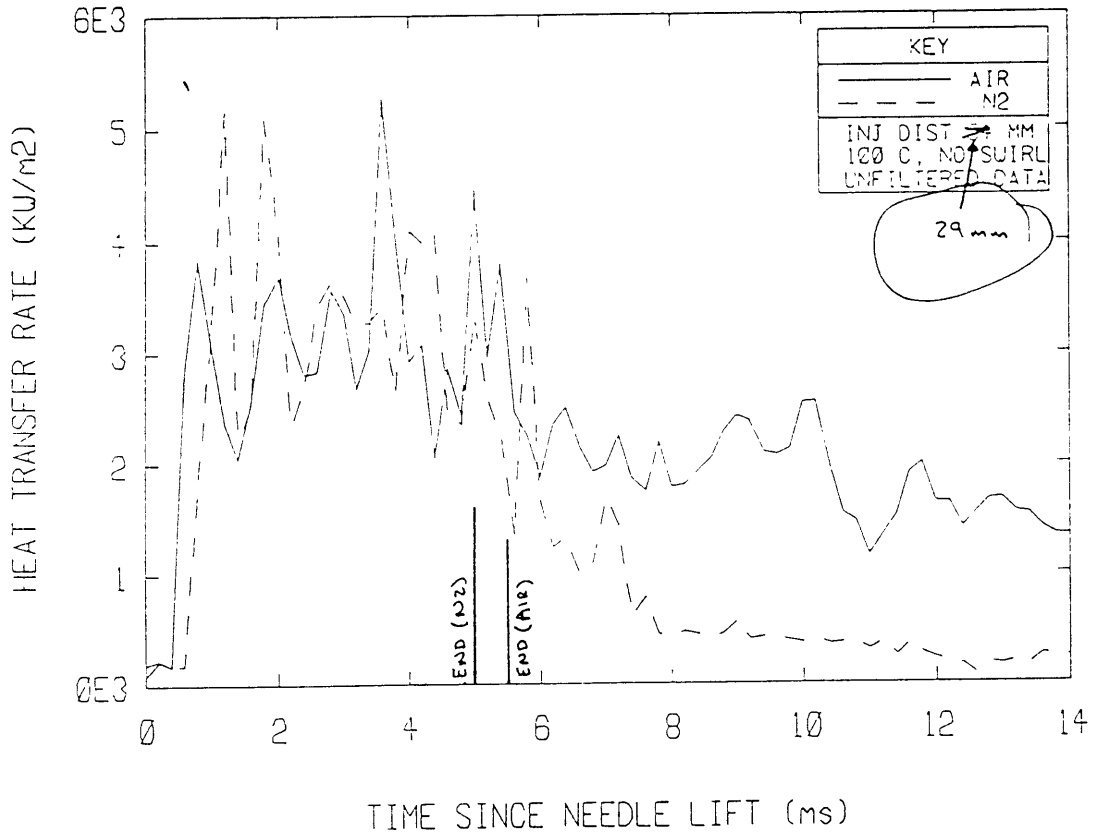


Figure 4.3. Impingement Point Heat Transfer in Air and Nitrogen
 (29 mm injection distance)

Next, the data suggests that the heat transfer rate with an infinite injection distance (e.g. without injection) would be approximately 260 kW/m^2 . We can verify this by examining the cylinder pressure lapse rate after compression but before injection. The cylinder pressure was observed to decay 174 kPa in 0.025 seconds. The leak rate was measured at 0.57% of this value, thus the pressure lapse rate was due almost entirely to gas cooling. The cylinder-average heat transfer rate corresponding to the measured pressure lapse rate was 278 kW/m^2 , which is consistent with the extrapolation of the impingement point heat flux data to an infinite injection distance.

4.4 REPEATABILITY

The experiment repeatability was assessed by running the RCM twice under identical conditions and comparing the resulting heat transfer rates. The heat transfer rates during the steady portion were determined for each thermocouple location, and were slightly different for each run. The difference between the two measurements (the "range") was plotted against the average of the two measurements (the "mean") for all fifteen sensors (figure 4.3). The average range was 14.6% of the corresponding mean, indicating a $\pm 7.3\%$ difference in the heat transfer between runs (analogous to a cycle-by-cycle variation for continuously operating engines). Ferguson, et. al.,^[21] claim an uncertainty of $\pm 9\%$ for this technique in diesel engines, thus the repeatability obtained here was considered acceptable.

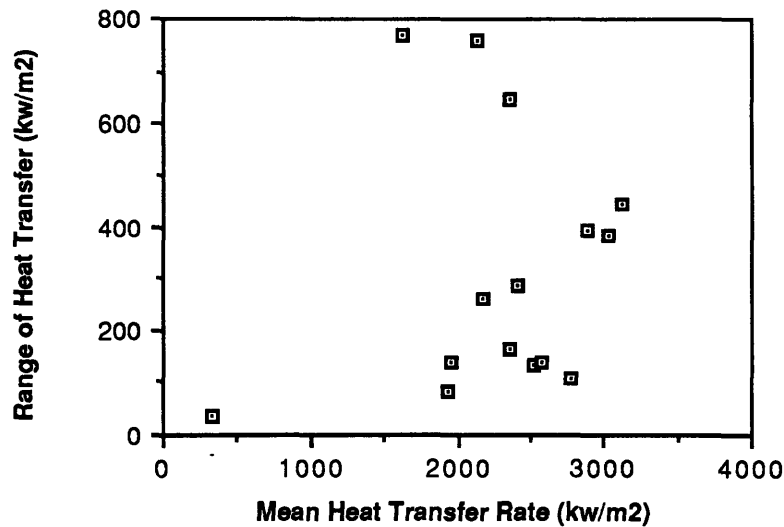


Figure 4.3. Experiment Repeatability

4.5 HEAT TRANSFER SURVEYS

Heat transfer rates were determined for all of the surface-mounted thermocouples. These are displayed in three separate, but similar, graphs for each experimental run. Each graph consists of multiple lines of heat transfer rate versus time since needle lift (time since start of injection). These heat transfer rates are extracted from first-order filtered temperatures. Figure 2.6 is reproduced here as figure 4.4 in order to show the location of the thermocouples.

The following sections show the experimental results for the baseline case only. The corresponding data for the remaining runs is included as Appendix A.

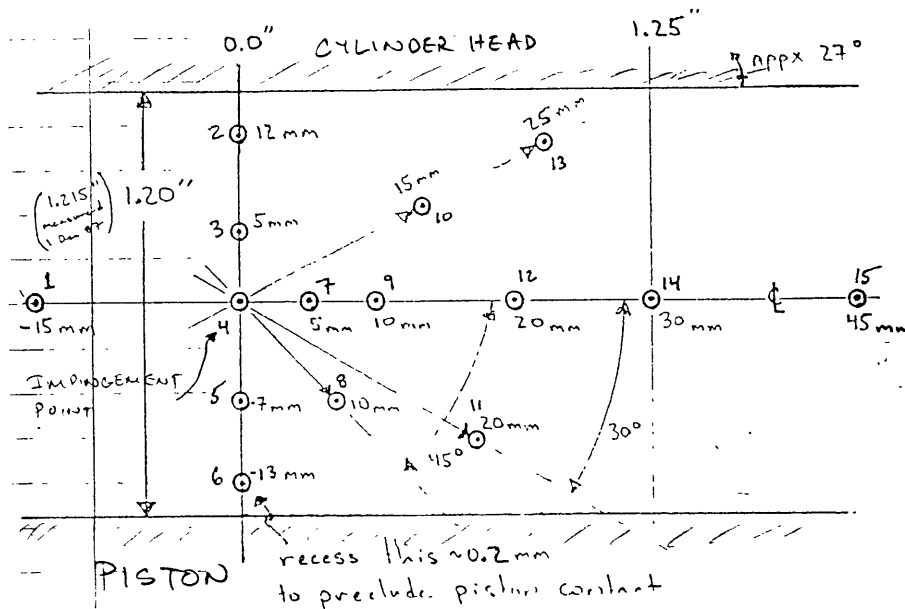


Figure 4.4. Thermocouple Locations

4.5.1 HORIZONTAL SURVEYS

The horizontal heat transfer survey for the baseline condition is presented in figure 4.5.

The six lines on this graph pertain to the thermocouples located midway between the piston face and the cylinder head on the "horizontal centerline". The distances referred to in the legend are distances from the jet impingement point along the horizontal centerline.

Referring to figure 4.3, these are thermocouples 4,7,9,12,14, and 15. These are located 0, 5, 10, 20, 30, and 45 mm from the impingement point, respectively. For the run with swirl, the air motion goes from the impingement point in the direction of increasing distance (e.g. thermocouples 7,9,12,14 and 15 are "downwind" of the impingement point).

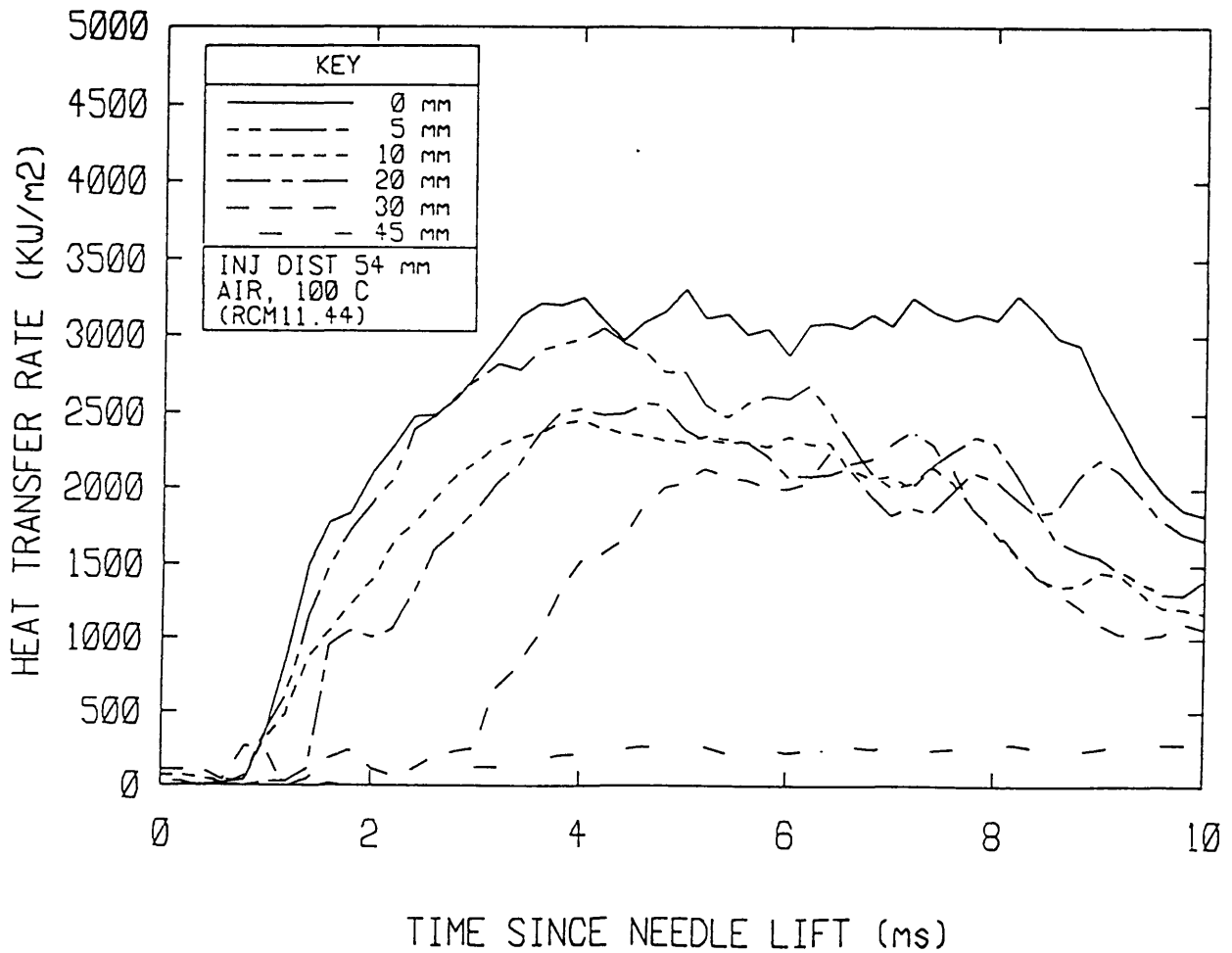


Figure 4.5. Horizontal Heat Transfer Survey

4.5.2 VERTICAL SURVEYS

The vertical heat transfer survey for the baseline condition is presented in figure 4.6. The five lines on this graph pertain to the thermocouples located on a line along the cylinder wall perpendicular to the piston face and intersecting the jet impingement point. The distances referred to in the legend are distances from the jet impingement point along this vertical line. Positive distances are closer to the cylinder head and negative distances are closer to the piston face. Referring to figure 4.3, these are thermocouples 2, 3, 4, 5, and 6. These are located 12, 5, 0, -7, and -13 mm from the impingement point, respectively.

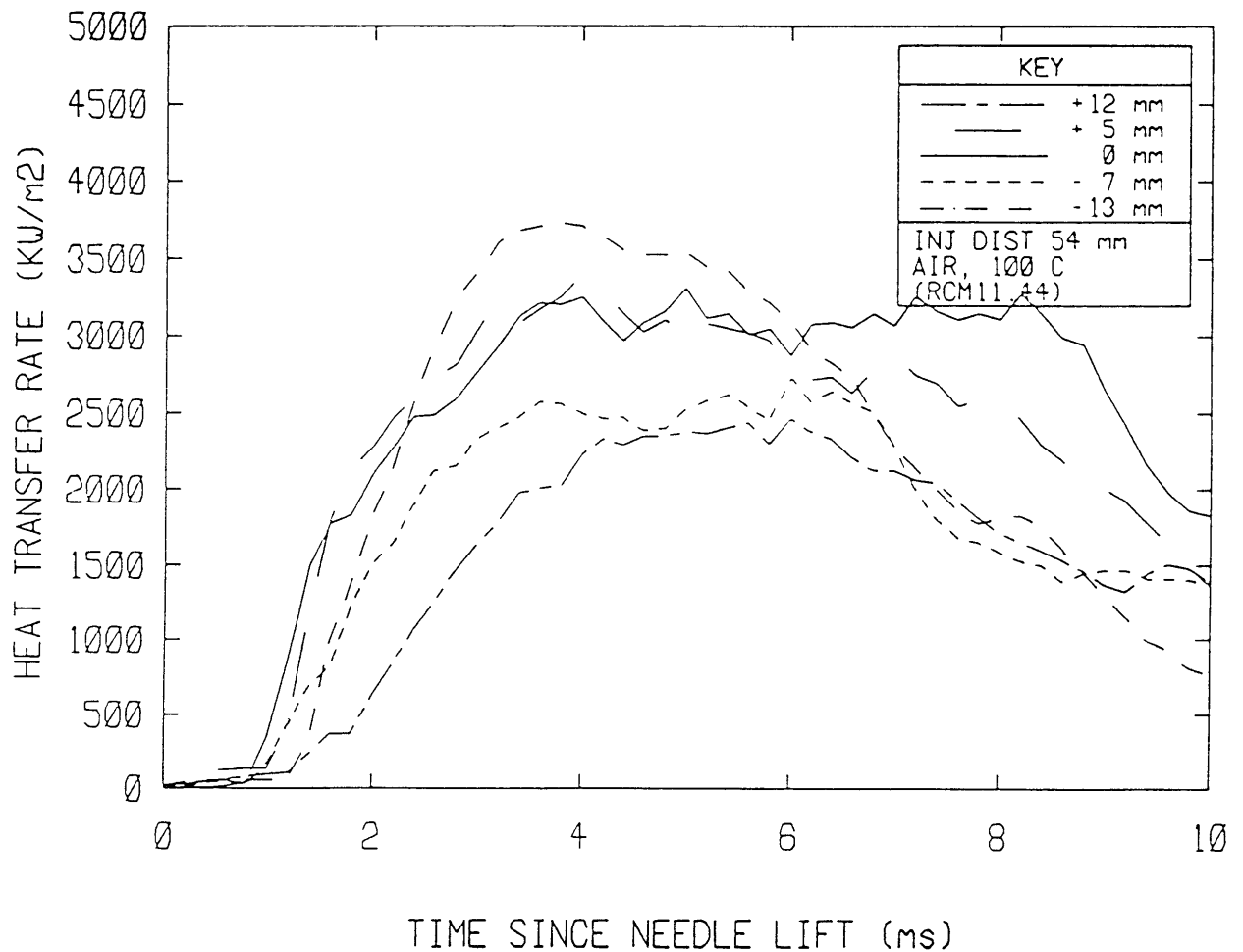


Figure 4.6. Vertical Heat Transfer Survey

4.5.3 MISCELLANEOUS SURVEYS

There were five thermocouples not included in the horizontal and vertical surveys. Referring to figure 4.4, these are thermocouples 1, 8, 10, 11, and 13. The heat transfer from these thermocouples are presented in figure 4.7. It turned out that for all runs without swirl, the heat transfer at thermocouple #1 was between those of thermocouples #9 and #12. This indicated that the heat transfer was symmetrical between the two sides.

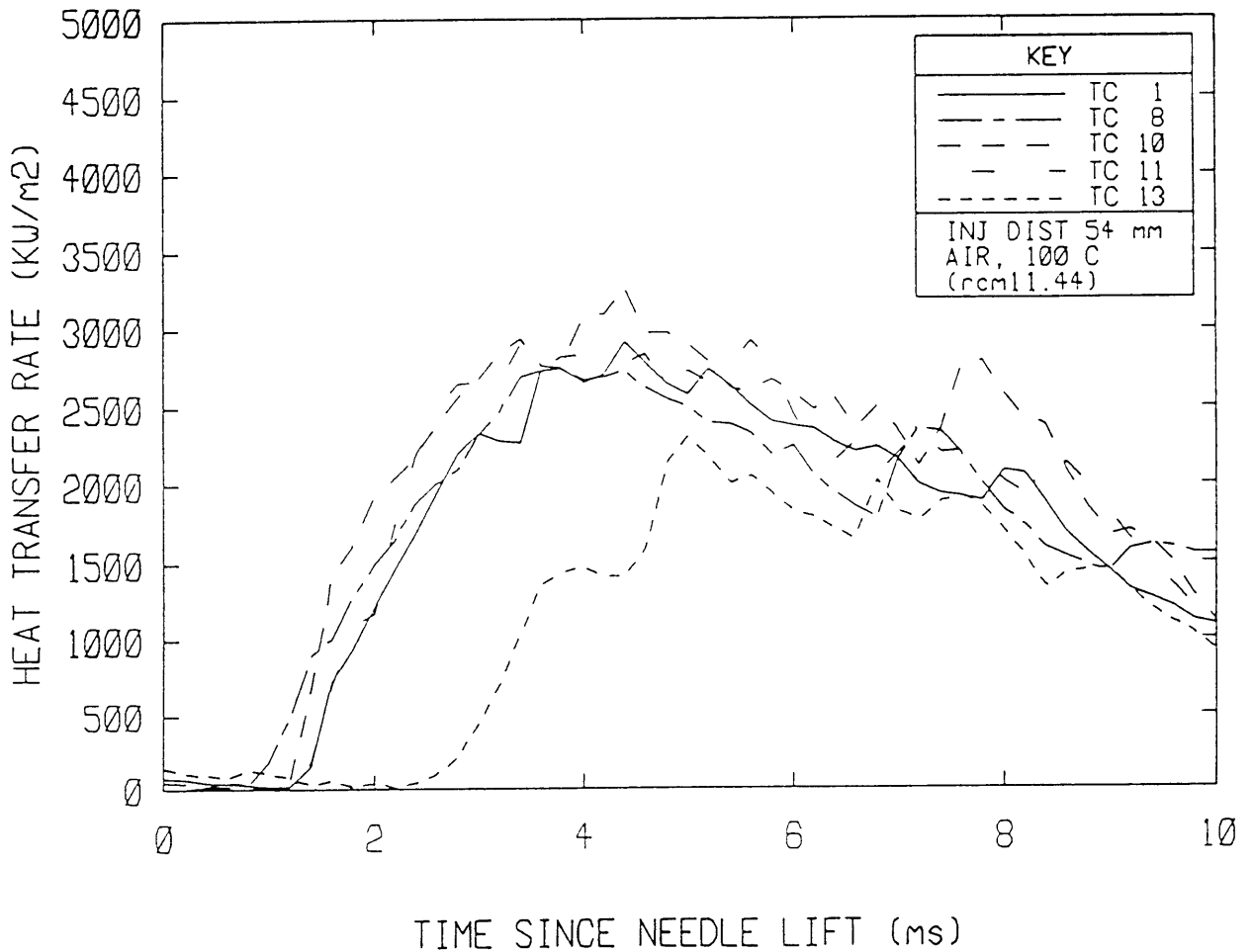


Figure 4.7 Heat Transfer Survey (Miscellaneous Thermocouples)

Chapter 5

Comparison to Steady Submerged Jet

5.1 MOTIVATION

There is little information in the literature about the heat transfer from transient two-phase heated jets to cooler walls. However, there is an abundance of information on the steady submerged jet, of which a small subset deals with the heat transfer therefrom. Modeling the fuel spray as a submerged jet is appealing since, if successful, the richer literature of the submerged jet^[22,23] could be brought to bear on the problem at hand.

We will start by considering the case of a non-burning fuel spray. We would like to relate the magnitude of the impingement point heat flux to some kinematic properties of the jet. We also want to develop a quantitative understanding of how the heat flux depends on distance from the impingement point. After accomplishing this, we want to determine whether the steady jet analogy can be extended to cover burning fuel sprays as well.

In this chapter we will accomplish the following:

- A) Identify a quasi-steady-state stage of the heat flux from transient fuel sprays. Determine the quasisteady heat flux for fuel sprays into air and nitrogen.
- B) Model the fuel spray as a gas jet in order to calculate a local air/fuel ratio, and use this air/fuel ratio to estimate the jet temperature as a function of distance from the nozzle tip.
- C) Show that the heat transfer coefficients for impingement point heat transfer are nearly identical both with and without combustion, and compare the heat transfer coefficients to correlations developed for air jets.
- D) Consider the circumferential variation of heat transfer with and without combustion.

5.2 QUASI-STEADY-STATE HEAT TRANSFER

The first step in the comparison of the transient spray to a steady jet was to see if a quasisteady period exists during the injection/combustion process, and to correlate the data in this period according to steady jet theory. In general, the heat transfer resulting from the fuel spray could be characterized as follows (fig. 5.1):

- A) a time delay during which the jet travels to the wall
- B) a period of nearly constant heat flux
- C) a period of decaying heat flux

Figure 5.1a shows the heat transfer at the impingement point for the baseline test conditions (54 mm injection distance, initial air temperature 100 C, no swirl), without filtering the temperature data. The three regimes described above can be clearly discerned. However, the heat transfer rate is hard to determine exactly due to the noise introduced by differencing the wall surface temperature. Figure 5.1b shows the heat transfer rate with a first-order filter applied to the temperature time-history as described in chapter 3. The filter introduced a non-negligible phase lag in the data. We are interested, however, in the magnitude of the quasi-steady heat flux only, so the performance of the filter is satisfactory in this regard.

As can be seen from figures 5.1a,b the heat flux remains very small until the jet impacts the wall. The heat flux then jumps very rapidly to an essentially constant level, where it remains during the entire injection period and somewhat beyond. The persistence of a high heat transfer rate even after the end of injection appears to result from continued burning of fuel in the post-injection mixing-controlled phase of combustion. When the fuel is totally consumed, the heat transfer rate then drops to a lower value.

For several reasons, the heat transfer rate during the post-burning phase is not directly applicable to real engines and will not be further studied. First, these experiments were done with a single fuel jet, rather than multiple jets as is common in engines. In order to have this single jet representative of one in an operating engine, the total amount of fuel injected is that corresponding to a single jet of a five-jet nozzle operating at 50% load. The chamber conditions at burnout are substantially different from those in a real engine due to the small amount of fuel injected, so we would not expect the heat transfer to be

DRAFT

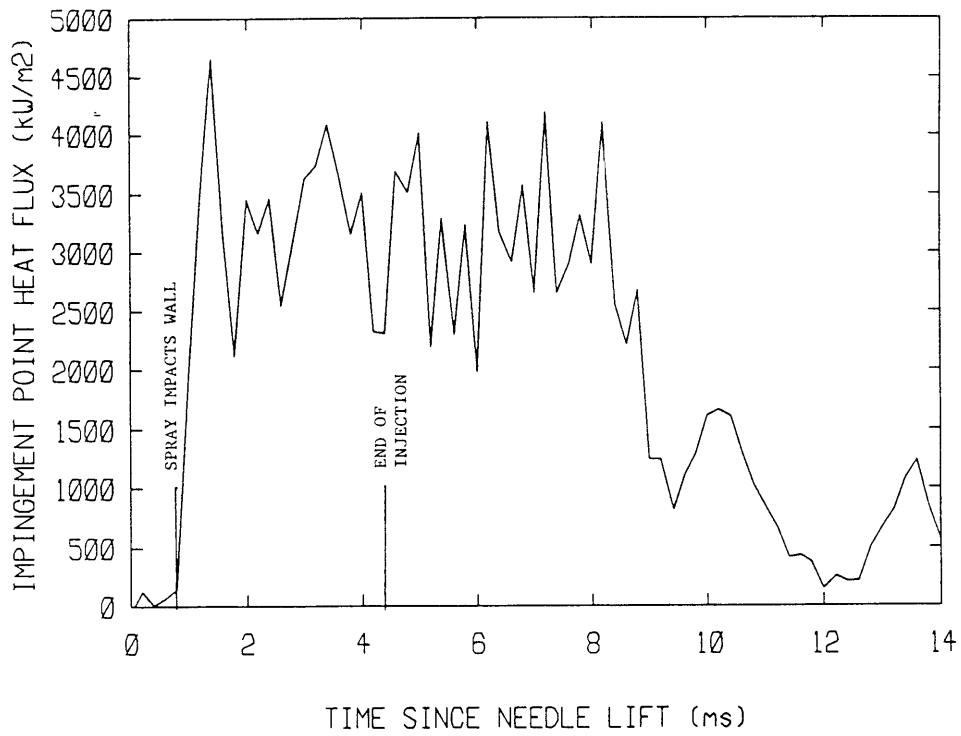


Fig. 5.1a Impingement Point Heat Transfer Time History
(Temperature data not filtered)

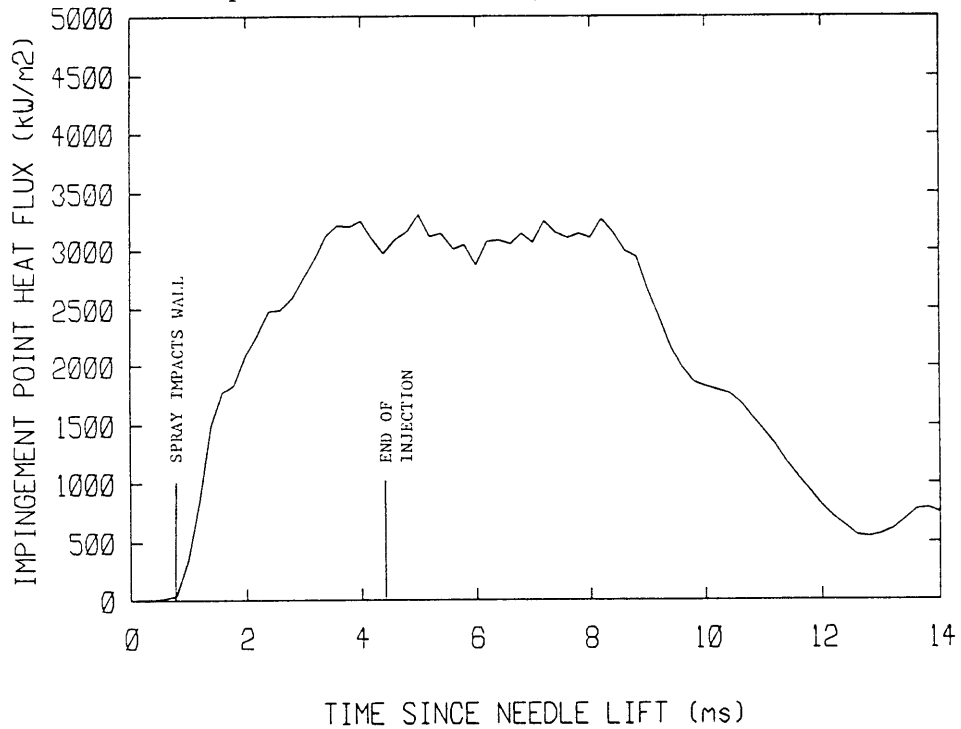


Fig. 5.1b Impingement Point Heat Transfer Time History
(Temperature data first-order filtered)

representative. Second, the combustion volume is fixed in the RCM, thus the expansion process which normally occurs at this part of the cycle was not simulated at all.

The heat flux during the near-constant period, known hereinafter as the "quasisteady heat flux", was determined for various sensor positions and served as the basis of the steady-state analog. Quasisteady heat transfer distributions were measured for fuel sprays into an inert gas (nitrogen) and also for fuel sprays into air.

5.3 DETERMINATION OF QUASISTEADY HEAT FLUX

The steady state period of heat flux was qualitatively determined by visual inspection of the heat flux traces. This served to identify an interval about 2 milliseconds in duration where the heat flux was most constant. This 2 ms interval was then quantitatively analyzed for the "flattest" point using a sliding window of 1 ms duration. The mean heat flux and standard deviation for each 1 ms interval was calculated, and the mean heat flux during the interval with the smallest (or nearly so) standard deviation was identified as the quasisteady heat flux. This process was repeated for each thermocouple location. Primary emphasis was placed on the thermocouples located along the horizontal (parallel to the piston face) centerline of the combustion chamber (# 1,4,7,9,12,14, and 15). These data are tabulated in Appendix A.

5.4 MODELING FUEL SPRAY AS SUBMERGED JET

In order to apply the theory of submerged gas jets to the fuel spray problem, we must first correct for the differences between the liquid spray and gas jets. The gas jet literature is primarily concerned with jets whose density and temperature matches that of the surrounding fluid. For those conditions, jet velocity distributions have been postulated and verified by experiment.^[11,12,14,24] These velocity distributions are key in prediction of heat transfer rates. In this case, however, we have a fuel spray whose density is much greater than the air into which it is sprayed. Second, the fuel is significantly cooler than the surrounding fluid. We must correct for these differences before we can apply the gas jet results to the problem at hand.

5.4.1 EQUIVALENT NOZZLE DIAMETER

The general relationships which have been developed for single, round, isodensity jets can be extended to non-isodensity jets by using the concept of an equivalent nozzle diameter.^[14] This concept is based on the assumption that the development of the jet is determined by the jet momentum flux. In a non-constant density system, the jet of density ρ_j entrains fluid of ambient density ρ_s and, because of the high rate of entrainment, the density of fluid within the jet approaches the density of the surrounding fluid within a short distance from the nozzle exit (say, 10 nozzle diameters).^[12] Therefore, the jet may be modeled as an isodensity jet with the same momentum and initial velocity, but with the density of the entrained fluid rather than the nozzle fluid. (This fast-mixing assumption is not totally valid for the present case because the homogenizing process is not limited by the entrainment process, but rather is limited by the evaporation of the droplets. Nevertheless, the isodensity jet approximation is a practical one.) The modelling is accomplished by replacing the actual nozzle diameter D with an equivalent nozzle diameter D_e per the following: ^[12]

$$D_e = D \left(\frac{\rho_j}{\rho_s} \right)^{1/2} = 0.254 \text{ mm} \left(\frac{848 \text{ kg/m}^3}{14.25 \text{ kg/m}^3} \right)^{1/2} = 1.96 \text{ mm} \quad (5-1)$$

5.4.2 DETERMINATION OF NOZZLE EXIT VELOCITY

The average nozzle exit velocity V_0 must be determined in order to find the initial jet momentum. This was accomplished by solving the continuity equation

$$V_0 = \frac{\text{fuel mass injected}}{T_{inj} \rho A} \quad (5-2)$$

where T_{inj} = injection duration and A = actual nozzle exit area. This was evaluated using the mean fuel mass (29.3 mg) and mean injection duration (4.88 ms) for 10 runs. The resulting nozzle exit velocity was 139.7 m/s.

5.4.3 ENTRAINED MASS

In order to calculate the local air/fuel ratio (which is necessary to estimate the local jet temperature), we need to know something about the entrainment of ambient fluid by the fuel jet. The mass flow rate M at any cross-section of the jet may be related to the fluid velocity u in the axial direction, the fluid density ρ , and the radial distance y by

$$M = \int_0^{\infty} 2 \pi \bar{\rho} \bar{u} y dy \quad (5-3)$$

where the over bar represents a time-averaged quantity. M may be calculated if axial velocity and density profiles are assumed, however, Ricou and Spalding^[25] have measured the mass flow rate and correlated it by the formula

$$\frac{M}{M_0} = 0.32 \left(\frac{\rho_1}{\rho_0} \right)^{1/2} \frac{x}{D} \quad (5-4)$$

where ρ_0 = initial jet density and ρ_1 = density of the surrounding fluid. Since the air mass flow rate $\dot{m}_a = M - M_0$, then the air/fuel ratio may be written as

$$\frac{\dot{m}_a}{\dot{m}_f} = \frac{M - M_0}{M_0} = \frac{M}{M_0} - 1 \quad (5-5)$$

Substituting (5-4) into (5-5) we obtain a relationship for the mean air/fuel ratio at a given jet cross-section

$$\frac{\dot{m}_a}{\dot{m}_f} = 0.32 \left(\frac{\rho_a}{\rho_f} \right)^{1/2} \frac{x}{D} - 1 \quad (5-6)$$

5.4.4 ESTIMATION OF JET TEMPERATURE

The temperature difference between the gas and the wall must be known to convert heat transfer rates to heat transfer coefficients. The wall temperatures were measured, but the gas temperatures were not. Therefore, the local gas temperatures were calculated. An accurate prediction of local gas temperature is difficult and requires more knowledge about

the detailed mixing and flame structure than is currently available, however, an approximate one-dimensional gas temperature model was developed in order to get a rough idea of the local temperature at the impingement point. This allowed a comparison of heat transfer coefficients in order to determine whether differences in heat transfer rates (between burning and non-burning jets) could be attributed primarily to temperature differences, or whether some more subtle fluid-dynamic effect was at work.

In order to make the calculations tractable, the following assumptions were made:

- A) Radial variations of air/fuel concentration are ignored, thus a mean air/fuel ratio at each axial distance was determined.
- B) In the absence of combustion, the mean jet temperature at a given distance from the nozzle tip equaled the thermodynamic equilibrium temperature between the fuel and the entrained gas.
- C) In the presence of combustion, the mean jet temperature at a given distance from the nozzle tip equaled the adiabatic flame temperature appropriate for the local equivalence ratio.

Knowing the air/fuel ratio, the results of Kamimoto and Matsuoka^[26] were used to determine the thermodynamic equilibrium temperature (the mean precombustion temperature) of the jet at any given distance. Mansouri^[27] provided the thermochemical properties of unburned diesel fuel vapor as a function of temperature. Then, the NASA chemical equilibrium code^[28] was used to determine the flame temperature. This procedure was accomplished for the actual injection distances used (Table 5.1).

<u>Injection Distance (mm)</u>	<u>Ma/Mf</u>	<u>Fuel/Air Equivalence Ratio</u>	<u>Equilibrium Temperature (K)</u>	<u>Fuel Vapor Enthalpy (cal/g-mol)</u>	<u>Flame Temperature (K)</u>
29	3.74	3.83	665	-14163	1376*
54	7.82	1.83	780	-1909	2161
68	10.11	1.42	810	1467	2476
79	11.90	1.20	830	3761	2637
105	16.15	0.89	855	6668	2603

*This temperature is unlikely due to the extreme fuel-rich equivalence ratio. The equilibrium temperature (665 K) should be used for this case.

Table 5.1. Mean Jet Temperatures at Various Injection Distances

5.5 IMPINGEMENT POINT HEAT TRANSFER

The quasisteady impingement point heat transfer rates were determined as explained above and plotted as a function of injection distance (fig. 5.3). Note that the heat transfer rate for the 29 mm injection distance is identical for both air and nitrogen. This suggests that the spray is not burning at the impingement point, probably because the local equivalence ratio is too rich to support combustion. Next, the data suggests that the heat transfer rate with an infinite injection distance (e.g. without injection) would be approximately 260 kW/m^2 . We can verify this by examining the cylinder pressure lapse rate after compression but before injection. The cylinder pressure was observed to decay 174 kPa in 0.025 seconds. The leak rate was measured at 0.57% of this value, thus the pressure lapse rate was due almost entirely to gas cooling. The cylinder-average heat transfer rate corresponding to the measured pressure lapse rate was 278 kW/m^2 , which is consistent with the extrapolation of the impingement point heat flux data to an infinite injection distance.

At first glance, there are striking differences between the results with combustion and those without combustion. When we examine the heat transfer coefficients, however, a different picture emerges.

The impingement point heat transfer coefficient h , defined by

$$\frac{Q}{A} = h (T_{\text{gas}} - T_{\text{wall}}) \quad (5-7)$$

was calculated using the gas temperatures from table 5.1 and, for the wall temperatures, the average of the wall temperature at injection and the peak wall temperature measured during the run (table 5.2). The resulting Nusselt number ($\text{Nu} = hD/k$) was evaluated using the equivalent exit diameter, and the thermal conductivity corresponding at the average of the gas temperature and the wall temperature.

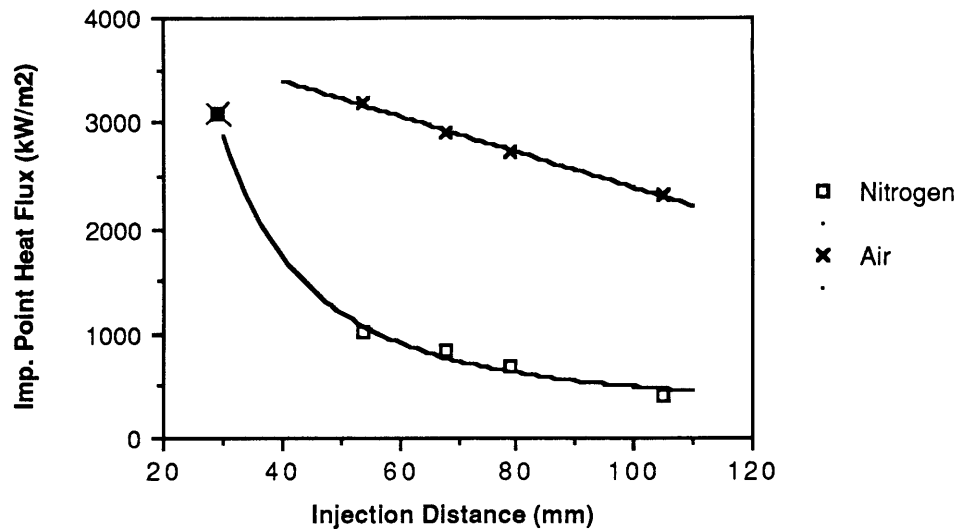


Fig. 5.3. Impingement Point Heat Transfer vs. Injection Distance (Air, Nitrogen)
 (Formula for line through nitrogen data is $y = 2.368E6 x^{-2} + 259$,
 Formula for line through air data is $y = -16.67 x + 4059$)

Injection Distance (mm)	Gas	Wall Temp (C)	Wall Temp (K)	Gas Temp (K)	Thermal Cond. (W/m-K)	ΔT (K)	Q/A (kW/m ²)	Heat Transfer Coefficient (kW/m ² -K)	Nusselt No.
29	N ₂	90	363	665	0.0395	302	3072	10.17	504.6
54	N ₂	81	354	780	0.0423	426	1031	2.420	112.1
68	N ₂	77	350	810	0.0430	460	851	1.850	84.3
79	N ₂	74	347	830	0.0435	483	678	1.404	63.3
105	N ₂	70	343	855	0.0440	512	396	0.773	34.4
29	Air	91	364	665	0.0404	301	3080	10.23	496.3
54	Air	95	368	2161	0.0784	1793	3185	1.776	44.4
68	Air	90	363	2476	0.0842	2113	2902	1.373	32.0
79	Air	86	359	2637	0.0869	2278	2721	1.194	26.9
105	Air	96	369	2603	0.0865	2234	2324	1.040	23.6

Table 5.2. Impingement Point Heat Transfer Coefficients

The impingement point heat transfer coefficients were compared to the results of Gardon and Cobonpue^[11] for impinging air jets (figure 5.4). Gardon and Cobonpue determined that for turbulent jets ($Re_e > 14,000$) in the region of fully developed flow ($S/D > 20$), the impingement point heat transfer coefficients could be correlated by

$$Nu = \frac{hD}{k} = 13 \sqrt{Re_e} \left(\frac{D}{S} \right) \quad (5-8)$$

where Re_e is the Reynolds number based on the nozzle exit diameter and the jet conditions at the nozzle exit.

It was not clear how to evaluate the jet Reynolds number in this experiment. The actual jet Reynolds number, using the actual nozzle exit velocity (139.7 m/s), the actual exit diameter (0.254 mm), and the kinematic viscosity of the liquid fuel ($1.35 \times 10^{-6} \text{ m}^2/\text{s}$) was 26280. However, we can calculate a Reynolds number for the equivalent gas jet as well. This was accomplished by using the mean cylinder density (14.25 kg/m^3), the nozzle exit velocity (139.7 m/s), the equivalent exit diameter D_e (1.96 mm), and the viscosity for air at the 950 K pre-injection temperature ($4.00 \times 10^{-5} \text{ kg/m-s}$).^[29] This yielded an equivalent jet Reynolds number of 97350.

The Gardon & Cobonpue correlation was calculated for both Reynolds numbers and compared to measured data. Using the actual jet Reynolds number, the Nusselt numbers were plotted against S/D (figure 5.4). Using the Reynolds number for the equivalent jet, the Nusselt numbers were plotted against S/D_e (figure 5.5). The Kamimoto results^[8] are plotted as well. In the Kamimoto experiment the jet Reynolds numbers (actual = 36700, equivalent = 97030) were close to those used in the current study (actual = 26280, equivalent = 97350).

The Nusselt numbers are different from those given by the Gardon & Cobonpue correlation. The correlation using the actual jet Reynolds number substantially underpredicts the impingement point Nusselt number, yet the correlation using the equivalent jet Reynolds number substantially overpredicts the Nusselt numbers. Further, the Nusselt number has a $1/S^2$ dependence for the cases without combustion and a $1/S$ dependence with combustion. The Gardon & Cobonpue correlation has a $1/S$ dependence.

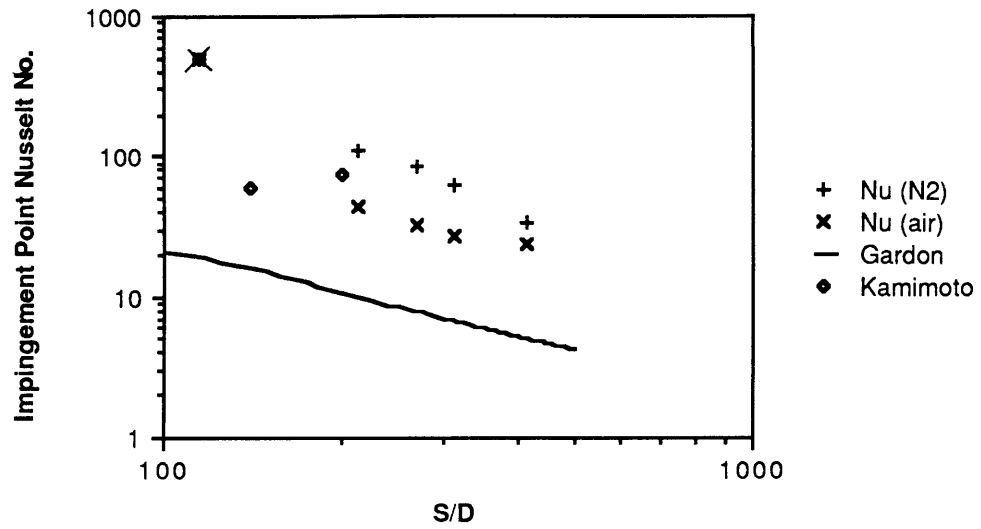


Fig. 5.4. Impingement Point Nusselt Numbers (Actual Jet Properties)

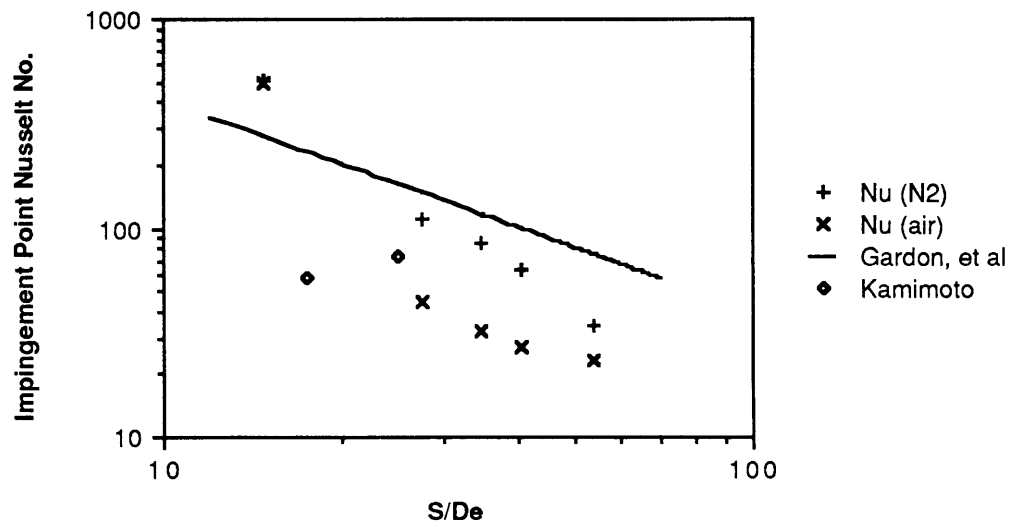


Fig. 5.5. Impingement Point Nusselt Numbers (Equivalent Jet Properties)

5.6 CIRCUMFERENTIAL VARIATION OF HEAT TRANSFER

Considering the circumferential variation of heat transfer rate, the quasisteady heat flux Q for each location was normalized by the heat flux at the impingement point Q_0 , and the distance from the impingement point X was nondimensionalized by the injector standoff distance S . Gardon and Cobonpue did this for an impinging jet of air for nozzle-to-plate distances greater than 10 nozzle diameters, and discovered that the normalized local heat transfer coefficients depend primarily on the dimensionless parameter X/S and only to a lesser extent on jet Reynolds number and S/D .^[7] They provided a range of values for the local heat transfer coefficients as a function of X/S (referred to in their paper as X/Z_n). Their findings are reproduced as figure 5.5.

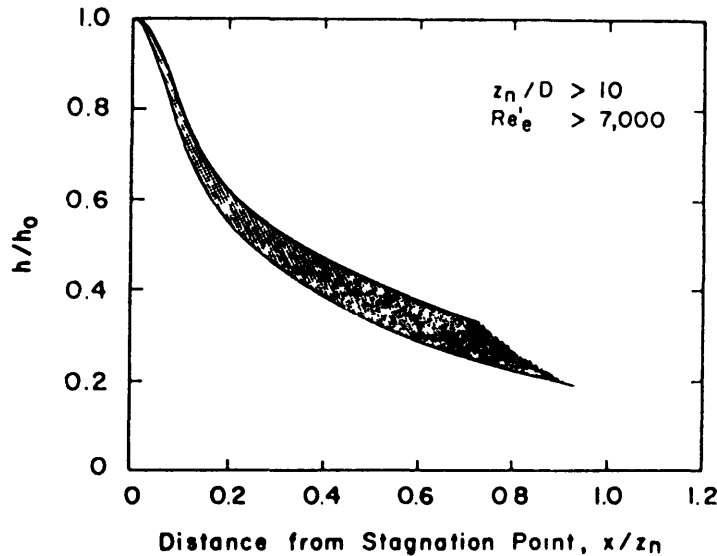


Fig. 5.5. Radial Variation of Normalized Heat Transfer Coefficients
Between a Plate and an Impinging Jet of Air (Gardon & Cobonpue)^[7]

The heat transfer data from the current investigation were normalized as described above and compared to the results of Gardon and Cobonpue. This was accomplished for fuel sprays into nitrogen (fig. 5.6) and fuel sprays into air (fig. 5.7). Reasonable agreement was obtained for fuel sprays into nitrogen, suggesting that non-burning fuel sprays can be modeled as submerged jets for heat transfer purposes. Local heat transfer coefficients were underpredicted for burning sprays, however. This is not surprising, as this analysis

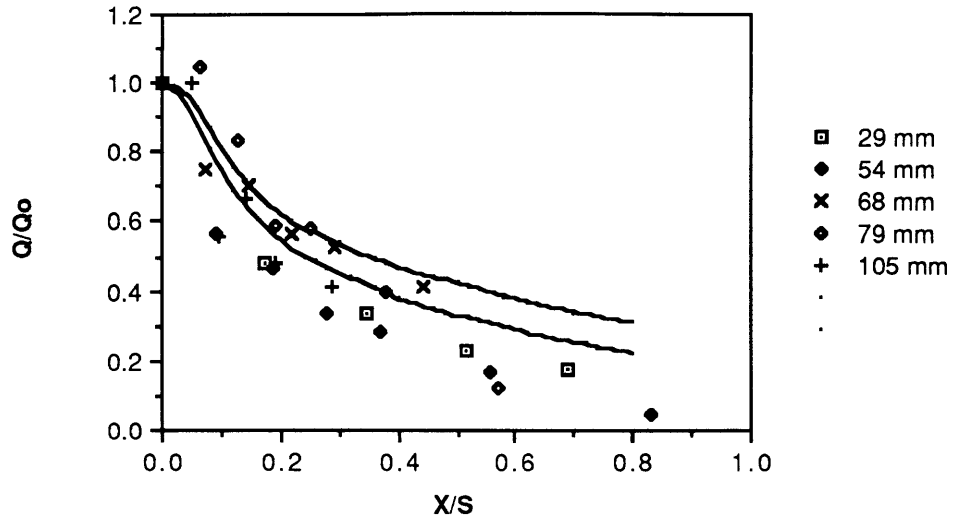


Fig. 5.6. Quasisteady Heat Flux Distribution for Fuel Spray into Nitrogen

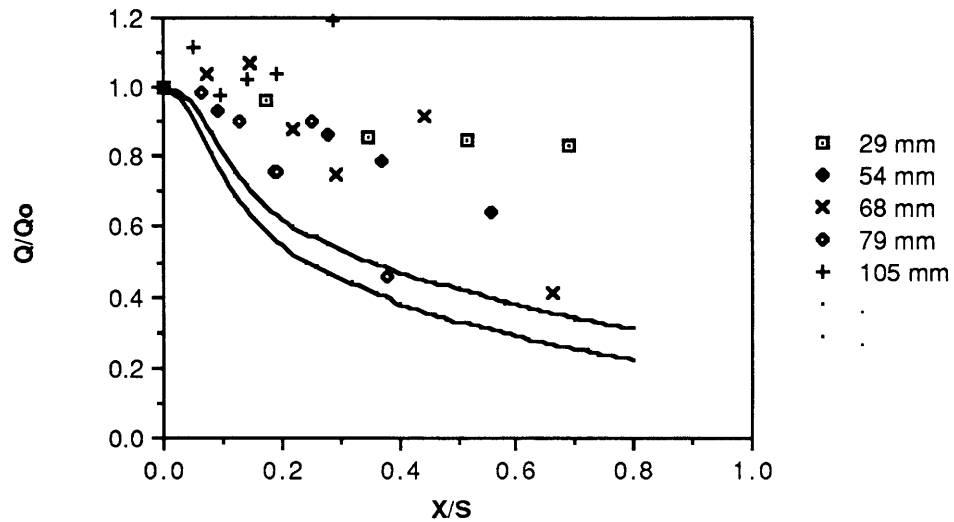


Fig. 5.7. Quasisteady Heat Flux Distribution for Fuel Spray into Air

assumes that local gas temperatures change only moderately. However, when additional air is entrained into the burning jet it allows the release of large amounts of energy via combustion, thus drastically altering the local temperature. It is possible that the burning jet results might be brought into agreement with the non-burning results via the incorporation of an estimate of the local gas temperature.

This possibility was examined by considering the data for a 54 mm injection distance. The heat transfer coefficient was assumed to decay with X/S as per Gardon and Cobonpue. The local gas temperature was increased until the measured heat transfer rates were reproduced. The gas temperature profile which results (figure 5.8) is that which must exist for the coefficient decay to behave as Gardon and Cobonpue determined while yielding the heat transfer rates which were observed in this experiment. As can be seen, the required temperatures are not plausible. Therefore, the heat transfer coefficients are not varying as do those for gas jets.

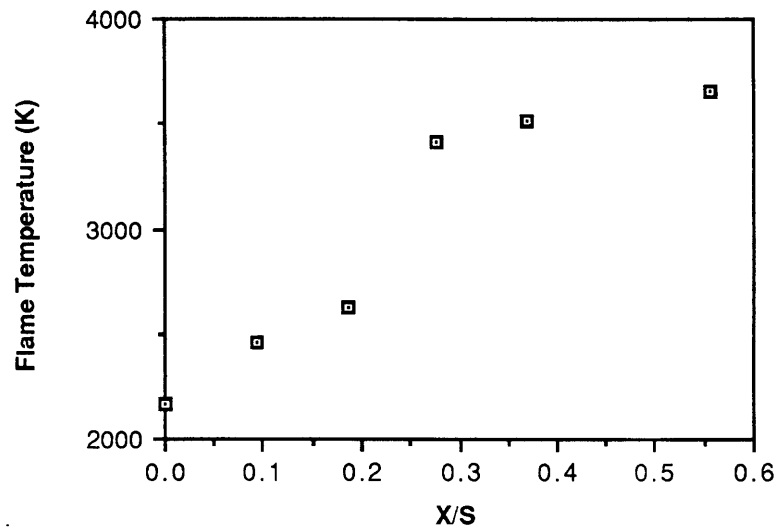


Figure 5.8. Flame Temperatures Required for Heat Transfer Coefficients to vary as do those in Gas Jets (54 mm injection distance)

Chapter 6

Effect of Swirl

6.1 MOTIVATION

Swirl is used in diesel engines to promote more rapid mixing between the inducted air charge and the injected fuel. Intake-generated swirl usually persists through the compression, combustion, and expansion processes.^[30] It is therefore necessary to consider the effect of swirl on the fuel spray, as significant changes in the flow patterns can result from this initial air motion. The success of the previous chapter at modeling the fuel spray as a gas jet into quiescent air suggests that similar success may be enjoyed for the swirling case as well.

6.2 TEST CONDITIONS

The RCM inlet air valve was oriented to direct air at 90 degrees to the cylinder axis (tangentially). The air velocity was increased to the highest level at which the air heaters could maintain an average cylinder air temperature of 100 C. Otherwise, the RCM was operated identically to the other data runs.

The amount of swirl present during injection was determined by tracking visible particles in the films, rather than a less direct measurement such as the tangential air velocity during the pre-firing sequence. This method was chosen since the angular momentum imparted to the air during induction decays through the compression process due to friction at the walls and turbulent dissipation within the fluid. Typically one-quarter to one-third of the initial angular momentum about the cylinder axis will be lost by the end of compression.^[30] There were several bright particles in the combustion chamber after compression but before injection. These were assumed to be either trace impurities in the supply air (probably compressor oil), or minute quantities of soot from around the piston/shaft attachment screws, which autoignited during the post-compression period. These particles were not numerous enough to give concern, and were in fact quite helpful in assessing initial charge motion. Most of these particles were located near the periphery of the combustion

chamber. However, a few were located sufficiently far from the edge so as not to be in the boundary layer. The rotation rate of the cylinder air at the time of injection was 2540 rpm. This was determined by tracking a bright particle through an angle of 50.7 degrees, which took 20 frames (3.33 ms) to accomplish.

6.3 RESULTS

The fuel spray and flame boundaries were deflected noticeably from those without swirl (fig 6.1a,b). The impingement point appeared to be deflected approximately 7 mm downstream of the jet aim point. The flame did not propagate upstream as far as downstream. In fact, the edge of the flame propagated upstream 14.6 degrees (13 mm) in 2.8 milliseconds and remained stationary until the fuel spray was terminated, at which point the flame was swept downstream. The edge of the flame propagated downstream somewhat faster than without swirl.

Quasisteady heat transfer rates were determined as previously (table 6.1). The heat transfer rates were compared to those without swirl (fig. 6.2). The heat transfer rate with swirl was somewhat higher than without swirl, however, the heat release rates were comparable (fig. 6.3).

<u>X</u> <u>(mm)</u>	<u>Heat Flux</u> <u>(no swirl)</u> <u>(kW/m²)</u>	<u>Heat Flux</u> <u>(with swirl)</u> <u>(kW/m²)</u>
-15	2761	299
0	3185	2601
5	2972	3522
10	2409	2892
20	2517	2488
30	2045	2026
45	254	1453

Table 6.1. Quasisteady Heat Transfer Rates

11.44.

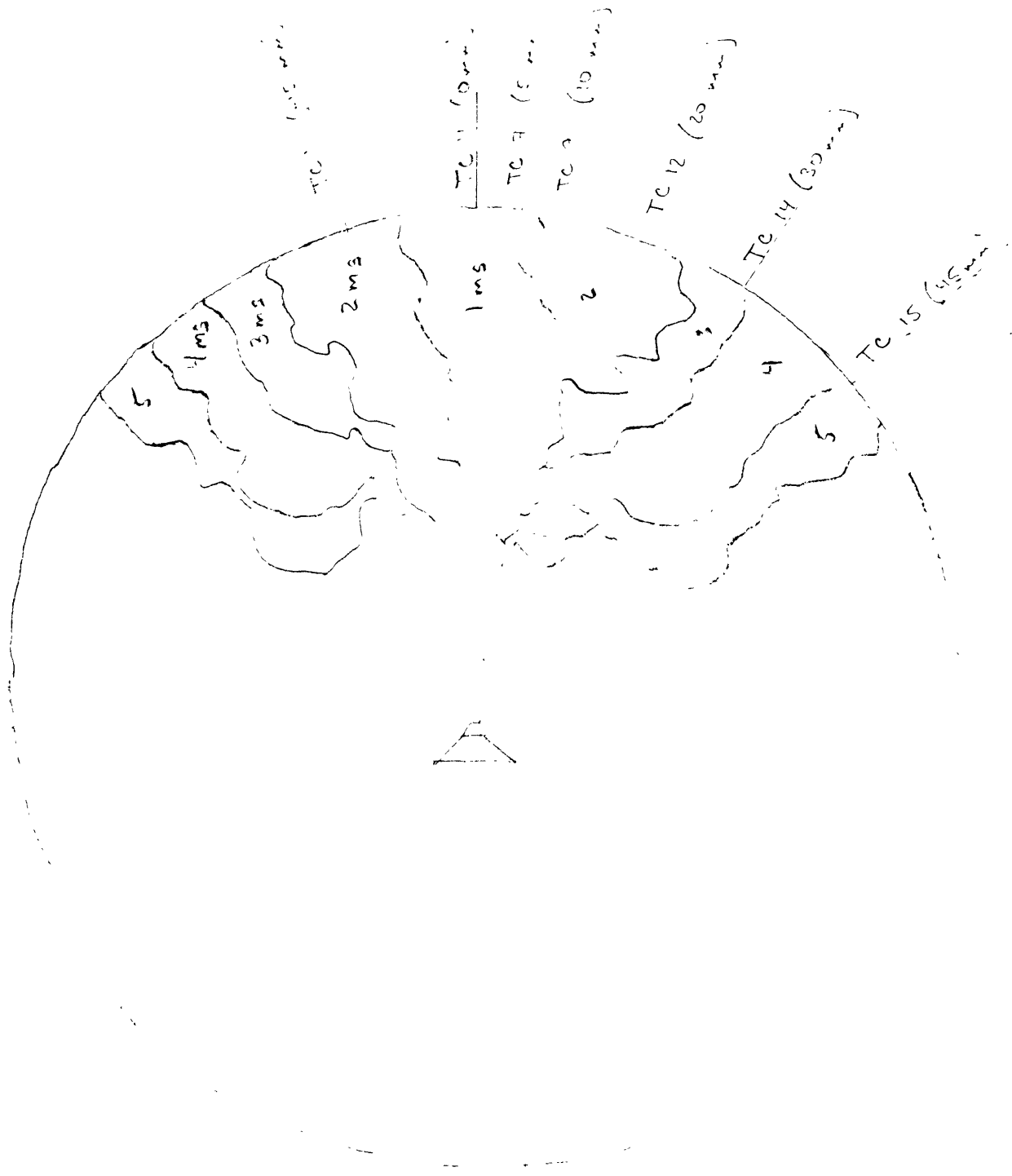


Fig 6. a Flame contours at different times (100 mm)

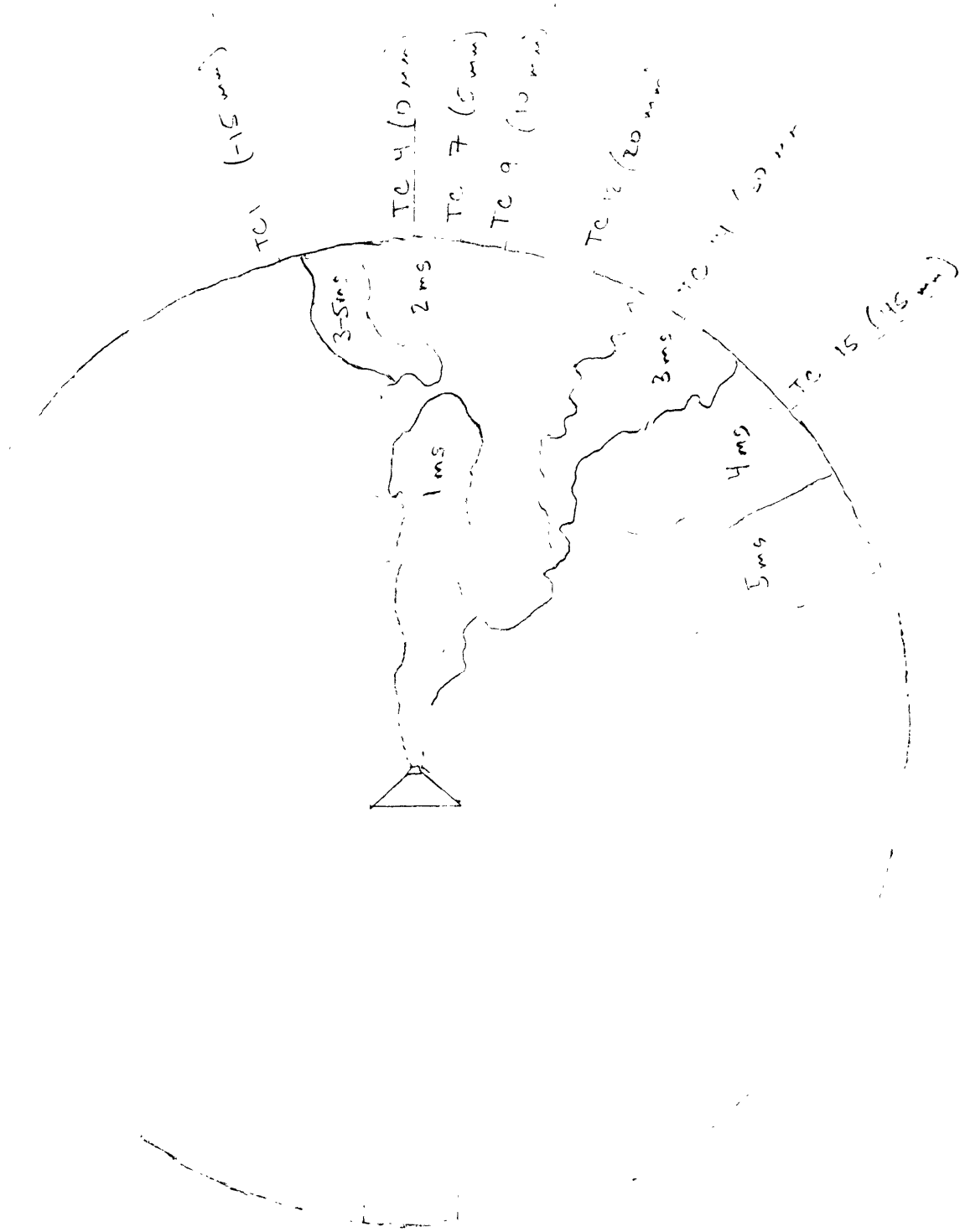


Fig. 6.1b Flame Temperature of ...
(2540 rpm ...)

The thermocouple located 5 mm downstream of the aim point was the sensor located closest to the impingement point, and in fact this thermocouple registered the highest heat transfer rate. The heat flux was severely attenuated in the upstream direction because of the absence of the flame and was enhanced in the downstream direction, relative to the heat transfer rates without swirl.

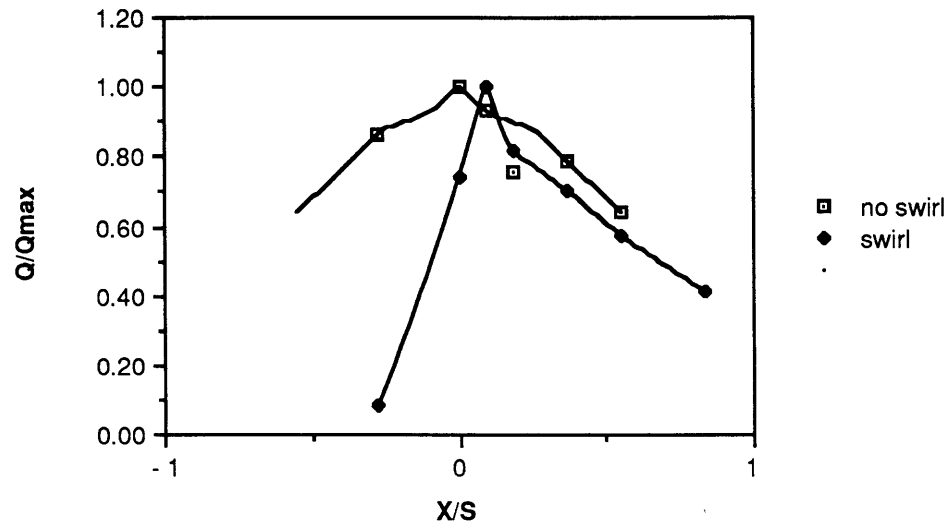


Fig. 6.2. Effect of Swirl on Circumferential Heat Transfer Distribution

EFFECT OF SWIRL

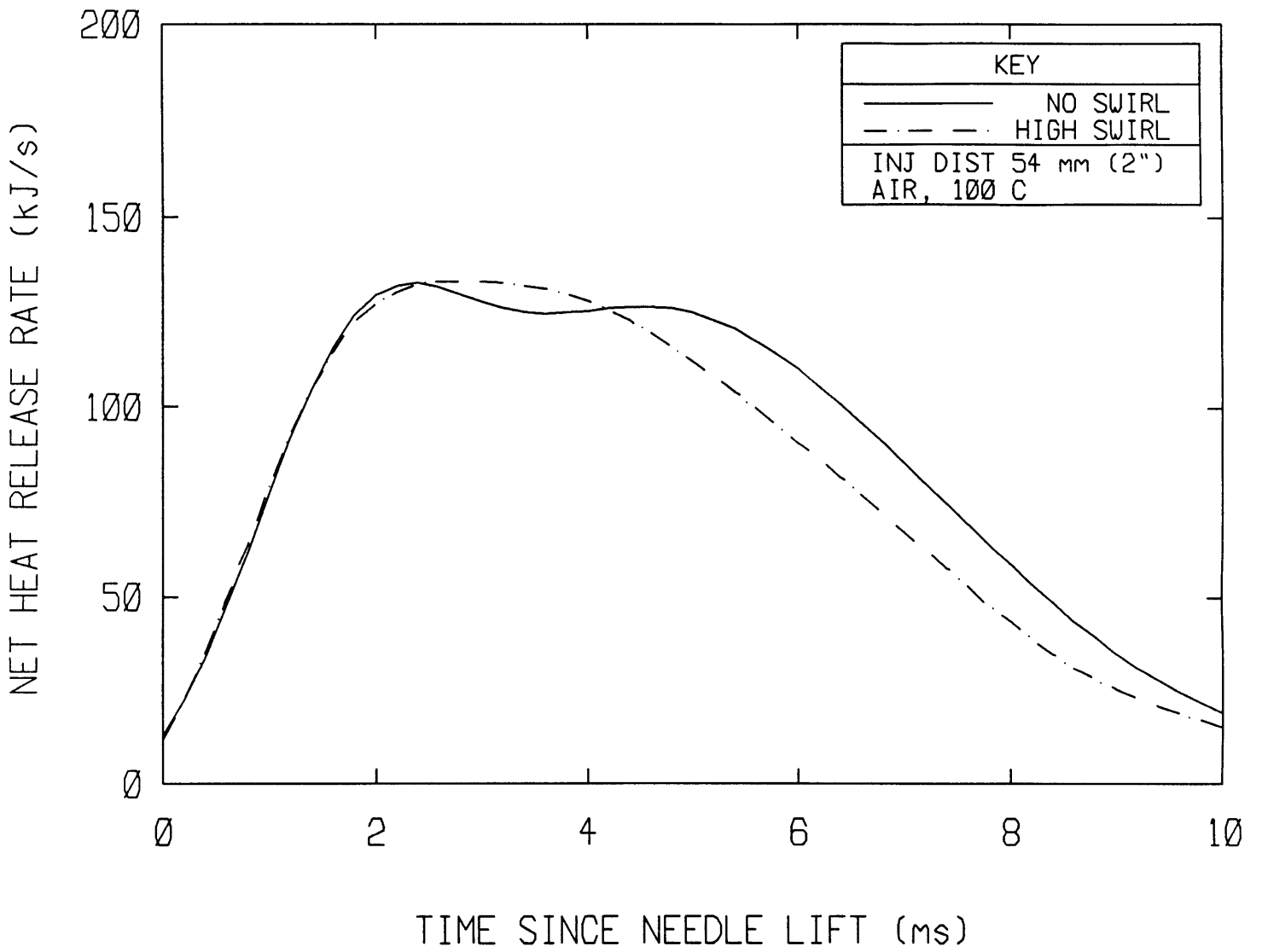


Fig. 6.3. Heat Release Rates with and without Swirl

Chapter 7

Effect of Charge Temperature

7.1 MOTIVATION

Diesel engines operate over a wide range of temperature conditions. The inlet air will be relatively cold when the engine is first started, and will gradually warm up to the vicinity of 100 C when the engine is in steady-state operation. Colella, et.al.^[15] studied the influence of charge temperature on the combustion event itself. They discovered striking variations in the instantaneous net heat release rates. Their conclusions were that decreasing the charge temperature lengthened the ignition time delay, which in turn allowed more fuel to be vaporized prior to the start of combustion. Since more fuel was burned in the characteristic premixed combustion phase, the rate of heat release was increased. Further, since less fuel remained to be burned during the mixing-controlled combustion phase, the total length of the combustion period was reduced. The effect was so strong that decreasing the inlet air temperature from 102 C to 27 C caused the peak net heat release rate to increase from 1500 kw to 5000 kw. The effect on heat transfer was investigated in the current research by varying the initial charge temperature from 30 C to 100 C in three increments.

The varying ignition time delay has a more subtle consequence, however. A longer ignition time delay allows more fuel to be vaporized prior to the start of combustion. This causes more of the fuel to be burned in the characteristic premixed combustion phase rather than the mixing-controlled combustion phase. We can therefore compare heat transfer rates in the two combustion phases by varying the initial charge temperature.

7.2 TEST CONDITIONS

Three RCM runs were accomplished with initial air temperatures of 30, 65, and 100 C. The injector standoff distance was 54 mm. The inlet valve shroud was oriented so as to direct air axially down the cylinder (no swirl). Pertinent test parameters are summarized in Table 7.1.

run	<u>11.57</u>	<u>11.59</u>	<u>11.44</u>
Initial Air Temp (C)	30	65	99.5
Avg Wall Temp (C)	30	61.5	74.5
Air Temp at Injection (K)	819	855	943
Ignition Delay (ms)	2.4	1.8	1.2

Table 7.1 Test Conditions for Temperature Survey

7.3 RESULTS

7.3.1 NET HEAT RELEASE RATES

Net heat release rates were extracted from cylinder pressure data using the method outlined in reference 16. The lower charge temperatures had higher peak heat release rates, which occurred later. This was due to the longer ignition time delays exhibited. The net heat release rates are presented in figure 7.1.

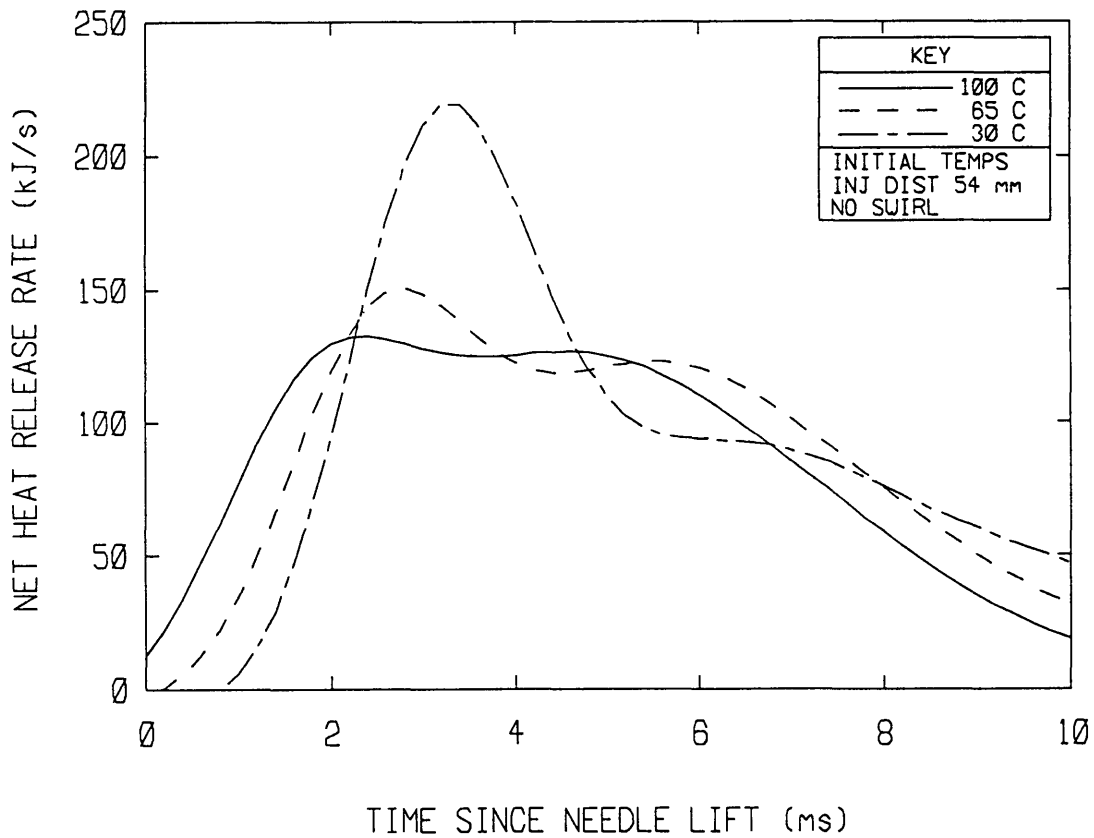


Figure 7.1. Net Heat Release Rates for Three Initial Air Temperatures

7.3.2 CORRELATION OF HEAT TRANSFER RATES WITH OTHER EVENTS

Figure 7.2 shows the impingement point heat transfer rate for the case of 30 C initial air temperature. On this trace, the heat transfer rates corresponding to different causal mechanisms can clearly be distinguished. There is a large peak in heat flux when the as yet unignited fuel jet impacts the wall. Shortly after, there is another peak corresponding to the second fuel pressure peak which characteristically happens 2 ms after the first fuel pressure peak (see figure 2.5). Ignition happens immediately after this second peak. It is not clear that a high heat transfer rate accompanies the premixed phase of combustion; the heat flux does not rise dramatically until the luminous flame reaches the wall. However, the premixed combustion period extends until approximately 5 ms after needle lift, which is considerably after the luminous flame arrives. It is therefore difficult to discern the difference in heat flux between the premixed and mixing-controlled periods. The data suggests that the premixed phase heat transfer might be less than the mixing-controlled heat transfer, but the supporting data is scanty at best, thus this conclusion must be deferred until future data is available for confirmation.

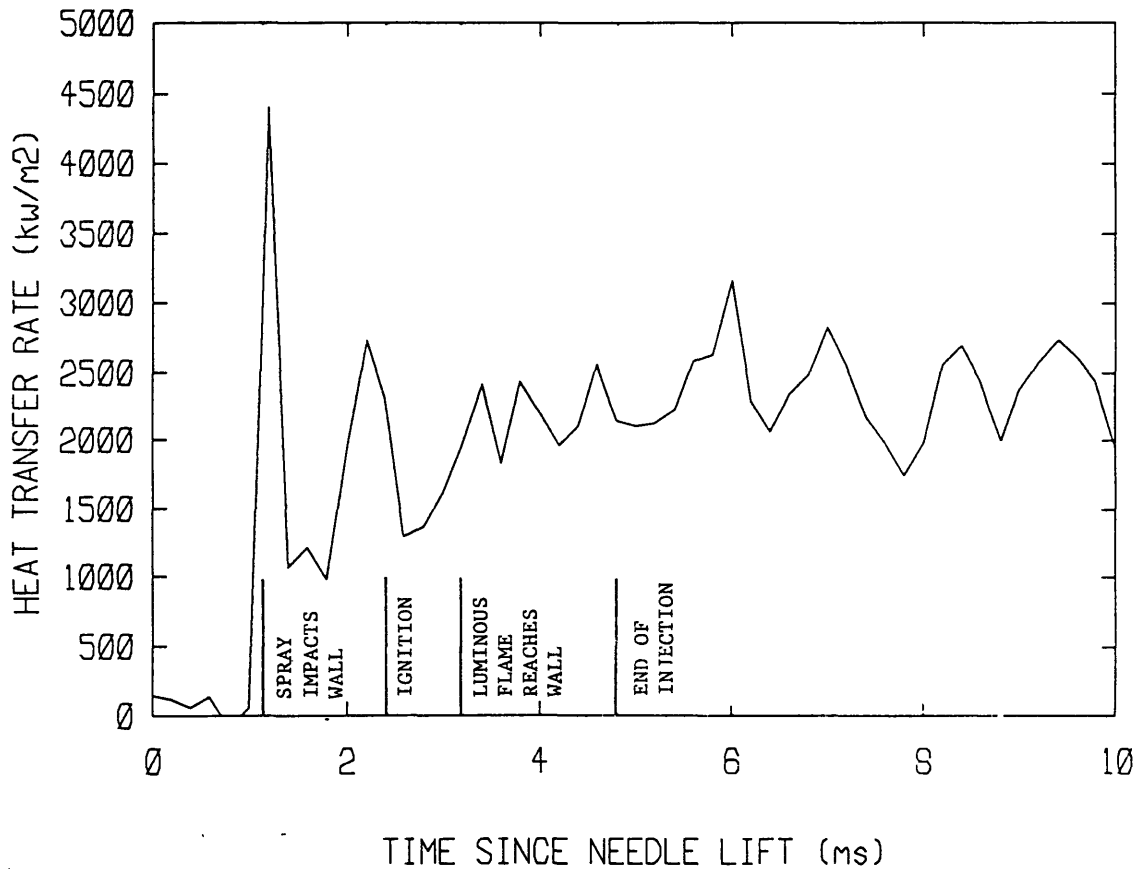


Figure 7.2. Impingement Point Heat Transfer (Initial Air Temp 30 C)

The impingement point heat transfer rates for all three initial temperatures is presented in figure 7.3. All three runs show similar characteristics, although the magnitude of the steady heat transfer period is greater for the higher temperature runs. This will be investigated more fully in the subsequent section.

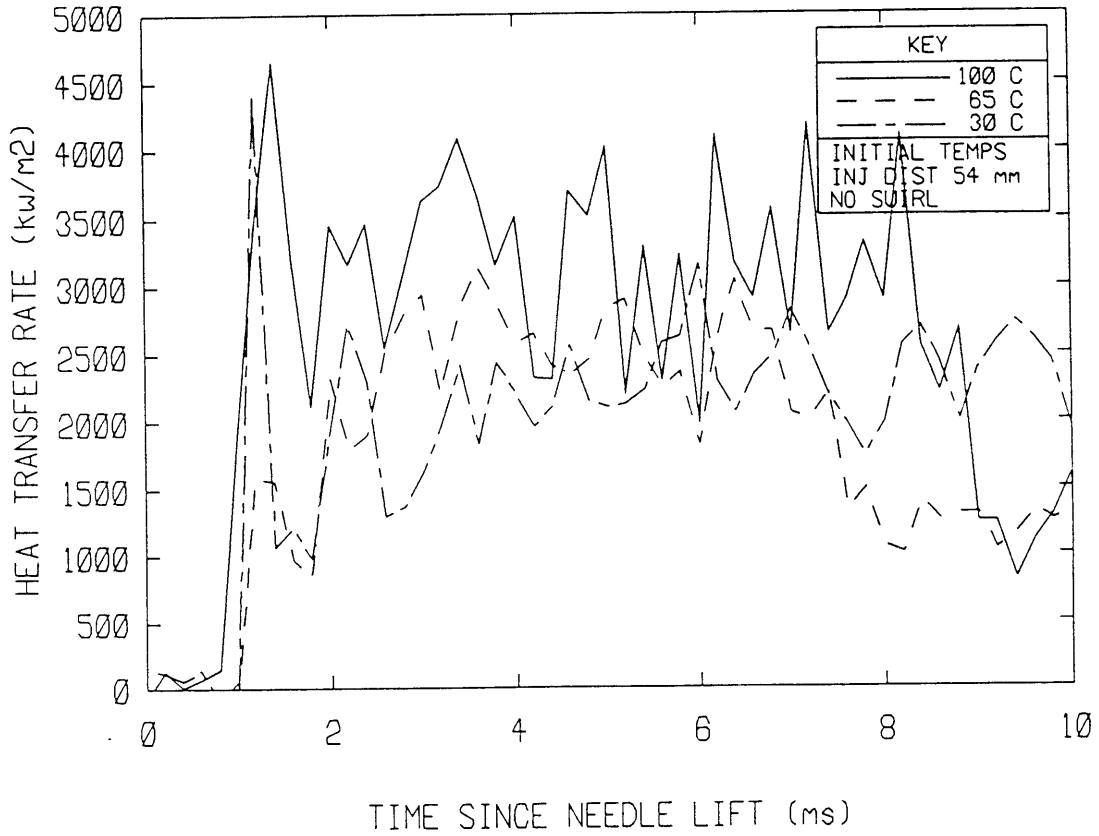


Figure 7.3. Impingement Point Heat Transfer (Three Initial Air Temps)

7.3.3 QUASISTEADY HEAT TRANSFER RATES

Quasisteady heat transfer rates were determined as previously (table 7.2, figure 7.4). The effect of initial air temperature is restricted to the immediate vicinity of the impingement point. The impingement point heat flux increases as air temperature is increased. However, away from the impingement point there is no discernable effect of initial air temperature. This is consistent, since the heat flux to these outlying regions occurs somewhat later than right at the impingement point. The later stages of combustion are characterized by a diffusion flame which is not sensitive to the initial charge temperature.

This also indicates that the central region is affected by the mechanics of vaporization and air entrainment to a greater extent than the periphery.

<u>X</u> <u>(mm)</u>	<u>Heat Flux</u> <u>(30 C)</u> <u>(kw/m²)</u>	<u>Heat Flux</u> <u>(65 C)</u> <u>(kw/m²)</u>	<u>Heat Flux</u> <u>(100 C)</u> <u>(kw/m²)</u>
0	2374	2521	3185
5	2185	2976	2972
10	2976	2891	2409
-15	2823	2739	2761
20	2146	2130	2517
30	1999	1786	2045
45	501	366	254

Table 7.2. Quasisteady Heat Transfer Rates

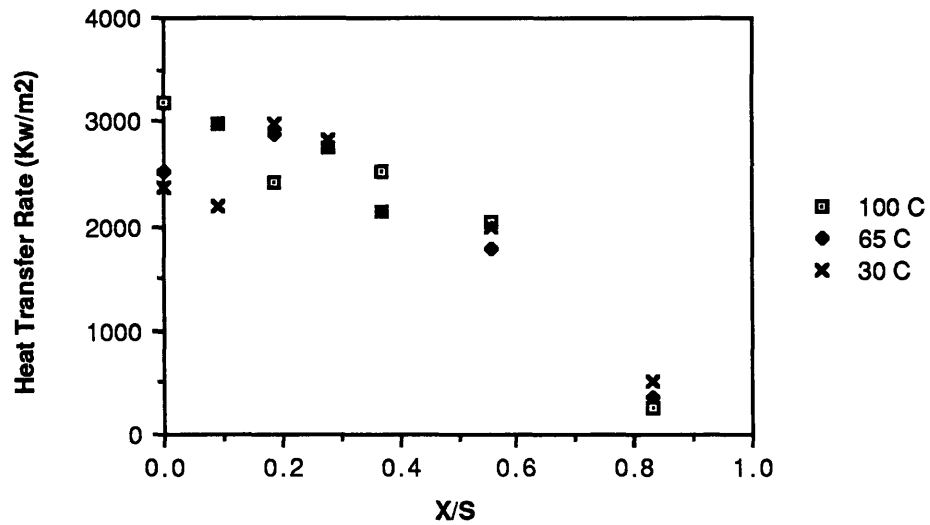


Figure 7.4. Heat Transfer Rates vs. Distance from Impingement Point

Chapter 8

Summary and Conclusions

Surprisingly little is known about the detailed structure of the diesel flame and therefore about the heat transfer therefrom. Although spatially-averaged heat transfer rates have been correlated successfully, there is currently no working model for prediction of local heat transfer rates in diesel engines.

A data base of diesel heat transfer experiments has been established. Major variables studied in this work were injector standoff distance, initial charge temperature, and swirl. Flame-induced heat transfer was separated from jet-induced heat transfer by conducting some experiments with nitrogen as the charge gas.

Wall surface temperature was the primary diagnostic tool used. The wall temperature time histories were converted to heat transfer rates by assuming one-dimensional heat conduction in the cylinder wall and numerically solving the heat conduction equation for the heat transfer rate. This model was verified by comparing the calculated temperature of a wall interior point to that measured by a thermocouple. A set of high-speed color movies were taken for all experimental runs, except those with nitrogen as the charge gas.

The heat transfer rate was small until approximately the time of jet arrival. At that time, the heat flux increased rapidly to attain an essentially steady value, which persisted until the fuel was consumed. Runs with a lower initial temperature, for which the ignition delay period was substantially longer than the jet travel time, revealed that large heat transfer rates accompany the jet arrival, and that essentially steady heat fluxes characterize the combustion period. If ignition happens when the jet arrives at the wall (which was typical in these experiments) then the first peak in heat flux will start a steady heat transfer period, but this will not generalize to cases where the jet travel time and the ignition delay period are unequal. Therefore, steady heat transfer starting immediately at jet arrival is somewhat of a coincidence, as the ignition delay times and the jet travel time for this set of experiments is nearly identical.

The nitrogen runs were different in that a heat transfer spike was observed at the end of injection. This was attributed to the establishment of a flowfield convecting hot cylinder

gas towards the wall. The gases were cooled somewhat by the vaporization of the fuel. When the fuel spray suddenly ceased, the cooling effect disappeared immediately while the flowfield took a finite time to decay. The sudden increase in gas temperature with no corresponding change in gas velocity caused the spike in heat transfer rate. As the gas velocity decayed, the heat transfer rate decayed as well.

The impingement point heat transfer rate received particular attention. The impingement point heat transfer rate was identical for both air and nitrogen runs for short (29 mm) injection distances. This was because the jet had not yet entrained enough air to support combustion at the jet center. This was clearly discernable from impingement point heat transfer traces showing both the air and nitrogen results. It is therefore concluded that the fuel spray undeniably contains a non-burning center which persists throughout the injection period, at least for some distance from the nozzle exit. This non-burning center was evident for a 29 mm injection distance, but was not observed for a 54 mm injection distance.

The impingement point heat transfer in nitrogen exhibited an inverse square dependence ($1/S^2$) on injection distance, whereas that in air exhibited a $1/S$ dependence.

The heat transfer from the fuel spray was compared to that from an impinging jet of air. This was accomplished by synthesizing a gas jet with the same initial momentum as the fuel jet. The local jet temperatures were estimated using results from gas jet theory. The heat transfer rates were nondimensionalized as Nusselt numbers for the impingement point and for locations on the cylinder centerline parallel to the piston face. These Nusselt numbers were compared to those predicted by correlations for air jets. The trends for burning fuel sprays were well-matched by the air correlations, but those for non-burning sprays exhibited a different slope. The Nusselt numbers predicted by the correlation were too high if the synthesized jet Reynolds number was used, and too low if the actual jet Reynolds number was used.

The local heat transfer coefficients (normalized by impingement point heat transfer coefficients) for non-burning sprays decrease with increasing distance from the impingement point similarly to air jets, though burning fuel spray heat transfer coefficients are consistently higher than those for air jets.

References

- [1] G. Borman and K. Nishiwaki, "A Review of Internal Combustion Engine Heat Transfer", *Progress in Energy and Combustion Science*, Vol. 13, pp. 1-46, 1987.
- [2] G. Woschni, "Universally Applicable Equation for the Instantaneous Heat Transfer Coefficient in the Internal Combustion Engine", SAE Paper 670931, SAE Transactions, vol. 76, 1967.
- [3] T. LeFeuvre, P.S. Myers, O.A. Uyehara, "Experimental Instantaneous Heat Fluxes in a Diesel Engine and their Correlation", SAE Paper 690464, SAE Transactions, vol. 78, 1969.
- [4] J.C. Dent and S.J. Suliaman, "Convective and Radiative Heat Transfer in a High Swirl Direct Injection Diesel Engine", SAE Paper 770407, *SAE Transactions*, vol. 86, 1977.
- [5] G. Woschni, W. Spindler, K. Kolesa, "Heat Insulation of Combustion Chamber Walls - A Measure to Decrease the Fuel Consumption of I.C. Engines?", SAE paper 870339, SAE International Congress, February 1987.
- [6] A.A. Amsden, J.D. Ramshaw, P.J. O'Rourke, J.K. Ducowicz, "KIVA: A Computer Program for Two- and Three-Dimensional Fluid Flows with Chemical Reactions and Fuel Sprays", LA-10245-MS, Los Alamos National Laboratory, February 1985.
- [7] R. Gardon and J. Cobonpue, "Heat Transfer Between a Flat Plate and Jets of Air Impinging on It", Proceedings of the 1961 International Heat Transfer Conference, 1962.
- [8] T. Kamimoto, H. Takahashi, H. Kobayashi, S. Matsuoka, "Convective Heat Transfer of an Impinging Diesel Flame in a Rapid Compression Machine", SAE Paper 821035, SAE SP-525, International Off-Highway Meeting, September 1982.
- [9] R.P. Durrett, D.C. Oren, C.R. Ferguson, "A Multidimensional Data Set for Diesel Combustion Model Validation: 1 - Initial Conditions, Pressure History and Spray

Shapes", SAE Paper 872087, SAE International Fuels and Lubricants Meeting, November 1987.

[10] D.C. Oren, R.P. Durrett, C.R. Ferguson, J. Timar, D.R. Tree, D.P. DeWitt, "A Multidimensional Data Set for Diesel Combustion Model Validation: 2 - Fuel Injection Rate and Boundary Conditions", SAE Paper 872088, SAE International Fuels and Lubricants Meeting, November 1987.

[11] G.N. Abramovich, The Theory of Turbulent Jets, MIT Press, 1962, pp. 586-600.

[12] J.O. Hinze, Turbulence, McGraw-Hill Book Co., 1959.

[13] R.B. Melton, "Diesel Fuel Injection Viewed as a Jet Phenomenon", SAE Paper 710132, 1971 Automotive Engineering Congress, 1971.

[14] J.M. Beer, and N.A. Chigier, Combustion Aerodynamics, Krieger Publishing Co., 1983.

[15] K.J. Colella, E.N. Balles, J.A. Ekchian, W.K. Cheng, J.B. Heywood, "A Rapid Compression Machine Study of the Influence of Charge Temperature on Diesel Combustion", SAE paper 870587, SAE International Congress, February 1987.

[16] E.N. Balles, "Fuel-Air Mixing and Diesel Combustion in a Rapid Compression Machine", Ph.D. Thesis, Massachusetts Institute of Technology, June 1987.

[17] E.N. Balles, "Fuel Injection Characteristics and Combustion Behavior of a Direct Injection Stratified Charge Engine", S.M. Thesis, Massachusetts Institute of Technology, September 1983.

*****FIX THIS *****

[18] Eric's SAE paper, "Influence of Charge Air Motion ...(or something like that)"

*****FIX THIS *****

[19] M.A. Theobald and W.K. Cheng, "A Numerical Study of Diesel Ignition", ASME Paper 87-FE-2, ASME Energy Sources Technology Conference, February 1987.

[20] W.K. Cheng and R. Gentry, "Effects of Charge Non-Uniformity on Diesel Heat Release Analysis", SAE Paper 861568, International Fuels and Lubricants Meeting, October 1986.

[21] C.R. Ferguson, D.R. Tree, D.P. DeWitt, S.A.H. Wahiduzzaman, "Design, Calibration and Error Analysis of Instrumentation for Heat Transfer Measurements in Internal Combustion Engines", Developments in Experimental Techniques in Heat Transfer and Combustion, AMSE-HTD-Vol. 71, 1987, pp. 67-82.

[23] J.W. Gautner, J.N.B. Livingood, P. Hrycak, "Survey of Literature on Flow Characteristics of a Single Turbulent Jet Impinging on a Flat Plate", NASA TN-D5652, 1970.

[23] P. Hrycak, "Heat Transfer from Impinging Jets: A Literature Review", AFWAL-TR-81-3054 (also AD-A106723), 1981.

[24] C.D. Donaldson and R.S. Snedeker, "A Study of Free Jet Impingement. Part 1. Mean Properties of Free and Impinging Jets", Journal of Fluid Mechanics, Vol. 45, part 2, pp. 281-319, Jan. 1971.

[25] F.P. Ricou and D.B. Spalding, "Measurements of Entrainment by Axisymmetrical Turbulent Jets", Journal of Fluid Mechanics, vol. 11, pp. 21-32, 1961.

[26] T. Kamimoto, S. Matsuoka, "Prediction of Spray Evaporation in Reciprocating Engines", SAE 770413, 1977.

[27] S.H. Mansouri, "Divided-Chamber Automotive Diesel Engine: Development and Validation of a Performance and Emissions Model", Ph.D. Thesis, Massachusetts Institute of Technology, December 1981.

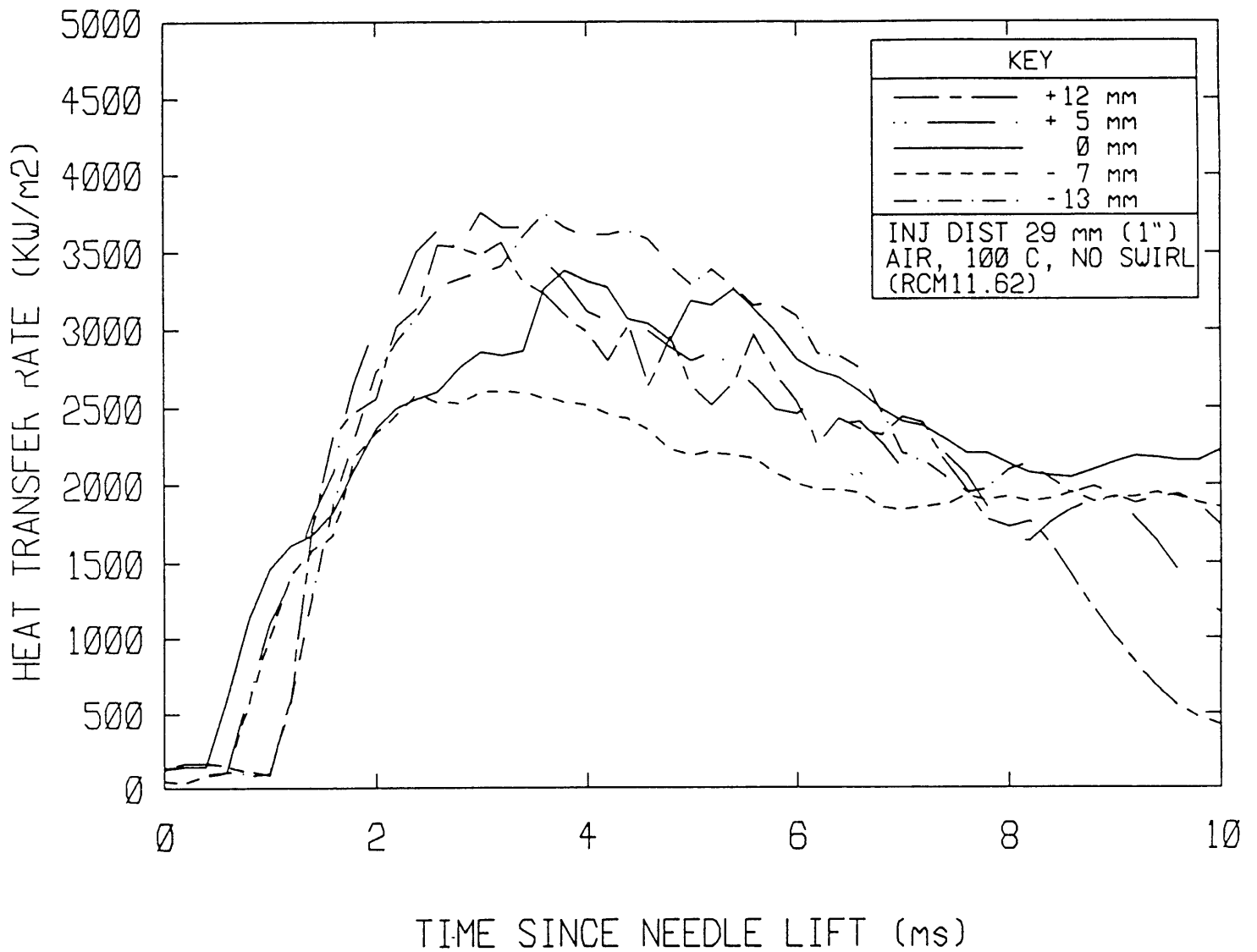
[28] S. Gordon and B. McBride, NASA SP-273, 1971.

[29] S.H. Mansouri and J.B. Heywood, "Correlations for the Viscosity and Prandtl Number of Hydrocarbon-Air Combustion Products", Combustion Science & Technology, vol. 23, pp. 251-256, 1980.

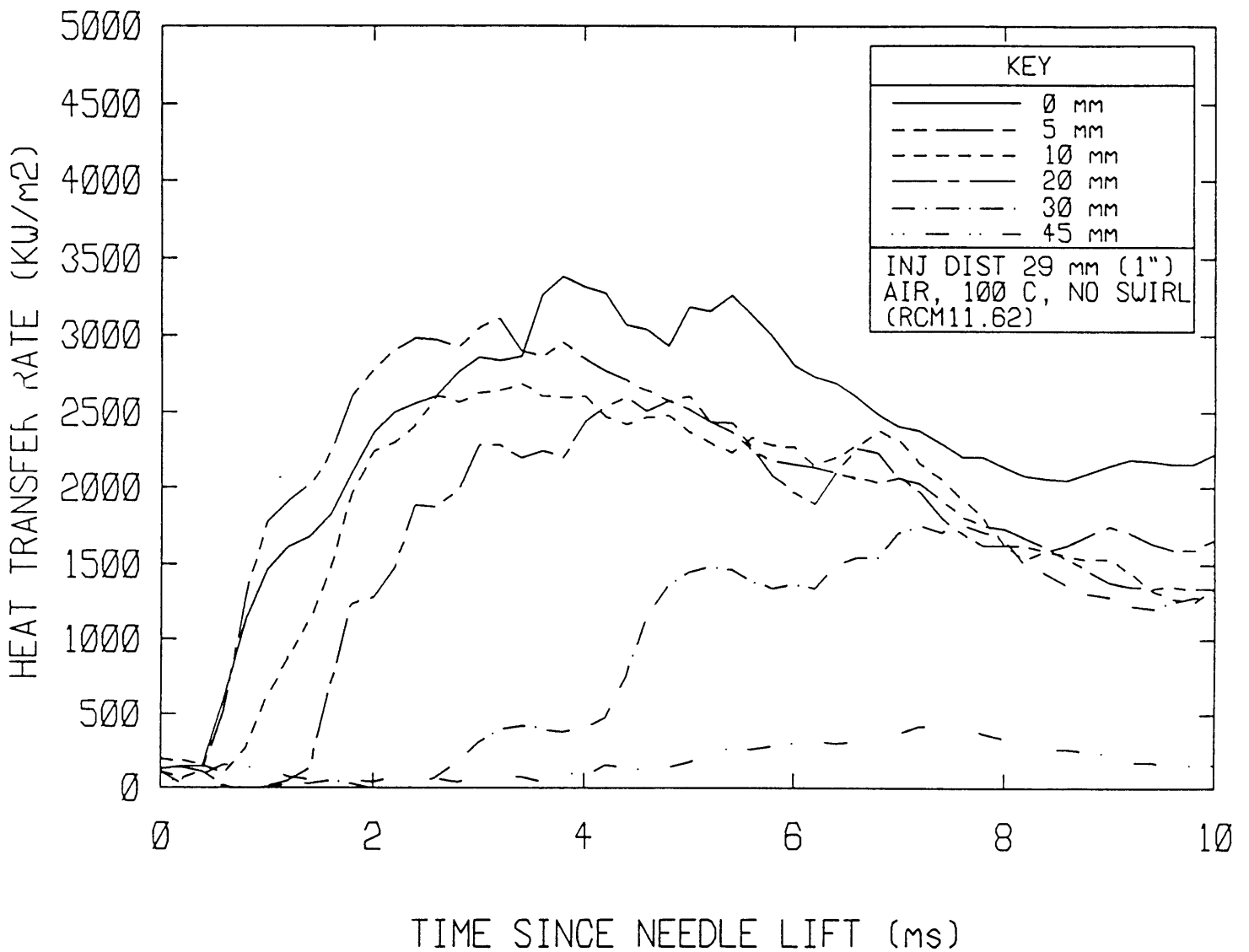
[30] J.B. Heywood, Internal Combustion Engine Fundamentals, McGraw-Hill, 1988.

APPENDIX A
HEAT FLUX SURVEYS

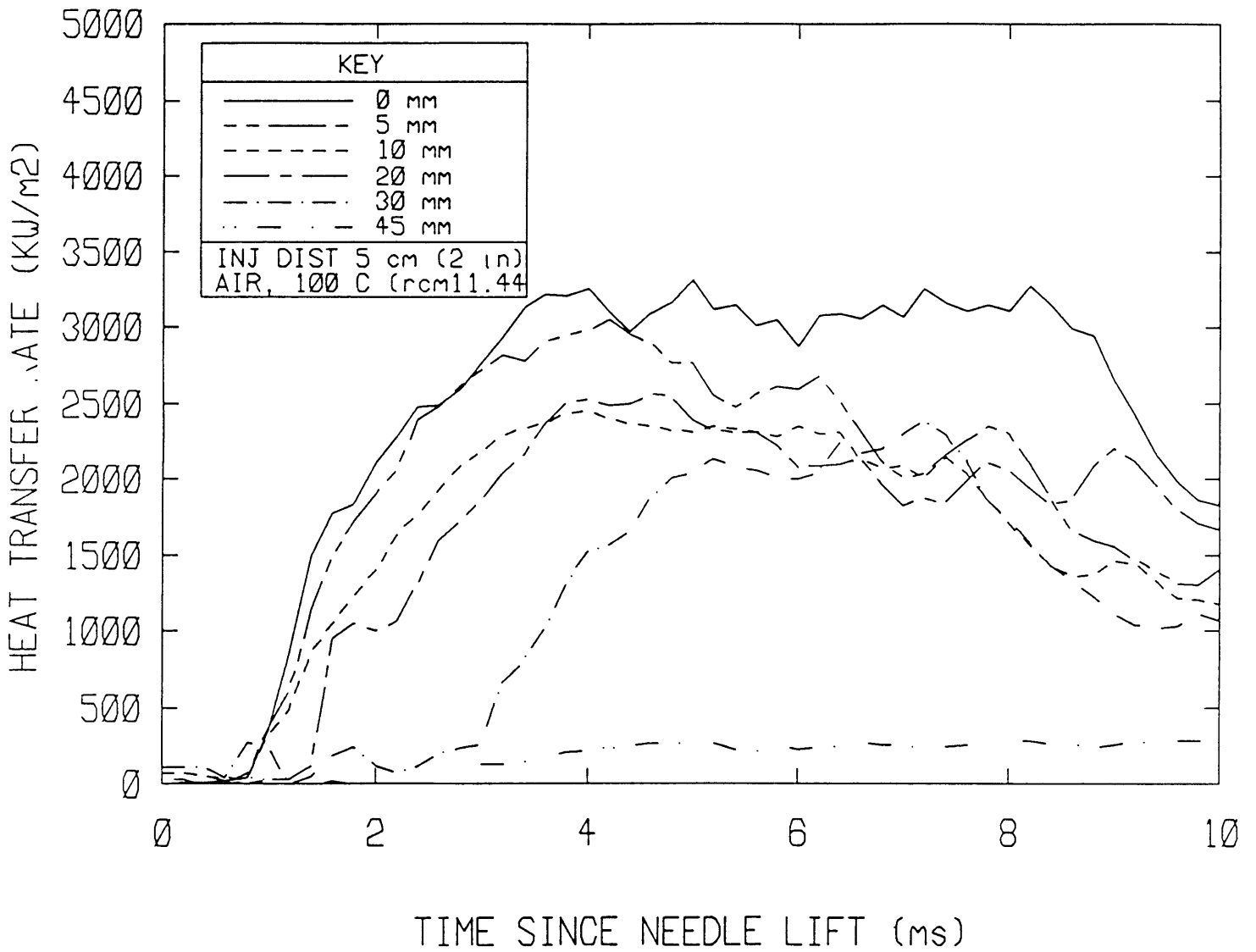
HEAT FLUX SURVEY (VERT)



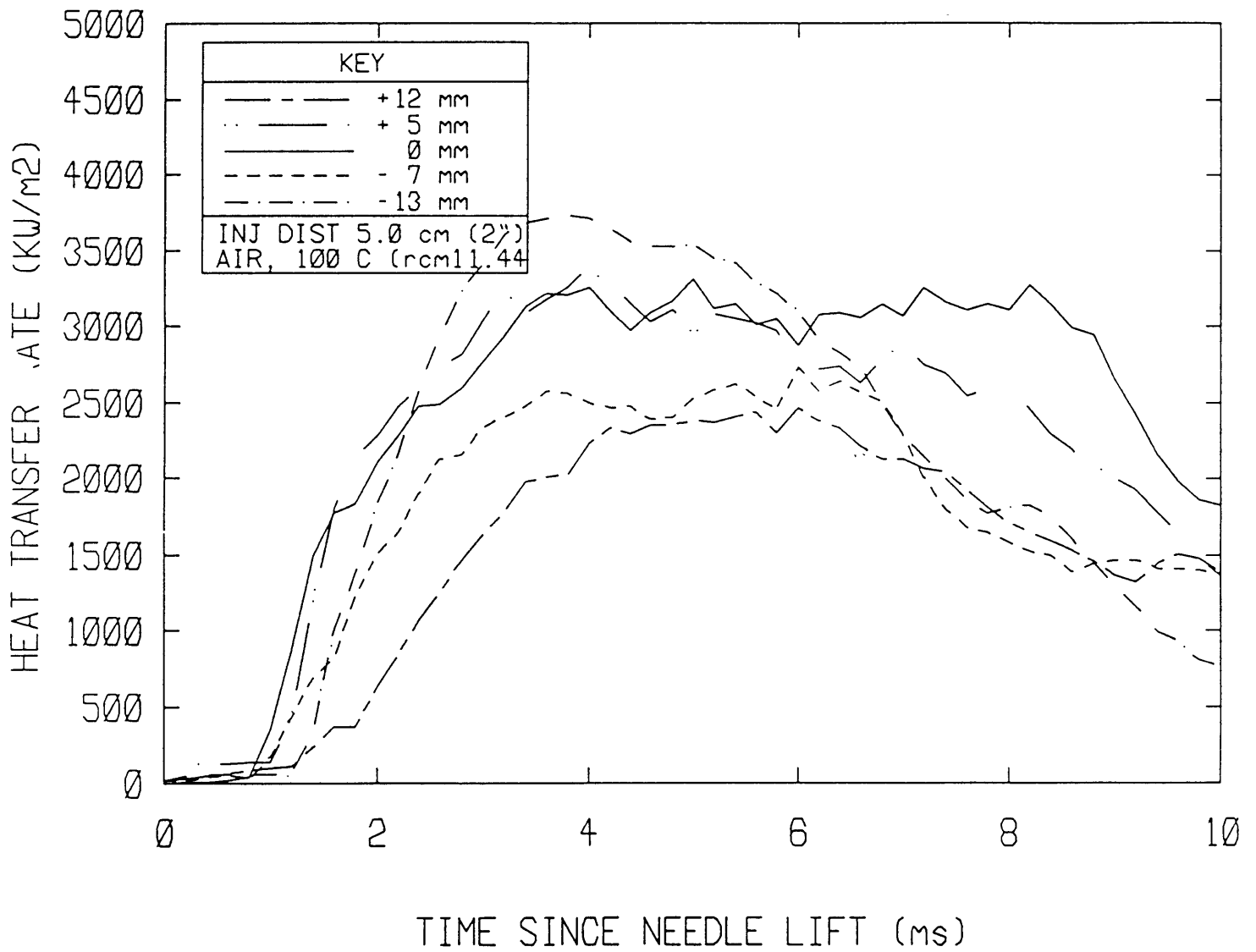
HEAT FLUX SURVEY (HORIZ)



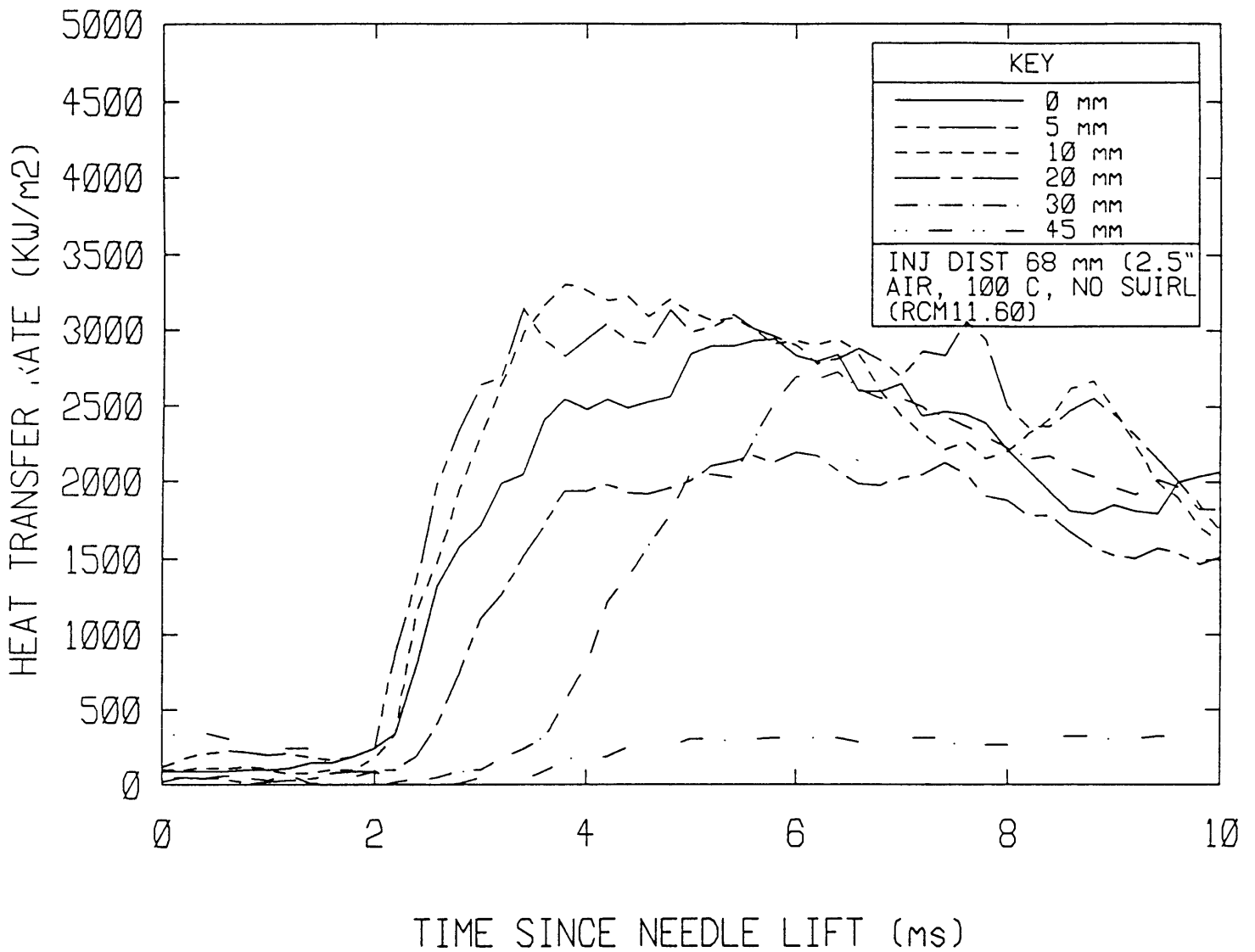
HEAT FLUX SURVEY (HORIZ)



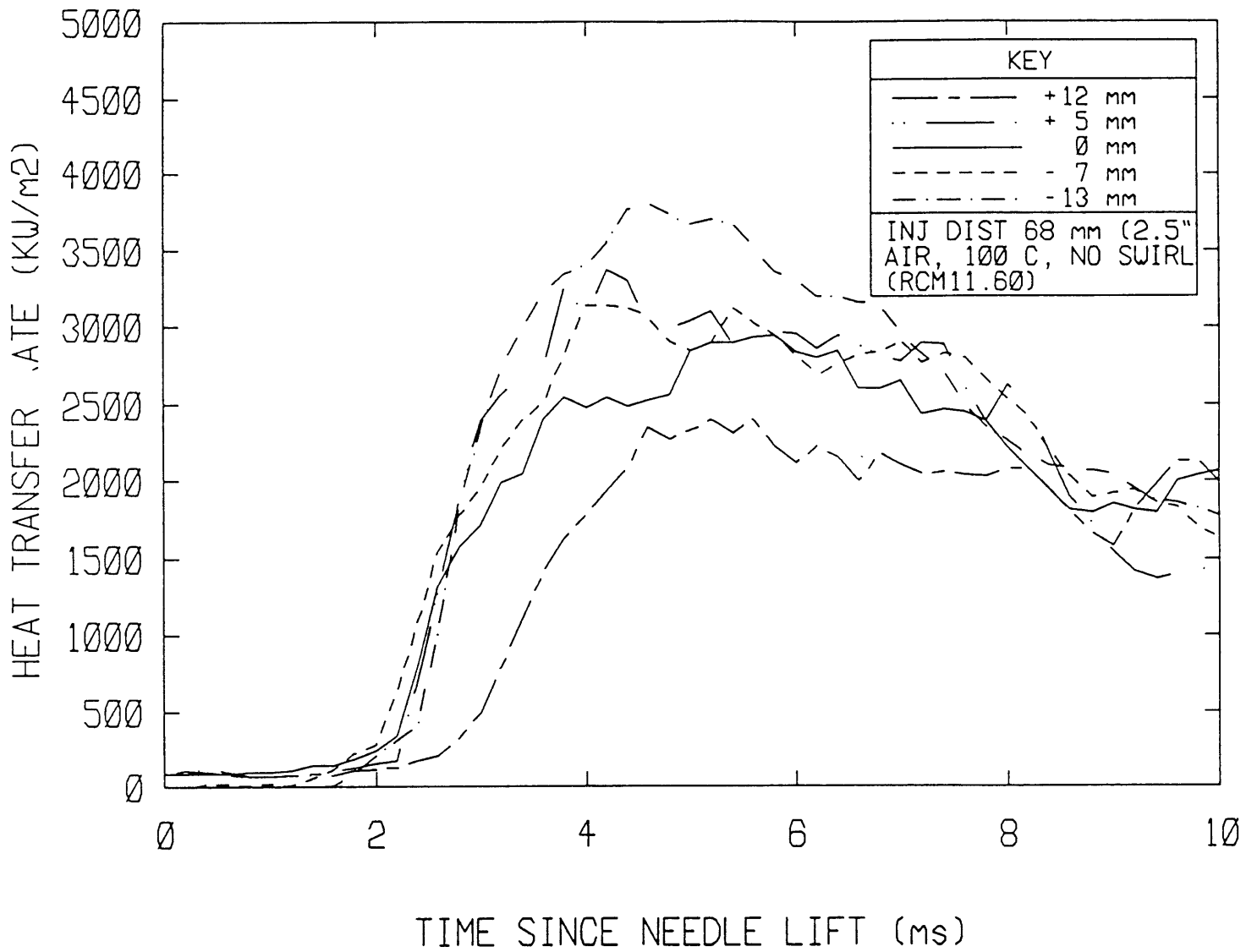
HEAT FLUX SURVEY (VERT)



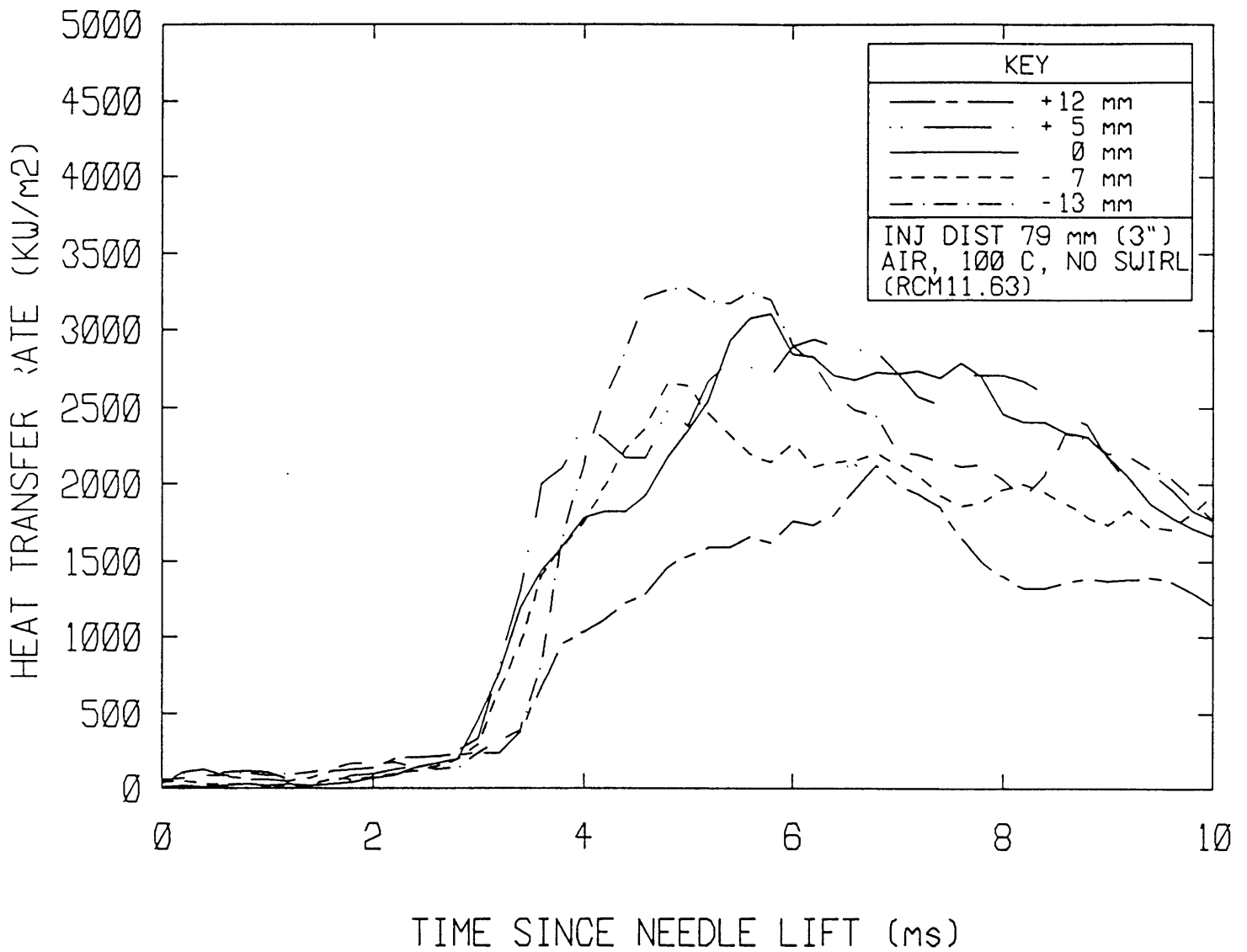
HEAT FLUX SURVEY (HORIZ)



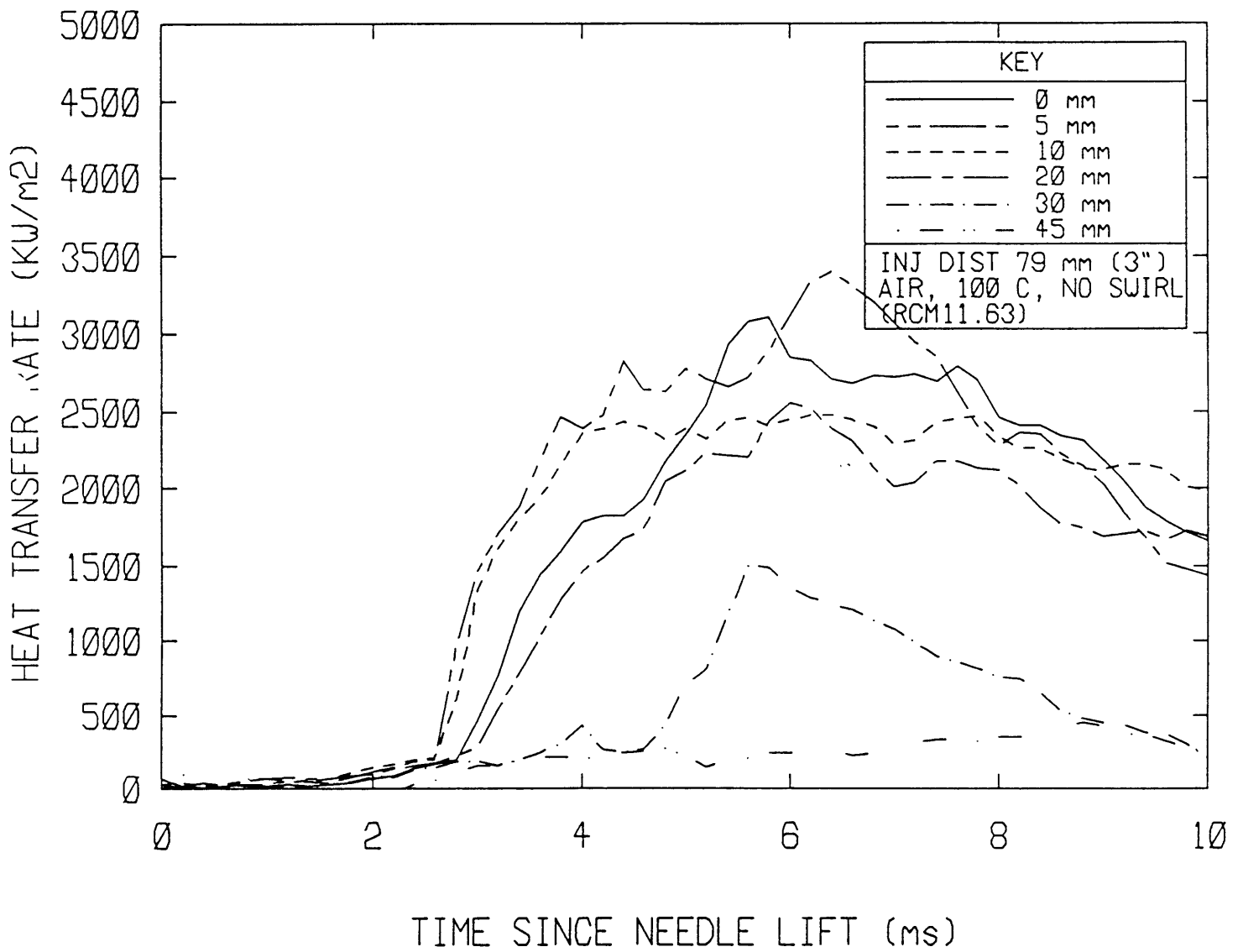
HEAT FLUX SURVEY (VERT)



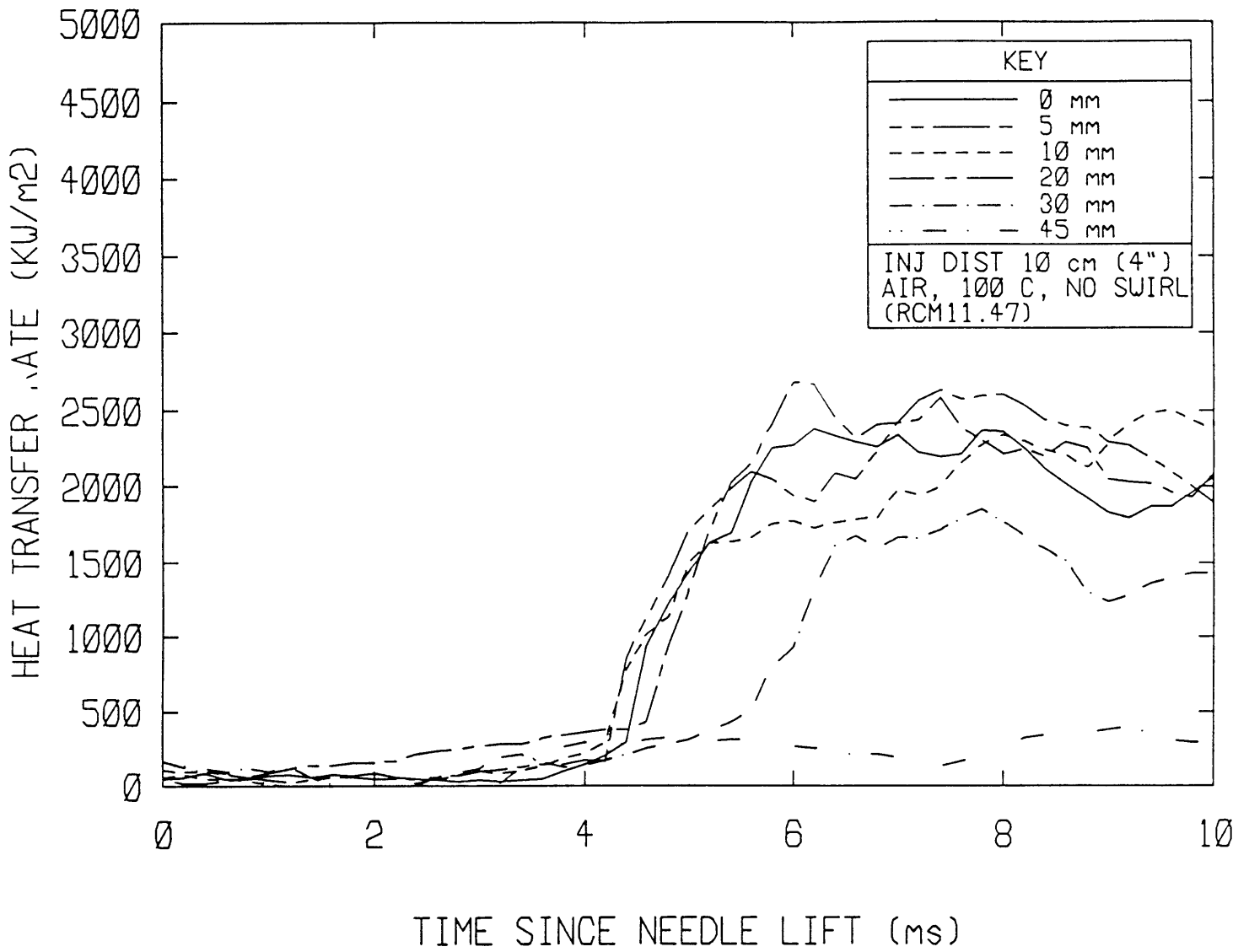
HEAT FLUX SURVEY (VERT)



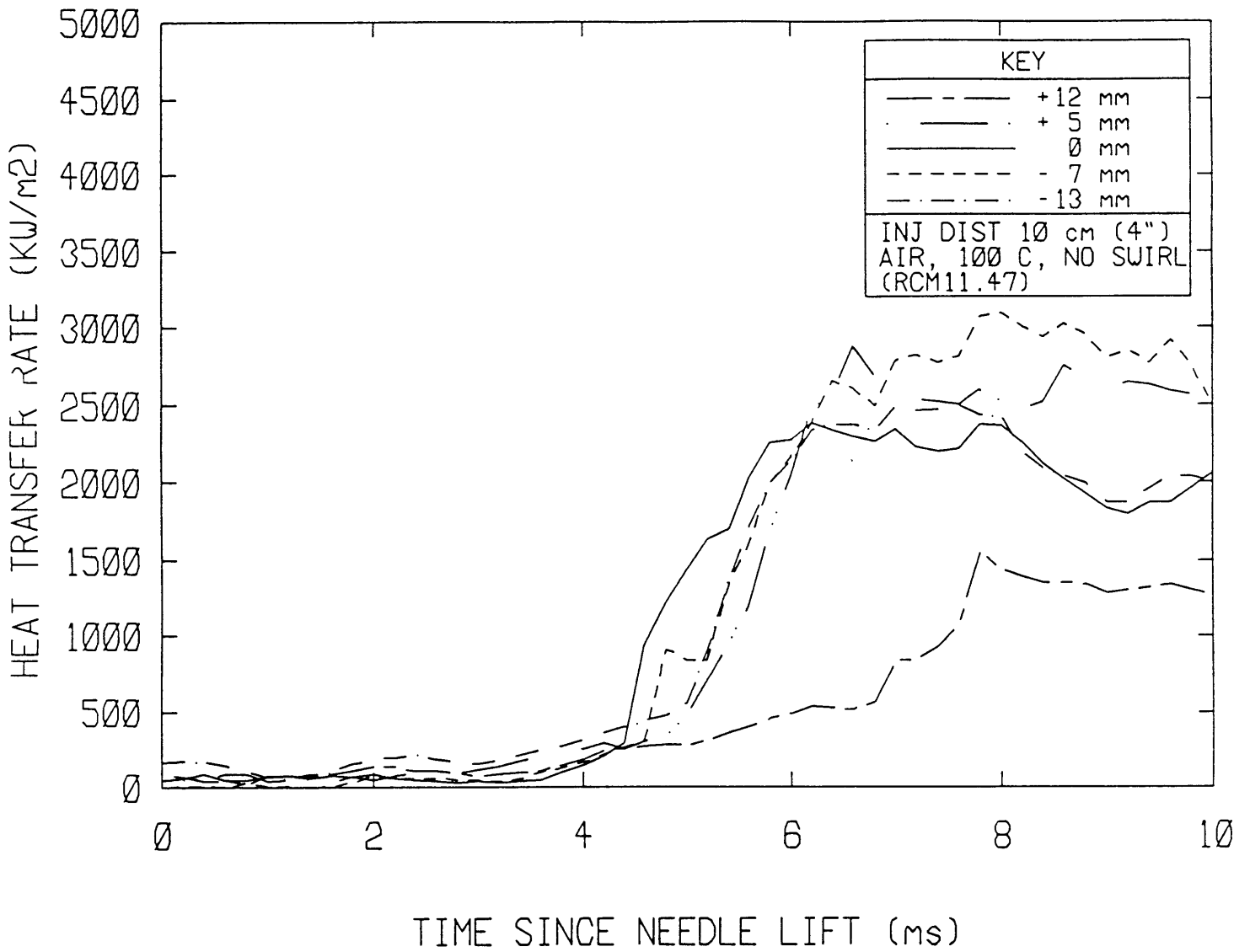
HEAT FLUX SURVEY (HORIZ)



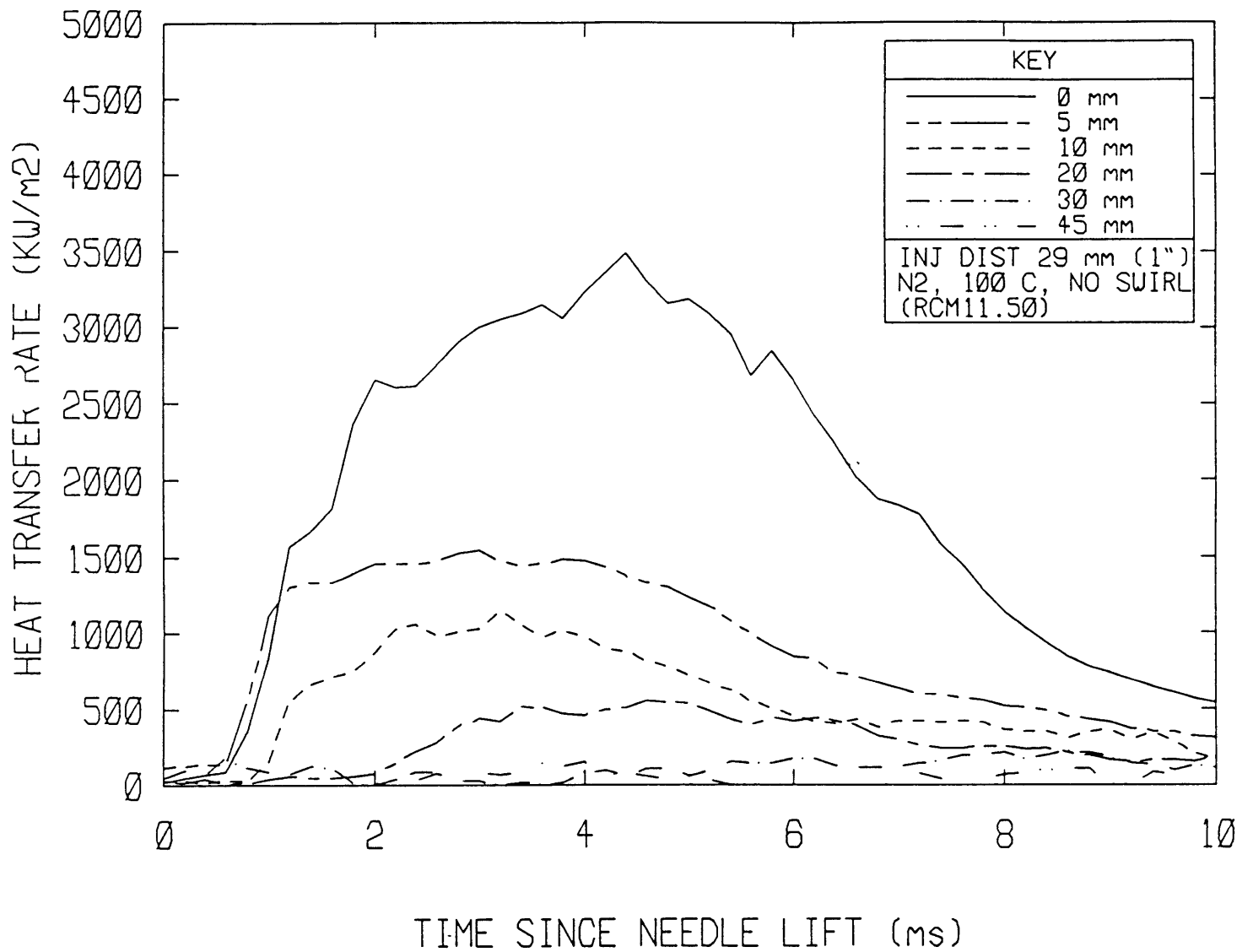
HEAT FLUX SURVEY (HORIZ)



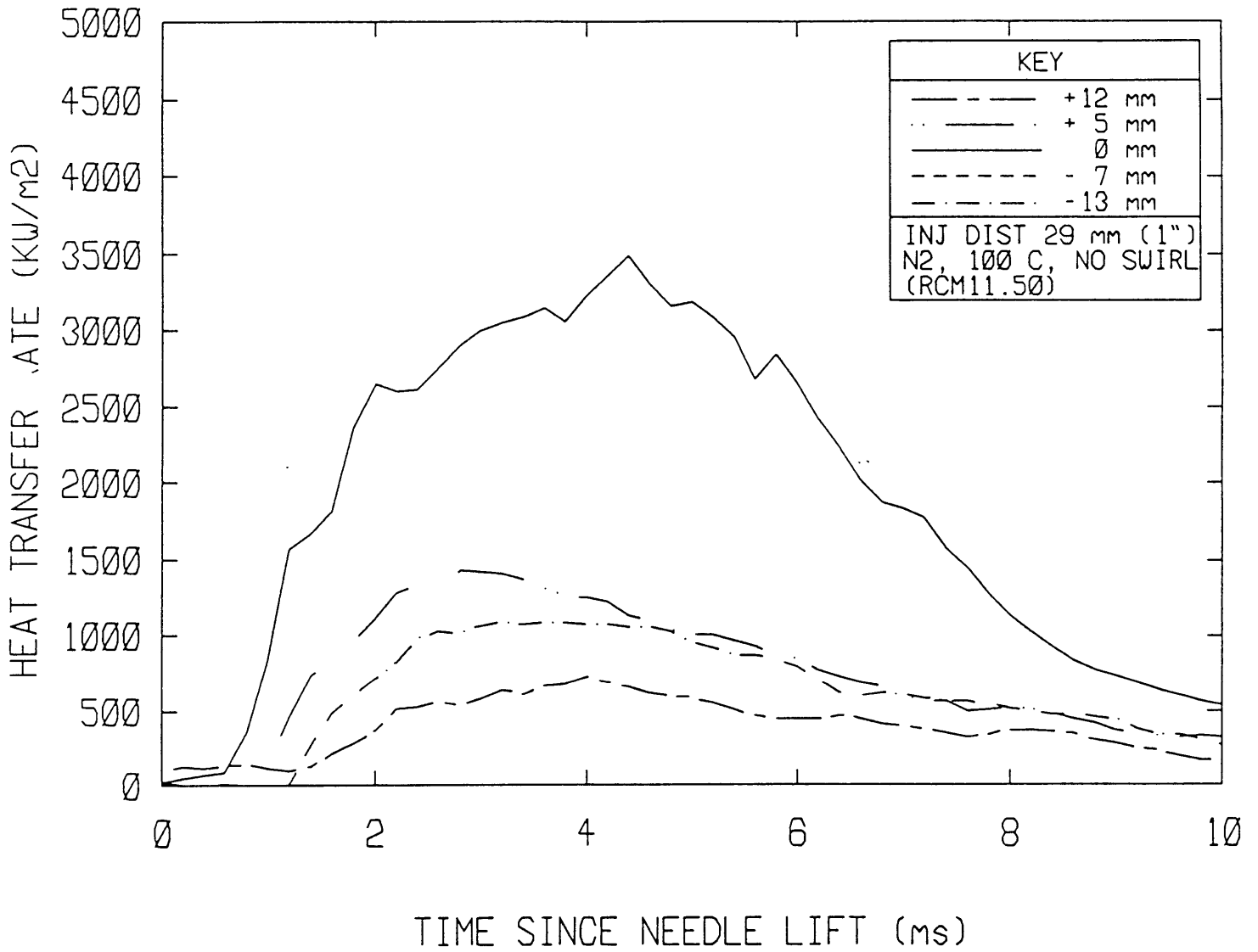
HEAT FLUX SURVEY (VERT)



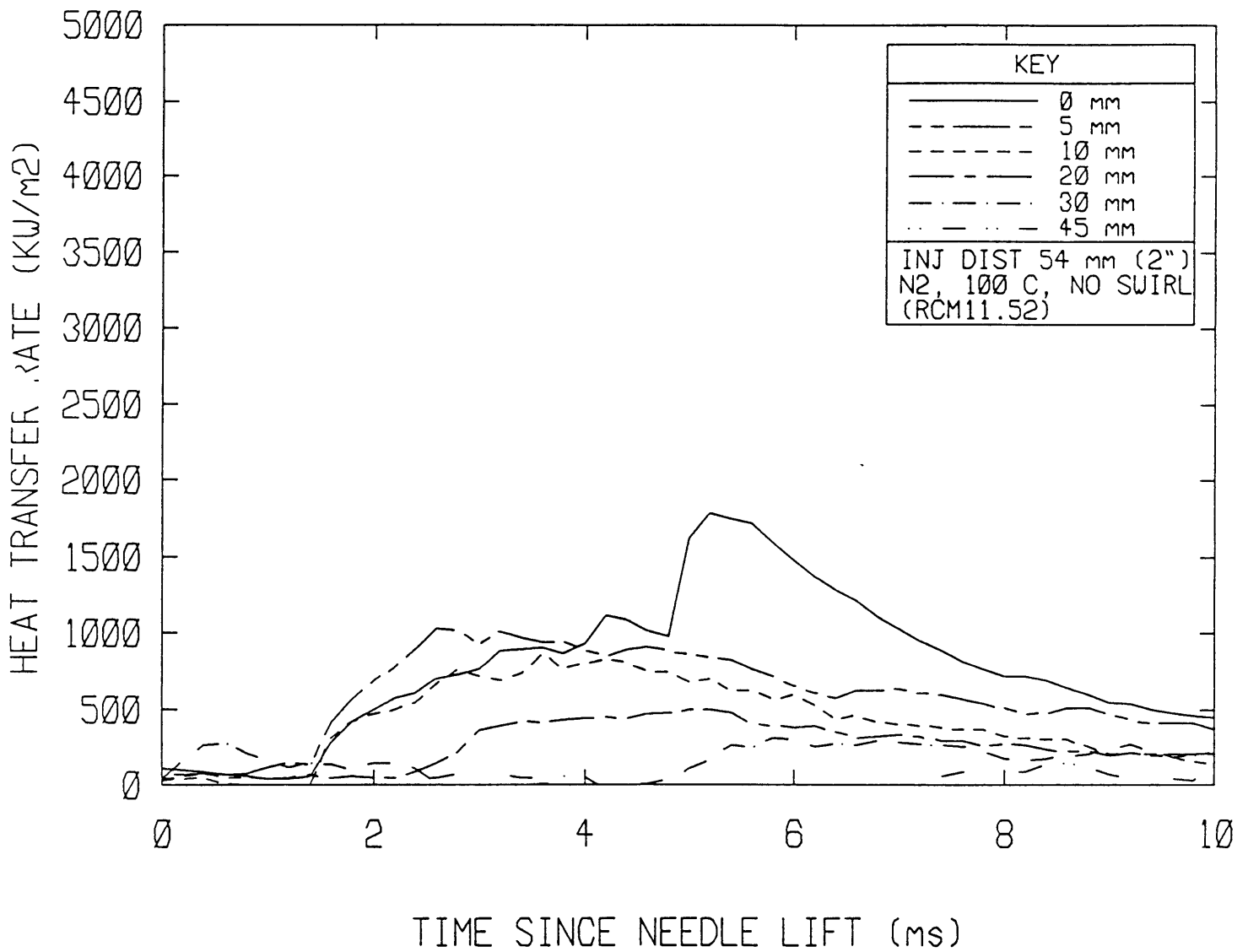
HEAT FLUX SURVEY (HORIZ)



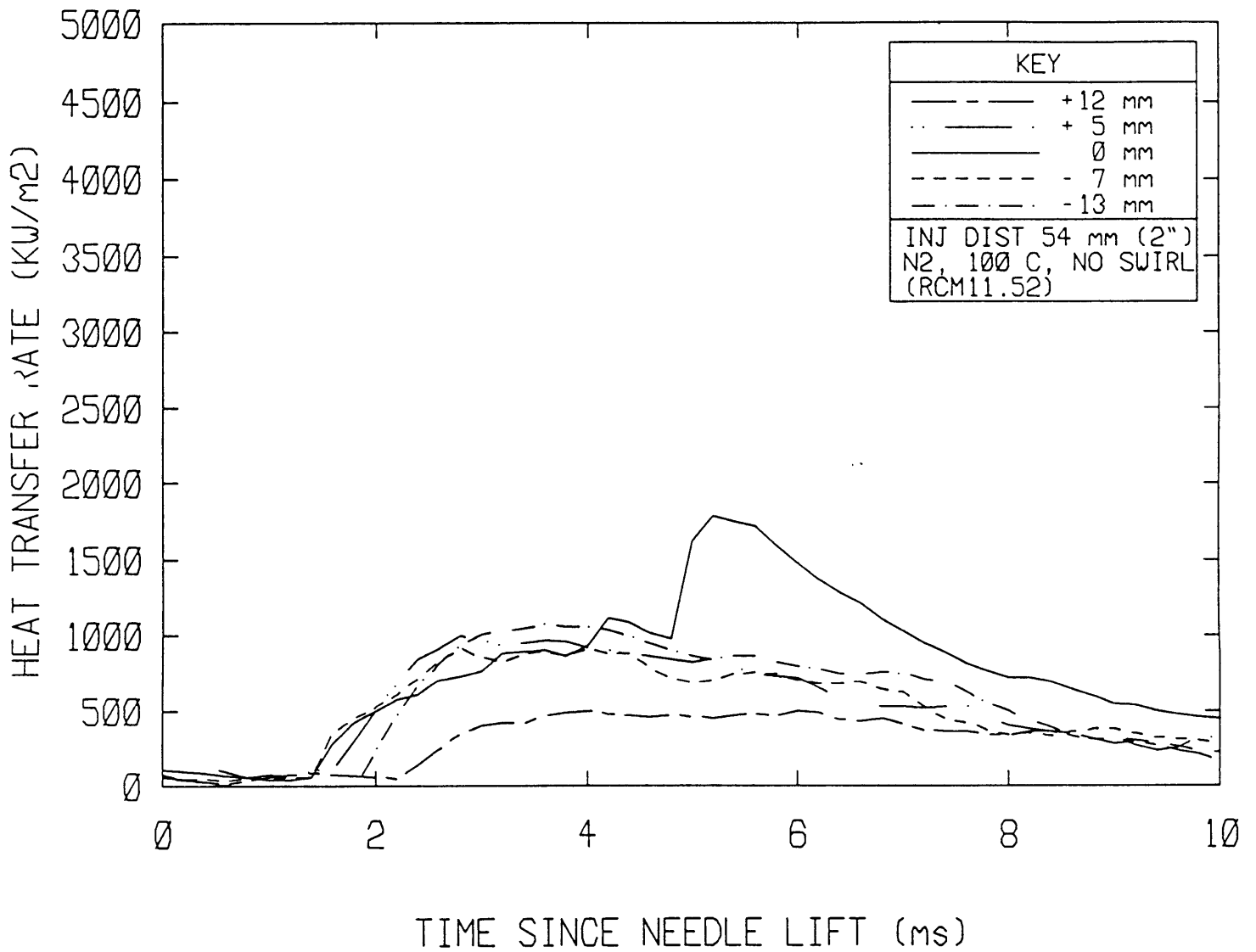
HEAT FLUX SURVEY (VERT)



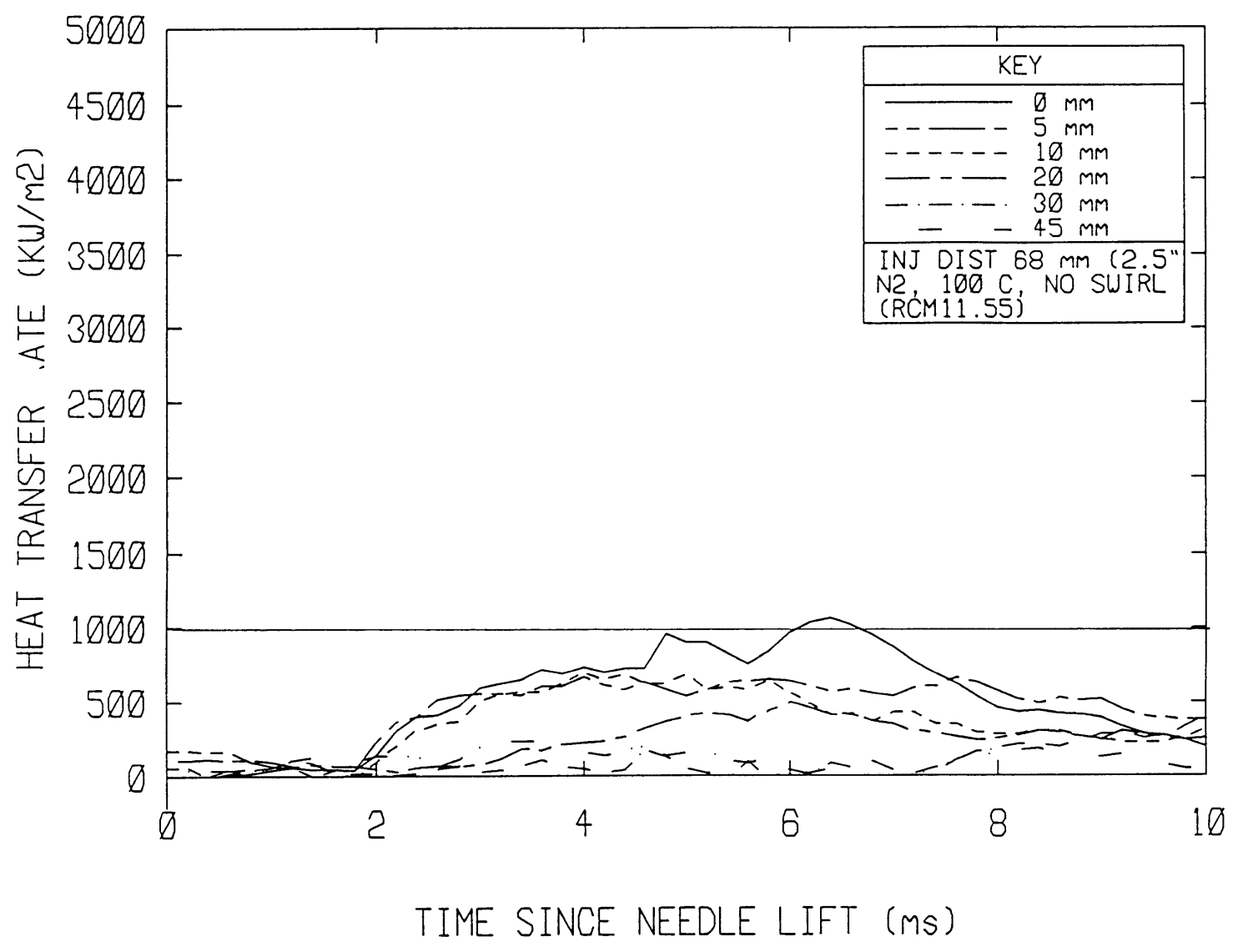
HEAT FLUX SURVEY (HORIZ)



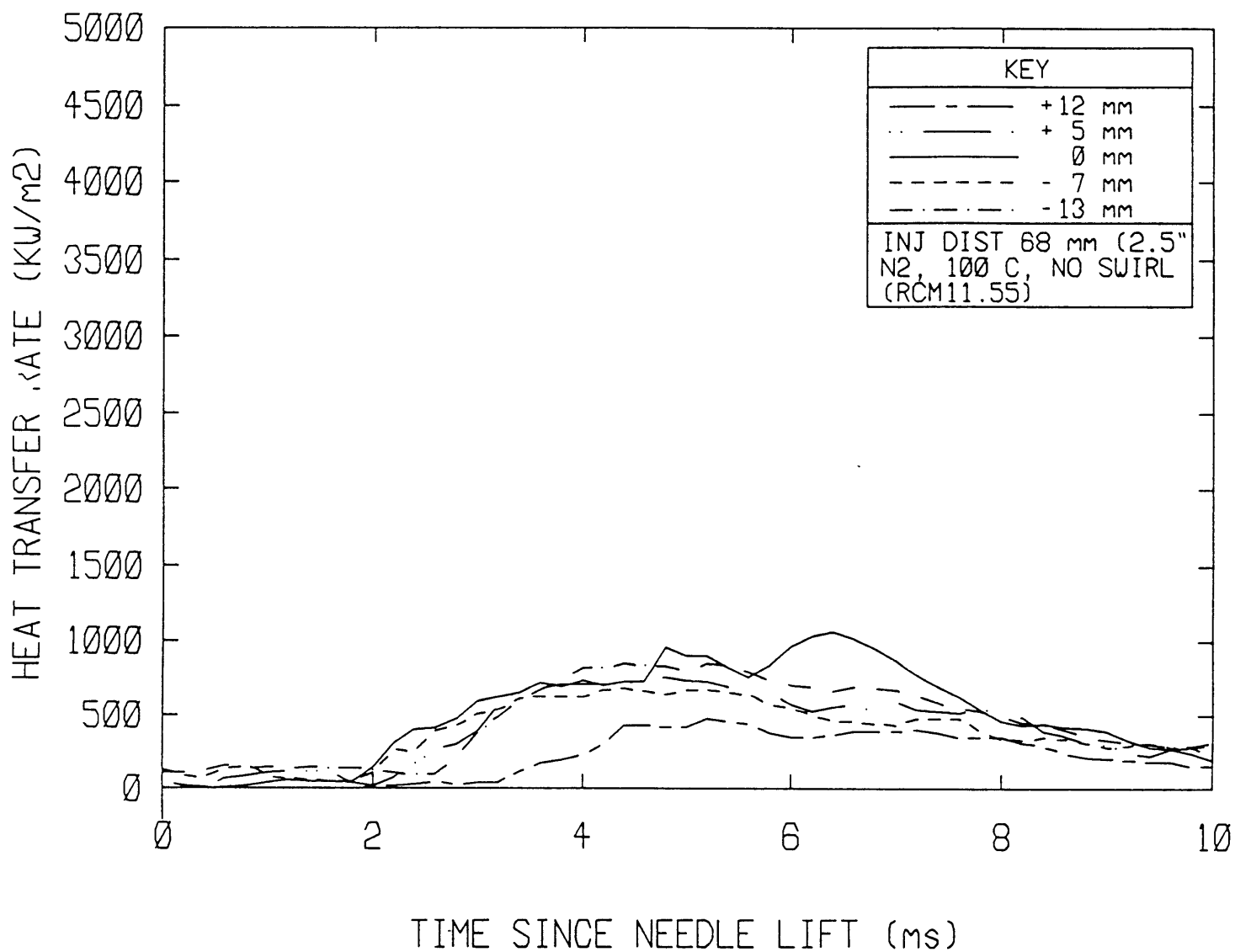
HEAT FLUX SURVEY (VERT)



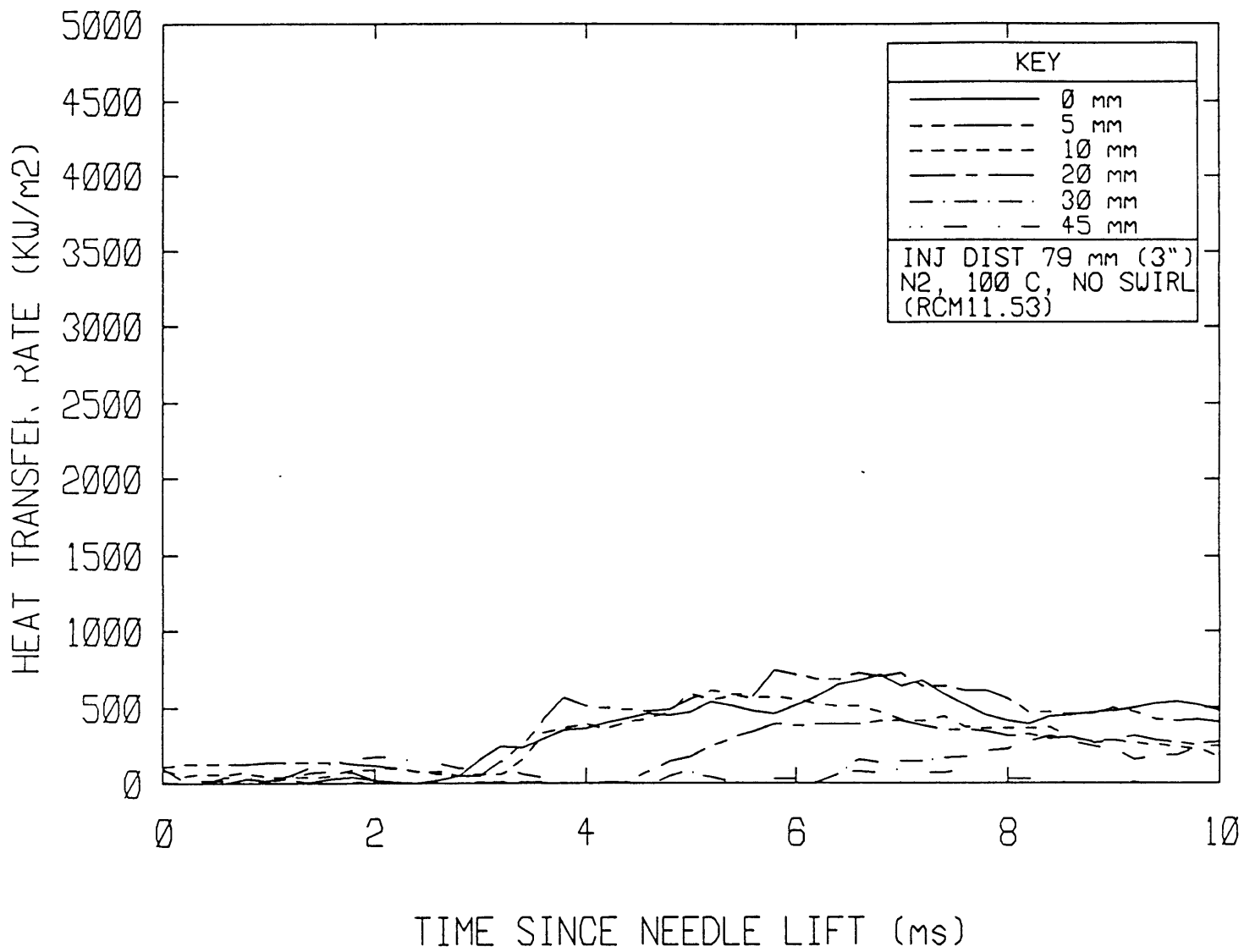
HEAT FLUX SURVEY (HORIZ)



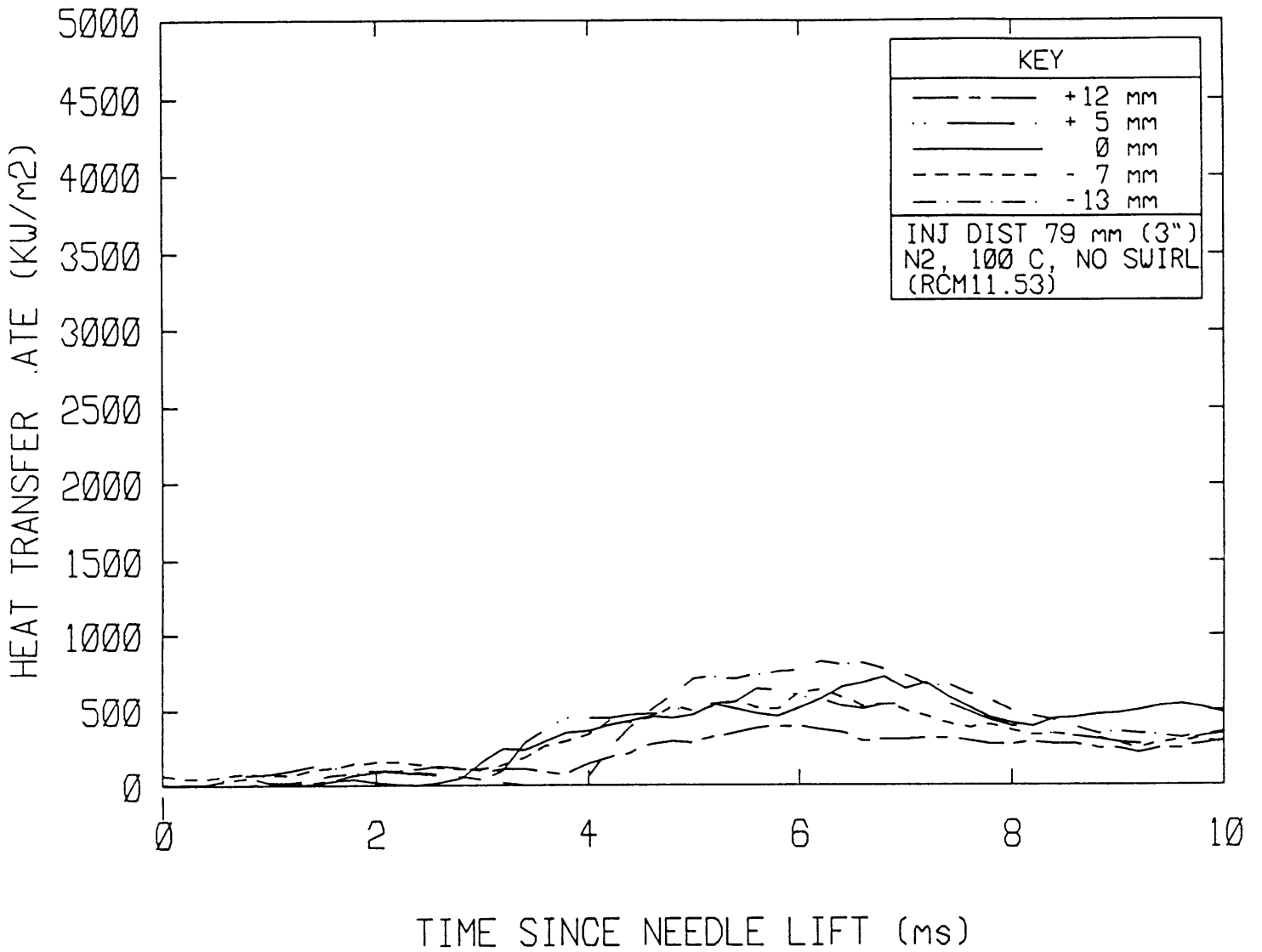
HEAT FLUX SURVEY (VERT)



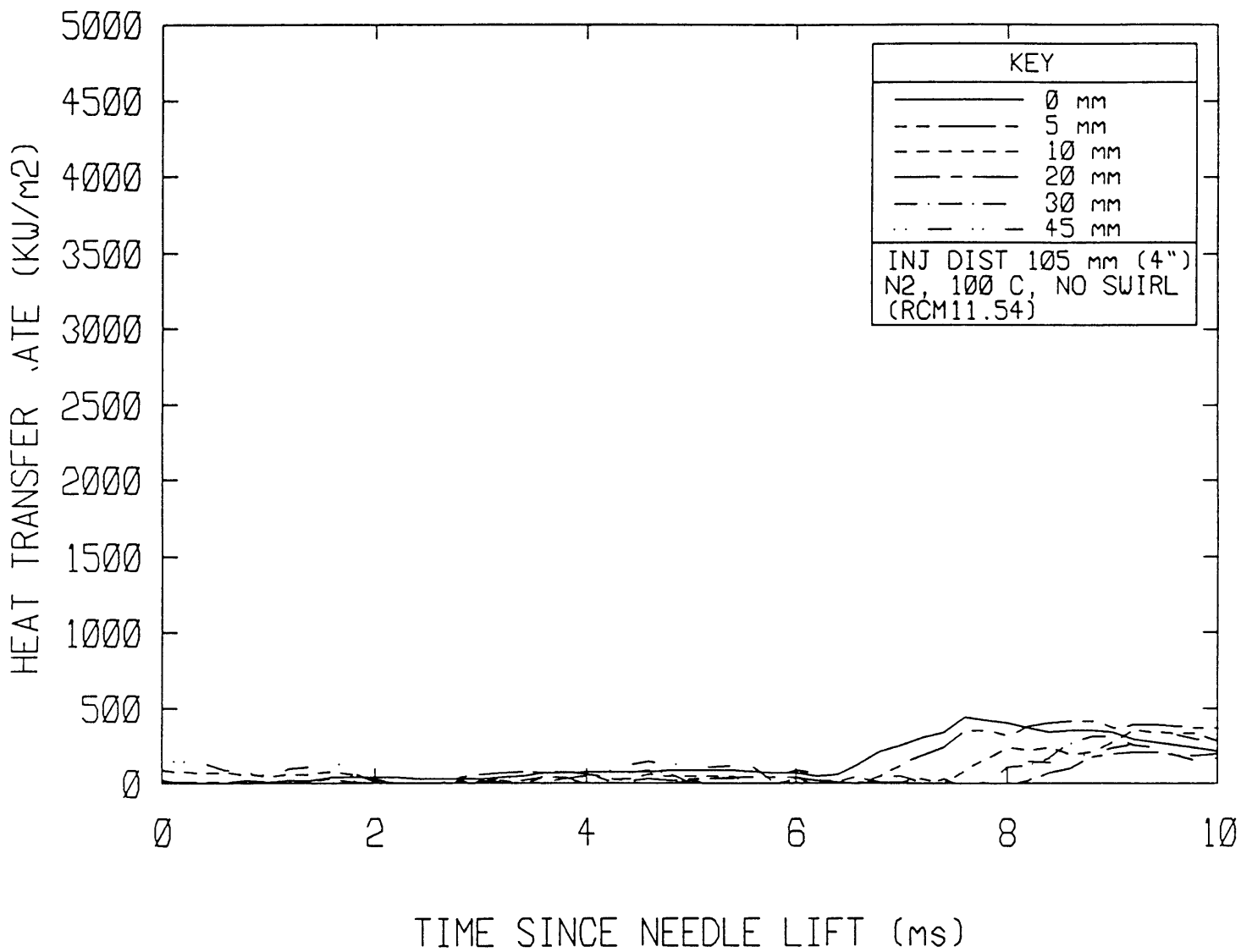
HEAT FLUX SURVEY (HORIZ)



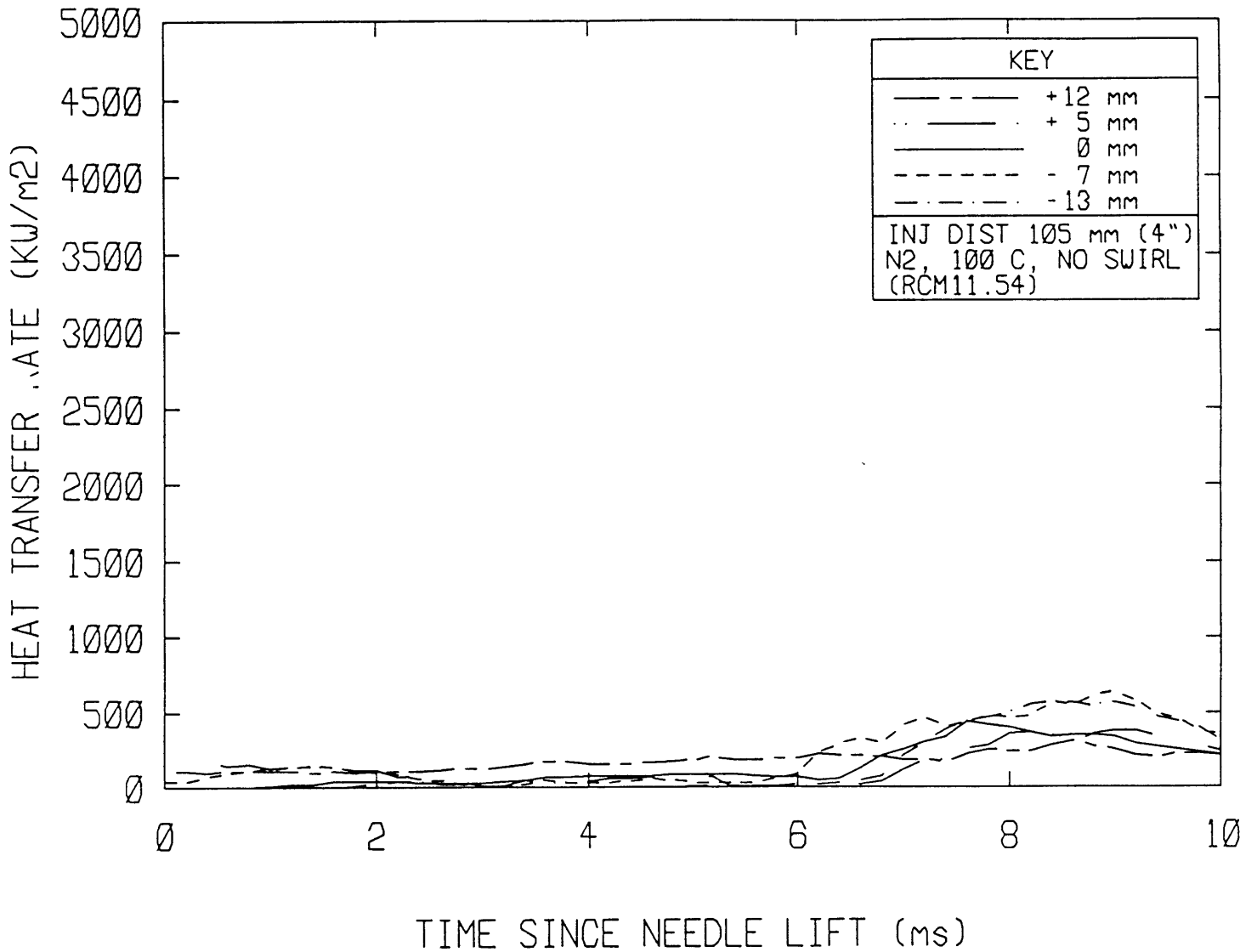
HEAT FLUX SURVEY (VERT)



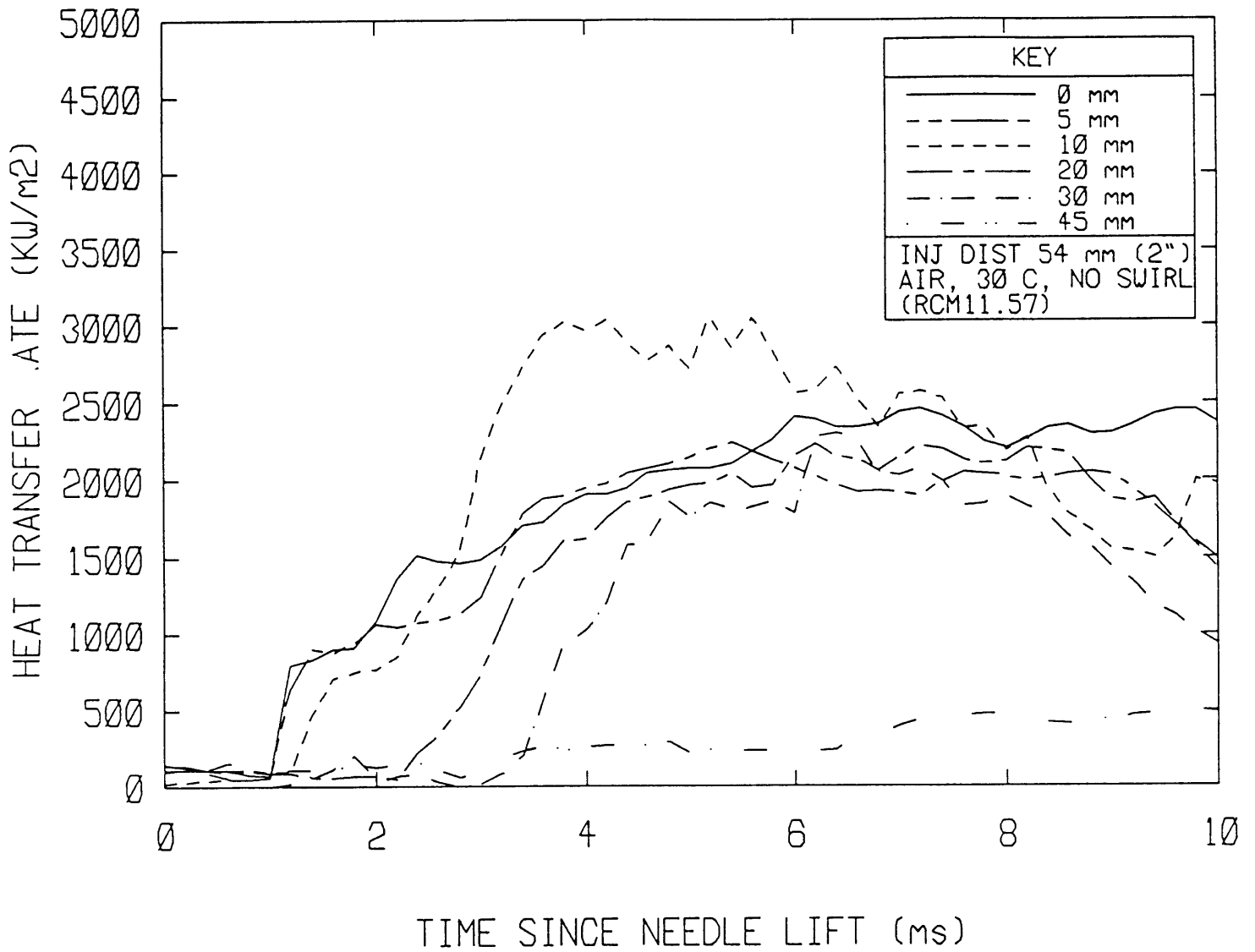
HEAT FLUX SURVEY (HORIZ)



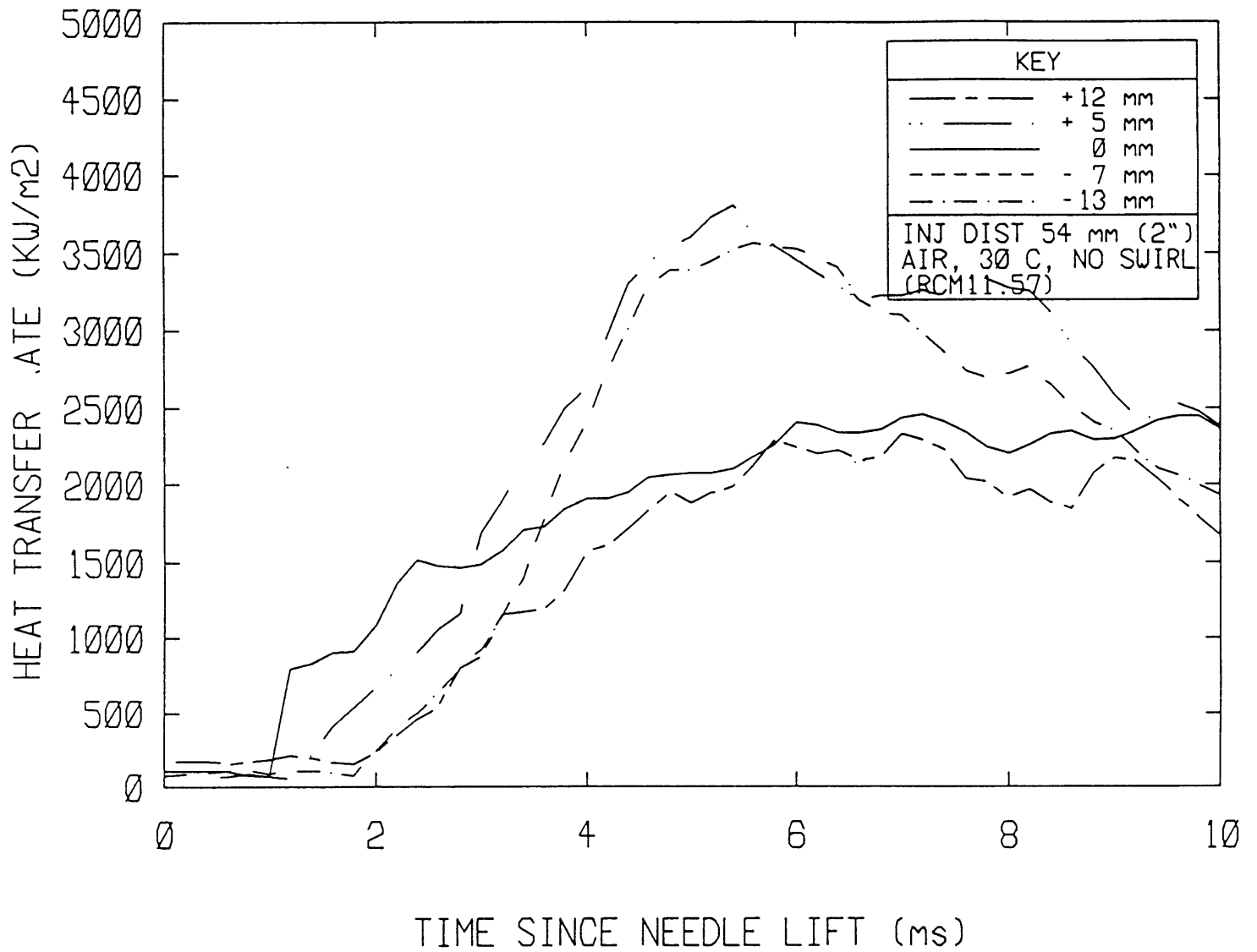
HEAT FLUX SURVEY (VERT)



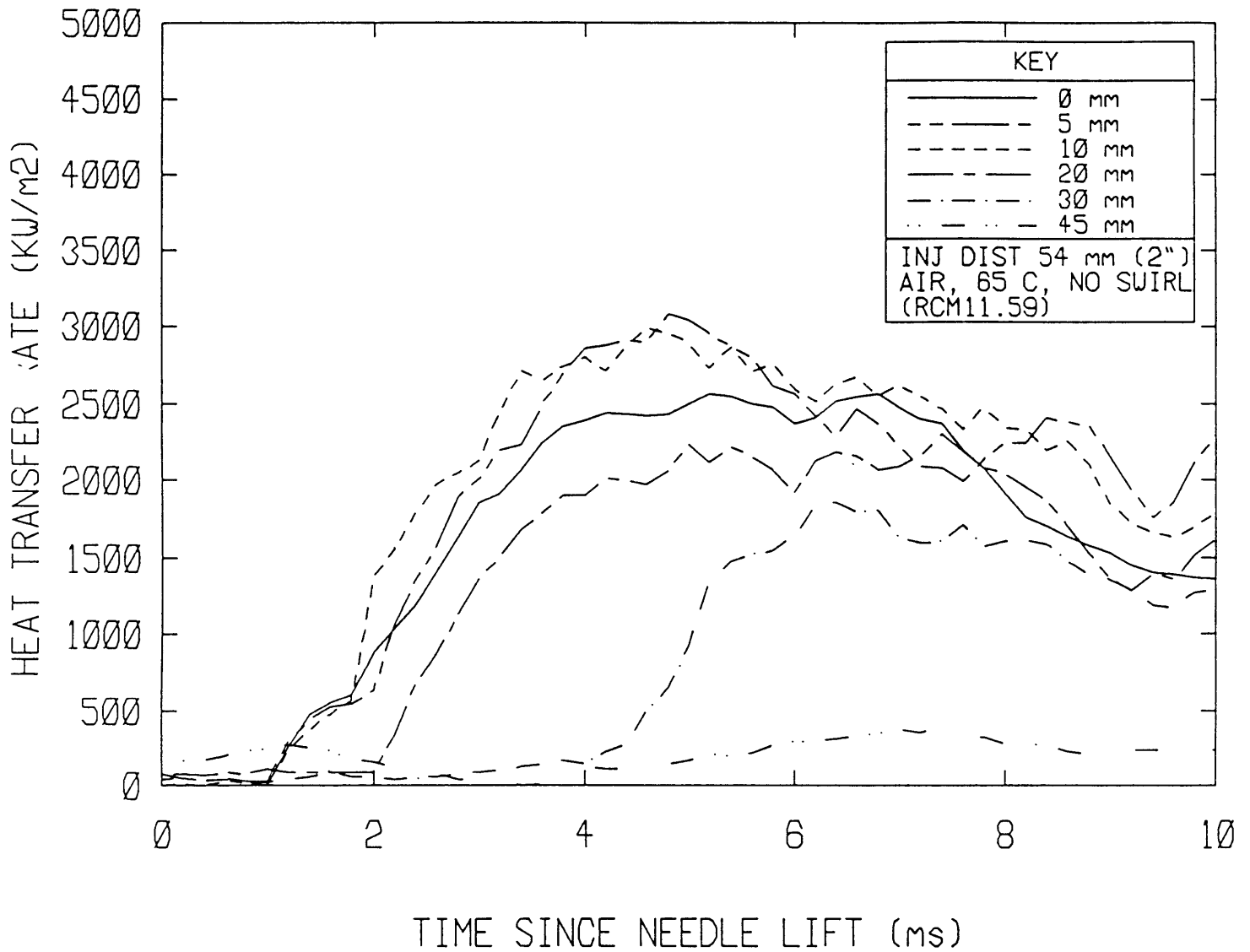
HEAT FLUX SURVEY (HORIZ)



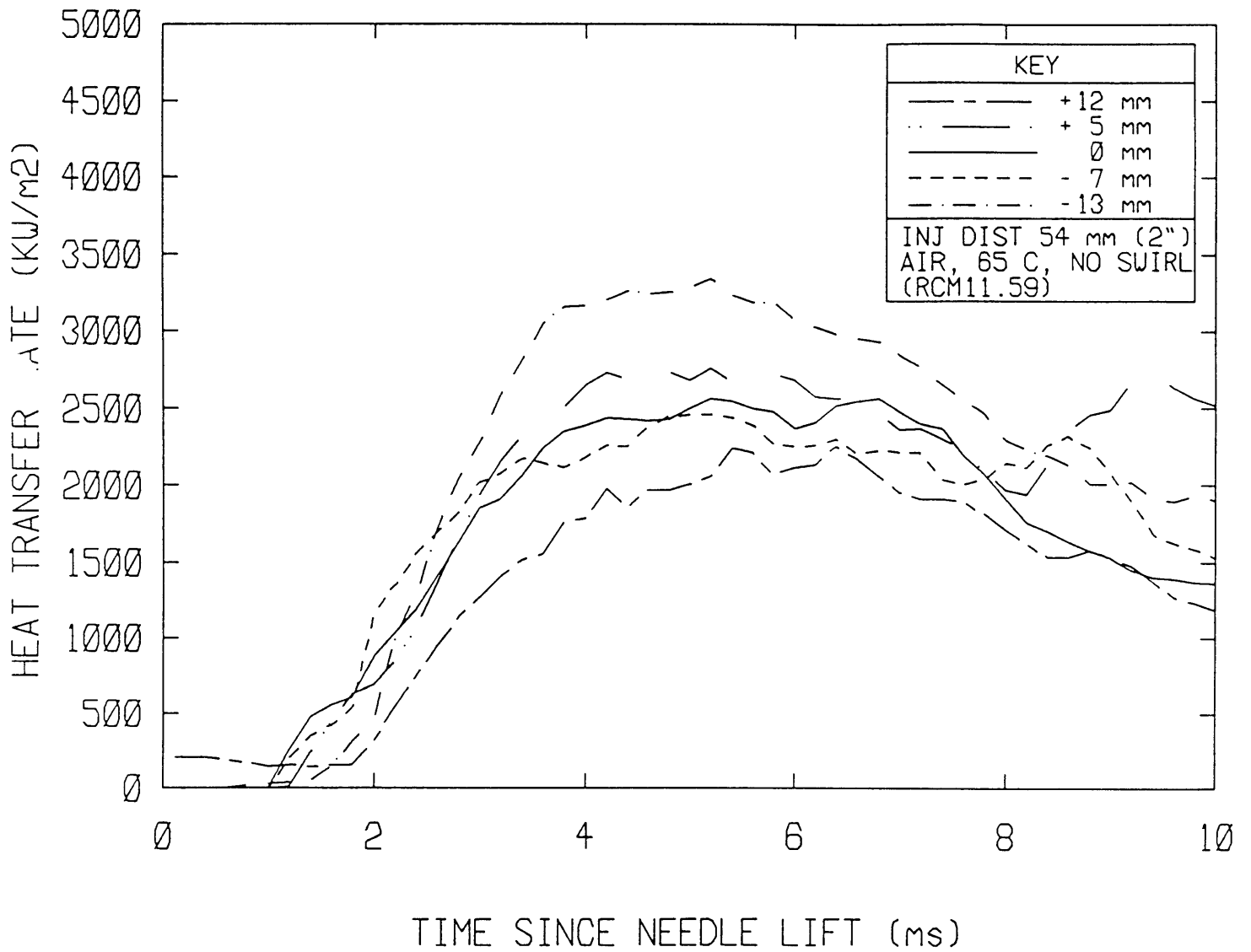
HEAT FLUX SURVEY (VERT)



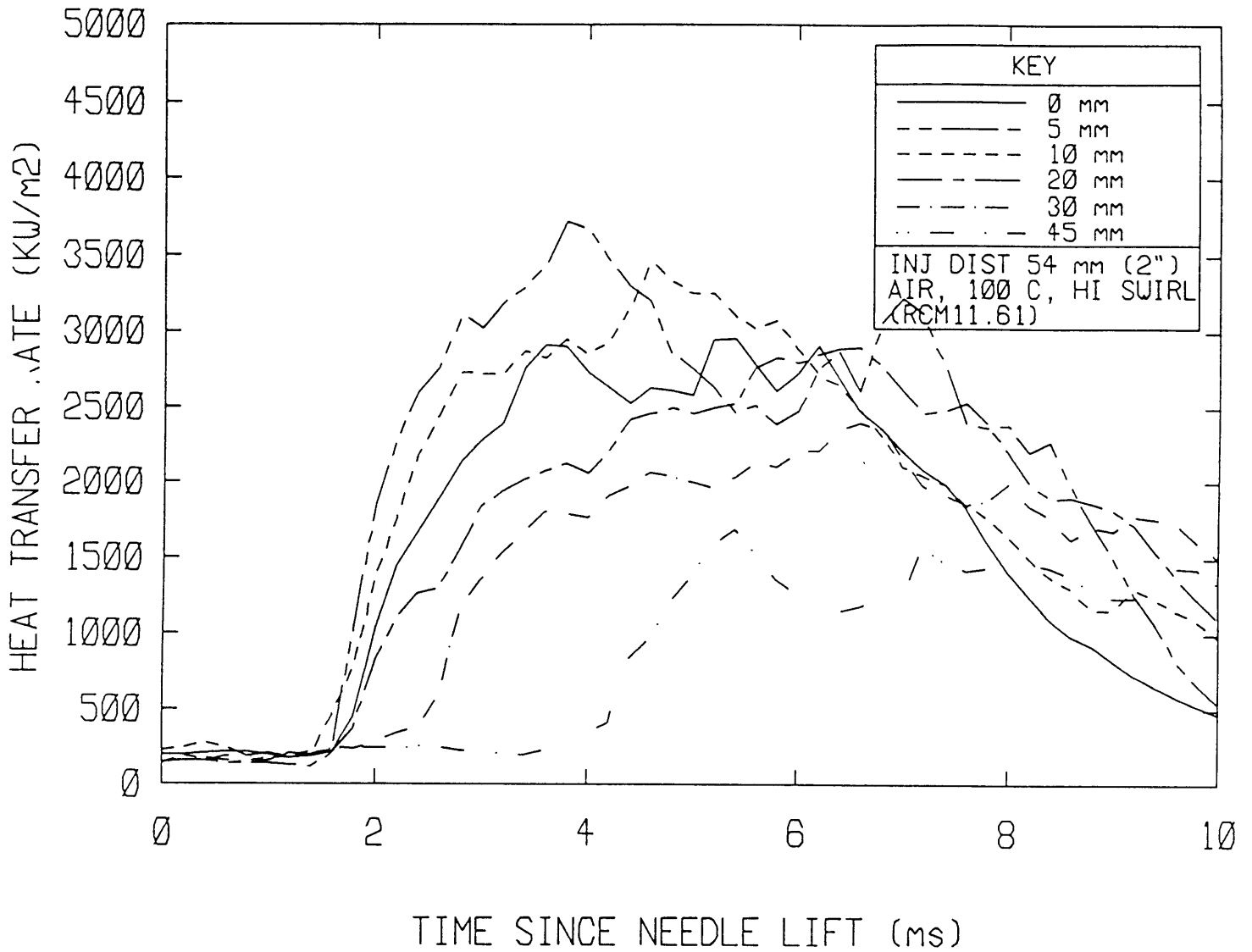
HEAT FLUX SURVEY (HORIZ)



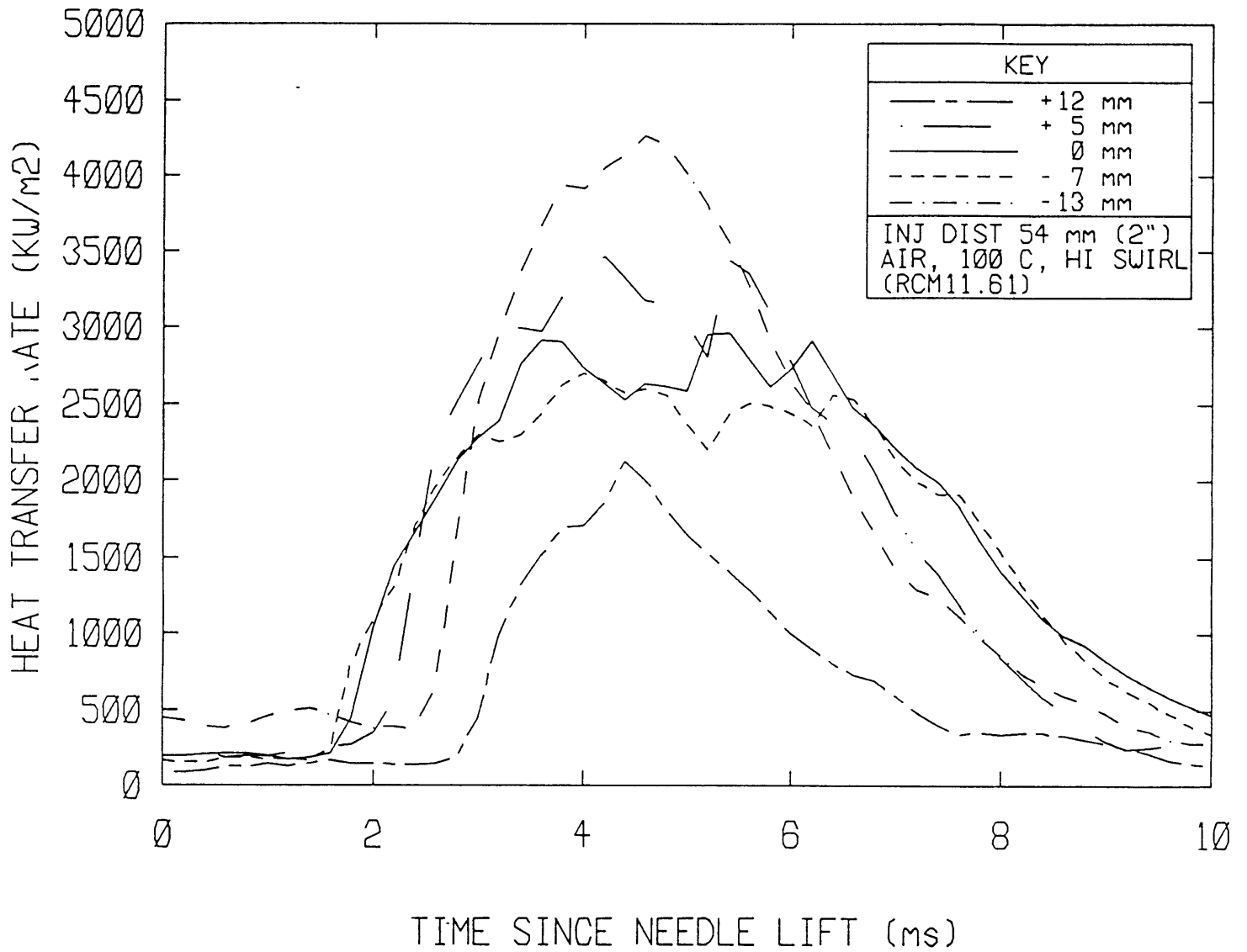
HEAT FLUX SURVEY (VERT)



HEAT FLUX SURVEY (HORIZ)



HEAT FLUX SURVEY (VERT)



DRAFT

Appendix B Steady State Heat Fluxes

Nomenclature:

x = horizontal distance from impingement point (mm)

All heat fluxes are kW/m²

NITROGEN

<----- injector standoff distance ----->

<u>X(mm)</u>	<u>29 mm</u>	<u>54 mm</u>	<u>68 mm</u>	<u>79 mm</u>	<u>105 mm</u>
0	3072	1083	851	678	396
5	1471	962	638	710	397
10	1027	797	598	565	222
-15	702	572	482	400	264
20	533	485	449	393	192
30	199	280	350	269	163
45	138	83		83	

AIR

<----- injector standoff distance ----->

<u>X(mm)</u>	<u>29 mm</u>	<u>54 mm</u>	<u>68 mm</u>	<u>79 mm</u>	<u>105 mm</u>
0	3080	3185	2902	2721	2324
5	2971	2972	3021	2688	2595
10	2631	2409	3114	2453	2278
-15	2606	2761	2557	2050	2382
20	2565	2517	2167	2445	2411
30	1730	2045	2661	1249	1767
45	402	254	317	339	350